

2010-12-15

Sustainable Composite Systems for Infrastructure Rehabilitation

Francisco Jose De Caso y Basalo
University of Miami, f.decasoybasalo@umiami.edu

Follow this and additional works at: https://scholarlyrepository.miami.edu/oa_dissertations

Recommended Citation

De Caso y Basalo, Francisco Jose, "Sustainable Composite Systems for Infrastructure Rehabilitation" (2010). *Open Access Dissertations*. 495.
https://scholarlyrepository.miami.edu/oa_dissertations/495

This Open access is brought to you for free and open access by the Electronic Theses and Dissertations at Scholarly Repository. It has been accepted for inclusion in Open Access Dissertations by an authorized administrator of Scholarly Repository. For more information, please contact repository.library@miami.edu.

UNIVERSITY OF MIAMI

SUSTAINABLE COMPOSITE SYSTEMS FOR
INFRASTRUCTURE REHABILITATION

By

Francisco J. De Caso y Basalo

A DISSERTATION

Submitted to the Faculty
of the University of Miami
in partial fulfillment of the requirements for
the degree of Doctor of Philosophy

Coral Gables, Florida

December 2010

©2010
Francisco J. De Caso y Basalo
All Rights Reserved

UNIVERSITY OF MIAMI

A dissertation submitted in partial fulfillment of
the requirements for the degree of
Doctor of Philosophy

SUSTAINABLE COMPOSITE SYSTEMS FOR
INFRASTRUCTURE REHABILITATION

Francisco J. De Caso y Basalo

Approved:

Antonio Nanni, Ph.D.
Professor of Civil, Architectural
and Environmental Engineering

Terri A. Scandura, Ph.D.
Dean of the Graduate School

Jacqueline P. James, Ph.D.
Assistant Professor of
Civil, Architectural and,
Environmental Engineering

Brian Metrovich, Ph.D.
Associate Professor of
Civil Engineering, Case
Western Reserve University

Fabio Matta, Ph.D.
Assistant Professor of
Civil and Environmental Engineering,
University of South Carolina

Tim Ibell, Ph.D.
Professor and Associate Dean
for Graduate Studies, Architecture
and Civil Engineering,
University of Bath

DE CASO Y BASALO, FRANCISCO J.
Sustainable Composite Systems for
Infrastructure Rehabilitation

(Ph.D., Civil Engineering)
(December 2010)

Abstract of a dissertation at the University of Miami.

Dissertation supervised by Professor Antonio Nanni.
No. of pages in text. (160)

The development of composite materials by combining two or more constituents with improved mechanical properties, when compared to either of the constituents alone, has existed since biblical times when straw or horse hair was mixed with clay or mud to produce bricks. During the second half of the twentieth century, modern composites known as fiber reinforced polymers (FRP) - consisting of a reinforcing phase (fibers) embedded into a matrix (polymeric resin or binder) - were developed to meet the performance challenges of space exploration and air travel. With time, externally-bonded FRP applications for strengthening of reinforced concrete (RC) structures gained popularity within the construction industry. To date, the confinement of RC columns using FRP systems is a convenient and well established solution to strengthen, repair and retrofit structural concrete members. This technology has become mainstream due to its cost effectiveness, and relative ease and speed of application with respect to alternative rehabilitation techniques such as steel or concrete jackets. However, significant margins exist to advance externally-bonded composite rehabilitation technologies by addressing economic, technological, and environmental issues posed by the use of organic polymer matrices, some of which are addressed in this dissertation.

Articulated in three studies, the dissertation investigates the development of a sustainable, reversible, and compatible fiber reinforced cement-based matrix (FRC) composite system for concrete confinement applications in combination with a novel test method aimed at characterizing composites under hydrostatic pressure.

Study 1 develops and characterizes a FRC system from different fiber and inorganic matrix combinations, while evaluating the confinement effectiveness in comparison to a conventional FRP system. The feasibility of making the application reversible was investigated by introducing a bond breaker between the concrete substrate and the composite jacket in a series of confined cylinders. The prototype FRC system produced a substantial increase in strength and deformability with respect to unconfined cylinders. A superior deformability was attained without the use of a bond breaker. The predominant failure mode was loss of compatibility due to fiber-matrix separation, which points to the need of improving fiber impregnation to enable a more efficient use of the constituent materials. Additionally semi-empirical linear and nonlinear models for ultimate compressive strength and deformation in FRC-confined concrete are also investigated.

Study 2 compares through a life cycle assessment (LCA) method two retrofitting strategies: a conventional organic-based, with the developed inorganic-based composite system presented in Study 1, applied to concrete cylinders by analyzing three life cycle impact indicators: i) Volatile Organic Compound (VOC) emissions, ii) embodied energy, and, iii) carbon foot print. Overall the cement-based composite provides an environmentally-benign alternative over polymer-based composite strengthening system.

Results also provide quantitative information regarding the environmental and health impacts to aid with the decision-making process of design when selecting composite strengthening systems.

Study 3 is divided into two parts, Part A presents the development of a novel “Investigation of Circumferential-strain Experimental” (ICE) methodology for characterization of circumferential (hoop) strain of composite laminates, while Part B uses the experimental data reported in Part A to explicitly evaluate the effect of FRP jacket curvature and laminate thickness on strain efficiency. Results showed that the proposed ICE methodology is simple, effective and reliable. Additionally, the ultimate circumferential strain values increased with increasing cylinder diameter, while being consistently lower when compared to similar flat coupon specimens under the same conditions. The ultimate FRP tensile strain was found to be a function of the radius of curvature and laminate thickness, for a given fiber ply density and number. The effect of these findings over current design guidelines for FRP confined concrete was also discussed.

To my family

Difficulties mastered, are opportunities won

Winston Churchill

ACKNOWLEDGEMENTS

Throughout the journey of this research, culminated in this dissertation, I have been accompanied by numerous individuals whom made this voyage possible and a worthwhile experience. These few lines, though not enough to acknowledge all their contributions, give me the opportunity to express my most sincere appreciation and thankfulness for their company.

To Dr. Antonio Nanni, as my advisor he taught me to persevere in my endeavors; as a sailor he taught me the importance of patience; as a friend I learned from him that passion is fundamental in everything I embark on. I hope to keep learning from him.

To Dr. Tim Ibell, Dr. Jacqueline James, Dr. Fabio Matta, and Dr. Brian Metrovich, I am privileged for their participation as members of my committee and grateful for their technical and philosophical advice. Special thanks to Dr. Fabio Matta, whose continuous support and relentless guidance has made a significant difference to my work; and Dr. Tim Ibell who as my former mentor has continued to provide thoughtful advice.

The financial support of the National Science Foundation Industry/University Cooperative Research Center for the Integration of Composites into Infrastructure (CICI) is gratefully acknowledged, as without it, this voyage would not have been possible.

To my research colleagues, faculty members, administration staff and friends; I would have never been able to reach the heights or explore the depths without their company. Special thanks to Dr. Ronald Zollo, Dr. Carol Hays, Dr. Fernando Tinoco, Dr. Rodrigo Mora, Carol Kavooras, Dr. Antonio De Luca, Derek Schesser, Dr. Fabio Nardone, Yao Gao, Matt Trussoni, Christian Aquino, Annalisa Napoli, Monica Maher, Bailey Lozner, Reem Madkour, Jose Cueto, Patrick Kaimrajh, Tom Makowski, Luis Torres, Nick Feldt, Sean October, Tala Shakri, Navid Nemati, Matteo Di Benedetti, Giovanni Loreto, Hany Jawaheri, and in particular Renny Sie; for their time, help, and encouragement in this unforgettable expedition.

Many thanks to Dr. Terri A. Scandura, Dr. James Tien, Dr. William Green, Odalis Ruiz, Devika Milner, Ann Helmers, Gilberto Arias, David Pool, Rafael Torres, Mechelle Francis, Cai Svendsen, William Buchser, Austin McQuillen, Raul Hernandez, and Manuel Gonzalez; for sharing their knowledge and friendship, while inspiring me throughout this experience.

Distinct thanks to Bill Jacobs, Candido Hernandez, Fred Goodwin, Bob Gulyas, Walter Hanford, Will Gold, Tory Jensen, Paul Kleindienst and Phil Davis; for their technical

support in this journey, and extended thanks to the University of Naples Federico II, and the personnel at DIST for their assistance with testing.

Recognition to the staff of the College of Engineering and the Graduate School at the University of Miami, the Graduate Activity Fee Allocation Committee (GAFAC), the student members of the American Society of Civil Engineers (ASCE) UM Chapter, and UM's Graduate Student Association (GSA); for the opportunities that have enriched my work and time as a graduate student at UM, many thanks.

This acknowledgement would not be complete without expressing my deepest gratitude to my parents, Laura and Francisco, and my siblings, Rodrigo, Carolina, Emerico and Laura. Throughout the years their unwavering faith and confidence in my abilities is what has shaped me to be the person I am today. *Gracias por todo.*

TABLE OF CONTENTS

LIST OF FIGURES	ix
LIST OF TABLES	xiii
LIST OF SYMBOLS	xv
CHAPTER	
I INTRODUCTION	1
II <i>Study 1</i> _ FIBER REINFORCED CEMENT- BASED COMPOSITE SYSTEM FOR CONCRETE CONFINEMENT	10
III <i>Study 2</i> _ SUSTAINABLE COMPOSITE STRENGTHENING SYSTEM: QUALITATIVE AND QUANTITATIVE ENVIRONMENTAL IMPACT ANALYSIS.....	54
IV <i>Study 3</i> _ ICE METHODOLOGY	85
<i>PART A</i> : ICE METHODOLOGY FOR FRP CHARACTERIZATION .	88
<i>PART B</i> : EXPERIMENTAL EVALUATION OF FRP STRAIN EFFICIENCY USING ICE METHODOLOGY.....	109
V CONCLUSIONS.....	145
BIBLIOGRAPHY	151

LIST OF FIGURES

Figure 1 – Dissertation and outcomes.....	5
Figure 2 – Failed inorganic matrix cube compression specimens:.....	38
Figure 3 – Setup for concrete cylinder compression tests.	39
Figure 4 – Failure mode of FRC confined cylinders: predominant fiber rupture in specimen HDG-H-2 (a) and BGP-A-1 (b); and predominant fiber-matrix separation in specimen LDG-A-1 (c) and BGP-H-1 (d).	40
Figure 5 – Representative SEM image of FRC composite in failed concrete cylinder confined using LDG fiber sheets with Type A (a) and Type H (b) matrix.....	41
Figure 6 – Representative SEM image of interface between inorganic matrix (Type A left) and concrete substrate (right) in failed confined concrete cylinder.	42
Figure 7 – Axial stress-strain response of representative concrete cylinder specimens in compression: confined with low density glass (LGD) sheets (a); confined with high density glass (HDG) sheets (b); and confined with hybrid basalt/glass/PVA sheets (c)..	44
Figure 8 – FRC flat coupon drawing (dimensions in mm).	45
Figure 9 – FRC coupon longitudinal section, showing thickness and fiber/matrix layers for different number of plies.	45
Figure 10 – Test set up for direct tensile testing of flat FRC coupons.	46
Figure 11 – Axial stress–strain envelope for tensile coupon tests for:	47
Figure 12 – Failure of representative two- and four-ply FRC flat coupon samples (a); and failure close-up at tab location (b).	48

Figure 13 – Influence of amount of FRC reinforcement: experimental points and best fitting line for strengthening ratio (a) and $\epsilon_{cc} / \epsilon_c$ ratio (b) with respect to stiffness of confinement system.	49
Figure 14 – Response of representative 2-ply bonded (B) and unbonded (U) FRC confined concrete cylinders in compression: axial stress-axial strain (a); volumetric strain-axial strain (b).	50
Figure 15 – FRC jacket removed from failed unbonded specimen (2U-3): top view, illustrating the inner surface of the FRC jacket (a); and side view, showing separation between fibers and inorganic matrix (b).	51
Figure 16 – Experimental points and semi-empirical linear and nonlinear model for strengthening ratio as function of confining stress for FRC bonded specimens.....	52
Figure 17 – Experimental points and semi-empirical linear and nonlinear model for axial strain at maximum axial stress as function confining stress for FRC bonded specimens. 53	
Figure 18 – Life Cycle Stages [55].	76
Figure 19 – Summary of the evaluation range for BFRC and GFRP composites.	77
Figure 20 – Processes within the LCI of BFRC and GFRP composites.	78
Figure 21 – Sample preparation following the wet lay-up technique.	78
Figure 22 – PID instrument (a); and PID sensor module and components (b).	79
Figure 23 – Environmental chamber test setup (a); specimen within environmental chamber (b).	80
Figure 24 – Minimum, average and maximum concentration levels of emitted VOCs for representative: GFRP- (a); and BFRC-strengthening system (b).	81
Figure 25 – Comparison of average concentration of emitted VOCs of representative BFRC and GFRP strengthening systems.	82
Figure 26 – LCIA results for each composite system: Potential Energy (a); and Global Warming Potential (b).	83
Figure 27 – LCIA normalized results for each system component: Potential Energy (a); and Global Warming Potential (b).	84
Figure 28 – Phase diagram of water. Dash line represents average working temperature of ICE methodology environmental chamber.	127
Figure 29 – General ordinary ice crystal structure (a), ice prior freezing (b), ice after freezing (c).	127

Figure 30 – ICE methodology rig components.....	128
Figure 31 – Strain gauge (SG) configuration for metal can specimens: cross-sectional layout (a); longitudinal layout (b).....	128
Figure 32 – Strain-time- temperature response of a representative metal can specimen, (S-2) with cross-sectional strain layout (a), and (S-4) with longitudinal strain layout (b)..	129
Figure 33 - Representative failure mode of metal cans with large diameter (a); small diameter (b).....	130
Figure 34 – Hand lay-up GFRP cylinder specimen fabrication process.....	131
Figure 35 – Strain gauge (SG) configuration for GFRP specimens: plan view (a); front view for layout of two SG (b); and six SG (c).....	132
Figure 36 – Circumferential strain measurements for a representative GFRP specimen 3P-115-2 instrumented with the longitudinal layout.	133
Figure 37 – Strain-time-air temperature response of representative GFRP specimens with one ply (a); two plies (b); and three plies (c).....	135
Figure 38 – Strain-time response for the entire test length showing the difference between same design specimens: 1P-115-2 showing pressure loss (due to leak), and 1P-115-5 without pressure loss (good seal).....	136
Figure 39 – Failure mode of 171 mm diameter GFRP cylindrical specimens 1P-171-2 (a); 2P-171-5 (b); and 3P-171-1 (c).....	137
Figure 40 – Typical tensile failure observed on specimen 1P-171-2.....	138
Figure 41 – Specimen 1P-171-4 failed at the mid cross-section after testing, showing the inside of the specimen with the ice layer formation (a); ice block inside specimen	138
Figure 42 – Scheme of confinement action.	139
Figure 43 – GFRP flat coupon specimen drawing (dimensions in mm).....	139
Figure 44 – Test setup for GFRP flat coupon specimen tensile (a); and flat coupon specimen instrumentation (b).....	140
Figure 45 – Representative direct tensile axial stress-strain response for GFRP flat coupon, 1P-C (a); 2P-B (b); and 3P-C (c).....	141
Figure 46 – Representative tensile failure experienced by flat coupons,	142
Figure 47 – Strain efficiency factor, κ_e , vs cylinder diameter, D , at.....	143

Figure 48 – Strain efficiency factor, κ_ϵ vs. t'/R ratio showing specimens by: diameter (a); number of plies (b); and combined results (c). 144

LIST OF TABLES

Table 1 – Mechanical properties of inorganic cement-based matrices.....	34
Table 2 – Reinforcing fiber sheet properties used for preliminary FRC material selection.	34
Table 3 – Results of compression tests for preliminary evaluation of confinement effectiveness.....	35
Table 4 – Results of direct tensile characterization of FRC flat coupons.....	36
Table 5 – Results of compression tests for assessment of bonded and unbonded FRC system.	37
Table 6 – Embodied energy of selected thermoplastic and thermoset polymers [64].	73
Table 7 – Reinforcement and matrix/primer properties*	73
Table 8 – Externally-bonded confining retrofit design.....	74
Table 9 – Energy and Carbon inventory data.	74
Table 10 – Minimum, maximum and average concentration of emitted VOCs for BFRC and GFRP strengthening systems, based on an average of five specimens.....	75
Table 11 – LCIA summary results.....	75
Table 12 – Cylindrical metal can properties.	122
Table 13 – Results of cylindrical metal cans tested with ICE methodology.	122
Table 14 – Results of cylindrical hand lay-up manufactured GFRP specimens tested with ICE methodology, strains measured at mid-height of specimen.	123

Table 15 – ANOVA three-factor with replication test for ultimate circumferential strains at mid-section.....	124
Table 16 – Results of cylindrical hand lay-up manufactured GFRP specimens tested with ICE methodology, strains measured at $\frac{3}{4}$, $\frac{1}{2}$ and $\frac{1}{4}$ of cylinder height.	124
Table 17 – GFRP flat coupon tensile test results.....	125
Table 18 – ANOVA single factor test for flat coupon f_{fu} results.	126
Table 19 – Average ultimate tensile strain for cylindrical specimens and flat coupons.	126

LIST OF SYMBOLS

D	diameter of plain concrete cylinder, or internal diameter of cylindrical GFRP specimen
df	degrees of freedom
E^{chord}	tensile chord modulus of flat coupons
E_f	longitudinal elastic modulus of fiber reinforcement
E_{frp}	young modulus of elasticity of FRP laminate
F	F-test ratio of the Mean Square Effect to Mean Square Error
$F-crit$	value that F-test statistic must exceed to reject the null hypothesis, extracted from distribution of statistical tables.
F_{xmn}^i	fate and exposure pathway of chemicals and substances x which have been released to all medias m , with all modeled exposure routes n , for a specific indicator i
f_{co}	average cylinder compressive strength of plain concrete
f_{cc}	compressive strength of confined concrete cylinder
$f_{cc,FRC}$	average compressive strength of FRC-confined concrete cylinders
$f_{cc,FRP}$	average compressive strength of FRP-confined concrete cylinders
f_{fu}	ultimate tensile strength of flat coupons
f_{lu}	confining pressure exerted by FRC jacket at maximum axial stress
f_m	cube compressive strength of hardened inorganic matrix

f_r	tensile radial stress
f_θ	tensile circumferential stress
H	cylindrical GFRP specimen height
I_i	potential impact of chemicals and substances for a specific indicator i
K	adiabatic bulk modulus of ice
k_1, m	empirical constants in model of axial strength of confined concrete cylinders
k_2, n	empirical constants in model of axial strain at maximum stress in confined concrete cylinders
MS	mean square
M_{xm}	mass of the chemicals and substances x released to all medias m
n_p	number of plies of fiber reinforcement
p	confinement pressure
P_{xn}^i	potency of the chemicals and substances released to all medias m for a specific indicator i
$P\text{-value}$	probability value
R	radius of curvature for cylindrical GFRP specimen
SD	standard deviation
SS	sum of squares
t_f	thickness of one ply of fiber reinforcement
t	thickness of FRP laminate
t'	normalized laminate thickness
t_n	normalized thickness ratio
T_g	FRP glass-transition temperature
T_s	internal specimen temperature
ε_{co}	average ultimate axial strain of plain concrete cylinders

ε_{cc}	axial strain of confined concrete cylinder at maximum axial stress in confined concrete cylinder
$\varepsilon_{cc,FRC}$	average axial strain at maximum axial stress in FRC-confined concrete cylinder
$\varepsilon_{cc,FRP}$	average axial strain at maximum axial stress in FRP-confined concrete cylinder
ε_{fu}	ultimate direct tensile strain
ε_{lu}	average hoop strain in FRC reinforcement at maximum axial stress in confined concrete cylinder
ε_r	radial strain
ε_v	volumetric strain
ε^*_{fu}	computed ultimate direct tensile strain
$\varepsilon_{\theta u}$	ultimate tensile circumferential strain
ε'_{fu}	average computed ultimate tensile direct strain
$\varepsilon'_{\theta u}$	average ultimate tensile circumferential strain
ε_{90}	peak circumferential strain at the mid cross-section in the <i>no-lap</i> zone
ε_{e90}	equivalent <i>lap</i> strain
ε_{270}	peak circumferential strain at the mid cross-section in the <i>lap</i> zone
ν	Poisson's ratio of concrete
ρ_f	FRC reinforcement ratio
σ_t	splitting tensile strength of hardened inorganic matrix
α	ANOVA test level of the confidence limits
κ_ε	strain efficiency factor
κ_ν	bond-reduction coefficient
ρ	fiber sheet density

CHAPTER I

INTRODUCTION

The development of composite materials by combining two or more constituents with improved mechanical properties, when compared to either of the constituents alone, has existed since biblical times when straw or horse hair was mixed with clay or mud to produce bricks [1]. During the second half of the twentieth century, modern composites known as fiber reinforced polymers (FRP) - consisting of a reinforcing phase (fibers) embedded into a matrix (polymeric resin or binder) - were developed to meet the performance challenges of space exploration and air travel. While being corrosion resistant and light-weight, FRP offered high-strength, -stiffness, and -durability over conventional materials. By the late 1980s FRP systems were researched and developed worldwide by the construction industry for infrastructure strengthening and repair due to deterioration of structures resulting from lack of maintenance, poor initial design due to insufficient reinforcement, and demanding design codes with increasingly higher service loads [2]. With time, externally-bonded FRP applications for strengthening of reinforced concrete (RC) structures gained popularity [3][4][5]. To date, the confinement of RC columns using FRP systems is a convenient and well established solution to strengthen,

repair and retrofit structural concrete members [6]. It has become mainstream due to its cost effectiveness, and relative ease and speed of application with respect to alternative rehabilitation techniques such as steel or concrete jackets [7].

Numerous studies have shown that concrete confinement with FRP systems can increase the compressive strength as well as the deformability under vertical and lateral (e.g., seismic) loads by creating a triaxial-stress condition, while additionally it increases the shear resistance of circular columns and prevents premature spalling failures [8][9][10]. This evidence was translated into design guidelines and codes of practice, for example by ACI in the USA [11] and by CSA in Canada [12], respectively. Currently a wide range of organic polymer matrices, typically epoxy-based, are used due to the commercial availability of convenient resin systems that offer adequate compatibility with the reinforcing fibers and the concrete substrate, and durability under aggressive environments such as coastal regions, coupled with mechanical (strength, stiffness, toughness) properties that are suitable for structural applications.

Nevertheless, significant margins exist to advance externally-bonded composite rehabilitation technologies by addressing the following issues posed by the use of organic polymer matrices. a) Fire resistance: organic resins are flammable and, unless insulated against fire, degrade under temperatures that are close to or exceed that of glass transition [13], typically ranging from 60 to 82°C [11]; this process may also be accompanied by the release of toxic fumes, constituting a health hazard. b) Reversibility: the ability to easily remove and replace a composite system, impractical for epoxy-based FRP systems,

would simplify inspection and integrity assessment after a critical event; in addition, the technology would become more attractive for the conservation of historic structures, where reversibility is desirable [14]. c) Recyclability: excess organic resin from a rehabilitation application or from removal is considered a hazardous waste where its controlled disposal requires protocols not common in the construction industry, with limited available information [15]. d) Environment and health: research and development efforts to study the environmental and health impacts of FRP material systems are limited [16], where production relies on hazardous toxic constituents requiring high energy inputs. e) Cost: researching alternatives to reduce the initial cost of externally-bonded systems is essential to further the acceptance of this technology [17]. f) Characterization: with the increasing use of advance composite materials in infrastructure, safe and reliable designs require accurate prediction, which is achieved with well characterized material properties [6].

DISSERTATION OUTLINE

Articulated in three studies, the dissertation investigates the development of a sustainable, reversible, and compatible fiber reinforced cement-based matrix (FRC) composite system for concrete confinement applications in combination with a novel test method aimed at characterizing composites under hydrostatic pressure. The studies resulted in seven submitted or presented technical papers, conference proceedings and an extended abstract, clearly reported in the outline of the dissertation in Figure 1. The first study, *Study 1*, assesses the structural performance of a prototype FRC system through confined concrete cylinders tested under uniaxial compression; the second study, *Study 2*,

comparatively evaluates the proposed FRC with a traditional FRP system through a life cycle assessment method; and the last study, *Study 3*, presents the development of a unique ‘Investigation of Circumferential-strain Experimental’ (ICE) methodology for FRP characterization, while evaluating the strain efficiency of composite laminates.

Study 1 titled “Fiber reinforced cement-based composite system for concrete confinement” proposes a reversible FRC system from different fiber and inorganic matrix combinations, while evaluating the confinement effectiveness in comparison to a conventional FRP system. Additionally semi-empirical linear and nonlinear models for ultimate compressive strength and deformation in FRC-confined concrete are also investigated.

Study 2 titled “Sustainable composite strengthening system: qualitative and quantitative environmental impact analysis” compares two retrofitting strategies: a conventional organic-based, with the developed inorganic-based composite system presented in Study 1, applied to concrete cylinders by analyzing their life cycle impact in terms of Volatile Organic Compound (VOC) emissions, embodied energy, and carbon foot print.

Study 3 is divided in two parts; Part A titled “ICE methodology for FRP characterization” and Part B title “Evaluation of FRP strain efficiency using ICE methodology”. Part A presents a novel experimental technique to measure circumferential (hoop) strain of composite laminates, while Part B uses the experimental data reported in Part A to explicitly evaluate the effect of FRP jacket curvature and laminate thickness on the strain

efficiency. The effect of these findings over current design guidelines for FRP confined concrete is also discussed.

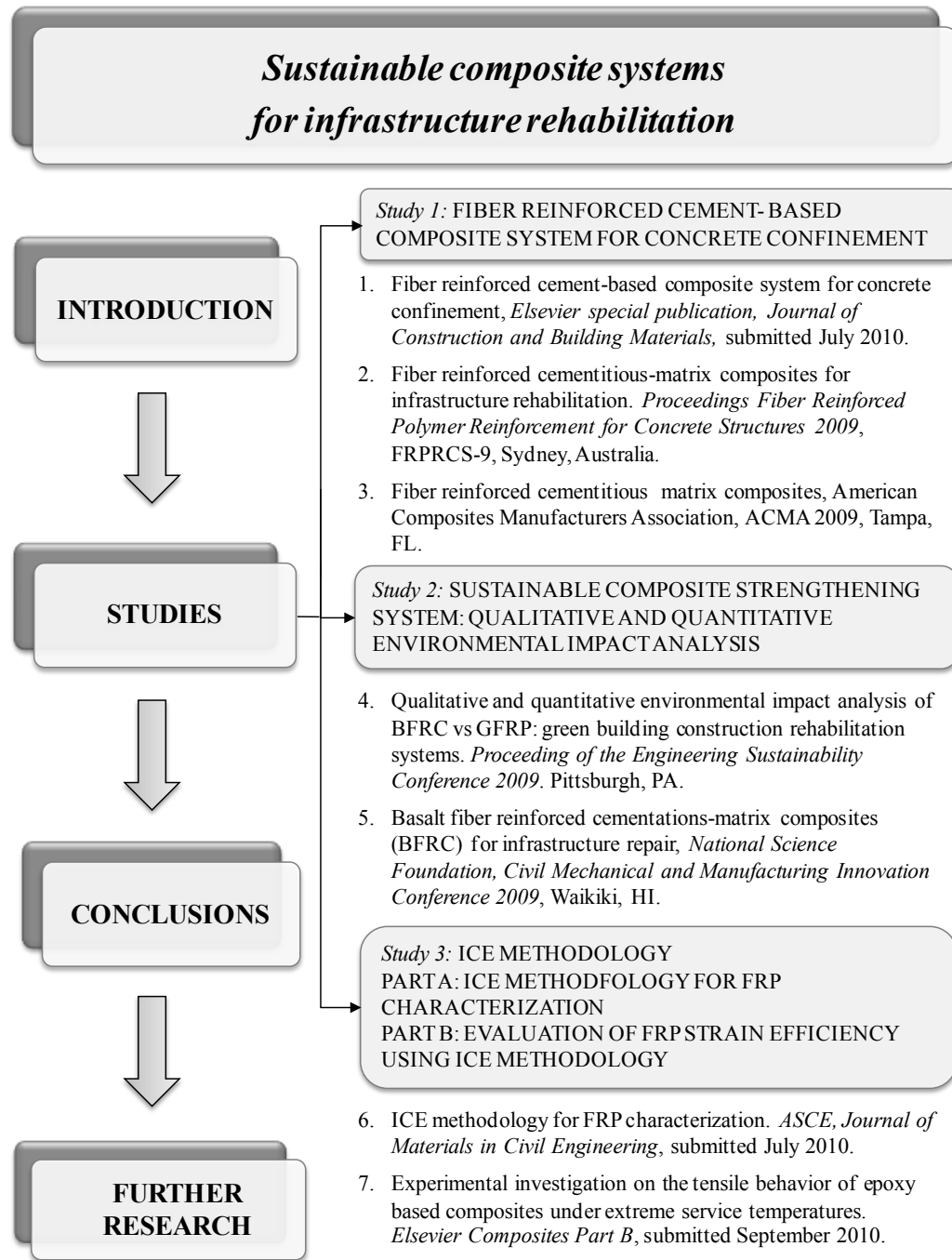


Figure 1 – Dissertation and outcomes

OBJECTIVES

Study 1 aims to:

- (a) develop a constructible and fully reversible confinement FRC jacketing system by verifying the workability and ease of installation on concrete cylinders;
- (b) examine the compatibility of the proposed system based on the quality of the concrete-FRC interface and the level of fiber impregnation;
- (c) evaluate the structural performance in terms of strength and deformability enhancement through confined concrete cylinders tested under uniaxial compression; and,
- (d) propose initial models for ultimate compressive strength and deformation in FRC-confined concrete.

Study 2 aims to:

- (a) apply a life cycle assessment methodology to compare organic- and inorganic-matrix composite systems, based on a functional unit;
- (b) investigate the life cycle contributions of the constituent materials for each composite in terms of three impact indicators including: i) experimental measurements of VOC concentration emissions, ii) embodied energy data, and iii) carbon foot print data; and,
- (c) determine qualitatively and quantitatively the relative level of sustainability within each composite system for confinement applications, contributing towards an environmentally-benign material system.

Study 3 aims to:

- (a) provide a cost-efficient and reliable experimental technique to measure circumferential strain of composite systems with different jacket diameters and laminate thicknesses;
- (b) understand the longitudinal and cross-sectional strain distributions of cylindrical FRP shells under hydrostatic pressure; and,
- (c) determine the effect of cylindrical FRP shell curvature and laminate thickness on the strain efficiency.

RESEARCH SIGNIFICANCE

With the increasing demand to strengthen, rehabilitate, and upgrade buildings and infrastructure [18][19], though initially costly, FRPs are particularly attractive reinforcement systems that may meet the increasing need. However, more environmentally-benign solutions are desired consistent with the growing demand for sustainable construction materials and systems [20][21]; this is reflected in the increasing number of green building projects on existing buildings through the United States Green Building Council's (USGBC) Leadership in Energy and Environmental Design (LEED) [22]. Additionally, the interest and funding of private and government agencies, such as the National Science Foundation (NSF) Industry/University Cooperative Research Center for the Repair of Buildings and Bridges (RB²C), reflects the significance of the work presented herein. Thus far, limited studies have provided a comprehensive analysis of the life cycle inputs and outputs of externally applied composites, while few studies have

explored alternative environmentally-benign structural rehabilitation composite systems such as fibers embedded within inorganic matrices (FRC). Additionally, the material properties of current organic- and the developed inorganic-based composite systems have not been characterized effectively, as experimental confined concrete cylinder values differ significantly from results obtained in standardized test methods [23]; characterization is fundamental to develop analytical models for design purposes.

The key novelties of the research presented herein consist of: the implementation of a life cycle assessment framework as a tool to engineering trade-offs (ETOs), to measure the transfer of direct and indirect environmental and health impacts associated with the use of composites strengthening systems to make a selection decision between the available systems; the development of a cement-based composite system for concrete confinement that responds to the growing need of sustainable material systems to strengthen and retrofit infrastructure; developing a fully reversible and fire resistant system that can be implemented as an alternative to existing polymer based composites, while providing significant increases in axial strength and deformability.

This research includes the development of a novel experimental test methodology using the property of water that expands when it changes state of matter from liquid to solid to apply a uniform internal hydrostatic pressure to composite cylindrical shells. This test arises from the fact that existing theoretical models and design guidelines available to predict the effects of FRP confinement on concrete rely on the common assumption that FRP fails when circumferential strain in the jacket reaches its ultimate tensile strain and

ruptures. The value for such critical parameter, the ultimate FRP tensile strain, is determined from material flat coupon tensile tests. While the characterization of the candidate FRC strengthening system is attempted for the first time in this research by means of direct tensile tests, extensive studies have suggested that ultimate FRP tensile strain determined experimentally according to flat coupon tests, could not be reached at the circumferential rupture of FRP jackets confining concrete cylinders [23][24][25]. Available experimental data has shown that the strain efficiency factor of externally applied FRP jackets, expressed as the ratio of the tensile circumferential strain in the FRP at failure to the average failure strain observed in FRP uniaxial tensile flat coupons tests, varies substantially from 0.58 to 0.91[26]. The causes for such differences are probably due to the effect of the radius of curvature, the multi-state of stress, or the uneven pressure exerted by the concrete resulting from its cracking. The evaluation of experimental results to determine the isolated effect of FRP jacket curvature and laminate thickness on the strain efficiency is also investigated in this research for the first time.

CHAPTER II

***STUDY 1_* FIBER REINFORCED CEMENT- BASED COMPOSITE SYSTEM FOR CONCRETE CONFINEMENT**

Though the application of externally-bonded fiber reinforced polymer (FRP) systems is a well established technique in the construction industry to strengthen and retrofit reinforced concrete (RC) structures, there is a need to address the economic, technological and environmental issues posed by the use of organic polymer matrices, previously summarized. This study aims to solve some of these issues by devising and evaluating the structural performance and behavior of a reversible fiber reinforced cement-based matrix (FRC) composite system for concrete confinement applications. First, six different combinations of commercially available inorganic binders and reinforcing fibers (including glass and basalt) were experimentally investigated to select a candidate system based on: constructability, where the FRC composites are applied on concrete cylinders to verify the workability of the matrix and ease of installation of the system; structural performance, evaluated at a developing stage of the system achieved by testing FRC confined concrete cylinders under uniaxial compression, together with

epoxy-based FRP confined counterparts used as benchmark; and compatibility, where the concrete-FRC interface and the ability of the matrix to penetrate the reinforcing fiber fabrics, both important factors in ensuring efficient stress transfer, are examined via scanning electron microscopy (SEM) analysis.

The selected FRC system was further characterized by testing additional confined concrete cylinders in compression, and by flat coupons tested in direct tension using three different external reinforcement ratios. For the cylinders both axial and in-plane (radial) deformations were measured to assess the confinement effectiveness. Reversibility was addressed by introducing a bond-breaker layer between the concrete substrate and the FRC composite jacket, where the behavior of bonded and un-bonded FRC jackets was also investigated. Analytical models to estimate strength increases and associated axial strains are also investigated.

BACKGROUND

Water-based inorganic binders (*i.e.*, cement-based grouts) are of interest as potential sustainable matrices for composite systems due to compelling properties, including non-toxic, recyclable, well known and used product in the construction industry, with high thermal stability [27][28], resistance to ultraviolet (UV) radiations and aggressive environments. Additionally, inorganic matrices have a high degree of chemical and mechanical compatibility with concrete substrates [29].

Their potential for use in structural rehabilitation was first successfully tested on RC beams strengthened in flexure using externally bonded carbon FRC laminates in the late 1990's [30]; comparable performance was attained in terms of flexural strength and post-cracking stiffness increase with respect to RC beams strengthened with carbon fiber sheets bonded using a two-part epoxy resin, with a minor reduction in ductility. It was also observed that inorganic matrices may be characterized by a different load transfer mechanism where local bond slip is accommodated by the formation of several hairline cracks in the matrix that do not propagate, typically resulting in failures due to fiber rupture rather than delamination [31]. Promising results were also obtained in increasing the shear strength of RC beams strengthened with carbon and glass FRC laminates [32][33].

Bond strength and integrity are not as critical in concrete confinement applications, where an intimate contact between the concrete substrate and the composite jacket is the key requisite to engage the strengthening system, thereby curtailing concrete dilation. Early attempts showed that comparable increases in axial strength and deformability were attained in concrete cylinders confined using a FRC-type composite system and a conventional two-part epoxy carbon FRP system [34][35]. A mortar-based composite that used textile carbon fiber reinforcement was developed and tested on confined cylinders and short rectangular columns, showing that jacketing provides a substantial gain in compressive strength and deformability [36], with a comparable confinement effectiveness to an epoxy-based carbon FRP system [37].

Recently, a study proposed the use of basalt reinforcing fiber sheets that were pre-impregnated with epoxy resin, and bonded with a cement-based mortar [38]; increases in compressive strength and axial strain were attained in plain concrete cylinders with respect to benchmark specimens strengthened with an epoxy-based glass FRP jacket.

SELECTION OF FRC SYSTEM

The objective of the first part of the feasibility study was to identify a candidate FRC system among different fiber/matrix combinations, on the basis of: ease of application, confinement effectiveness with respect to epoxy-based FRP systems with similar fiber reinforcement, ability to penetrate the reinforcing fibers, and ensure optimal stress transfer. Six fiber/matrix combinations were examined that included different inorganic matrices (water-based and acrylic-based), reinforcing fibers (including glass and basalt), and fiber sheet densities.

Inorganic Cement-Based Matrix

Two different inorganic matrices were investigated: the first based on a commercially available hydraulic cement-based mix formulated to produce a thixotropic matrix with high water retention, herein denoted as “Type H”; and the second based on a commercially available low-cost acrylic-modified Portland cement-based mix, herein denoted as “Type A”. The mixes include fine (powder) aggregates, ideal to penetrate the reinforcing fiber sheets when a sufficiently low viscosity matrix is used, and lend themselves to produce low-shrinkage matrices, thus providing dimensional stability. For both matrices, the ratio of liquid to powder weight was defined experimentally by trial-

and-error, where the desired outcome was to produce a matrix with a viscosity low enough to penetrate and permeate the reinforcing fibers, and high enough to hold the fiber reinforcement sheets in place onto the concrete substrate while curing, thus addressing constructability. Through this iterative process, a 27% water to powder weight and a 45% acrylic to powder weight ratios were selected for Type H and Type A matrices, respectively.

The cube compressive strength, f_m , and splitting tensile strength, σ_t , of the hardened matrices were determined according to ASTM C 109 [39] and ASTM D 3967 [40], respectively. The results are summarized in Table 1. For each property characterization, five samples were used that were cast from a single batch of either Type H or Type A mix, respectively, and tested after 28 days. All tests were performed using a servo-hydraulic frame under a displacement control rate of 0.64 mm/min. Type H had nearly 7 times the splitting tensile strength and over 12 times the cube compressive strength of Type A, failing in a brittle fashion, differently from the ductile behavior displayed by Type A, as shown Figure 2. The latter response is desirable in bond-critical applications (*e.g.*, flexural and shear strengthening) as it may accommodate interface slip and delay delamination [31], whereas it becomes less critical in confinement applications, which are contact-critical.

Reinforcing Fibers

Three different reinforcing fiber sheets were selected, whose properties are summarized in Table 2. Two are made of high-strength glass fibers, the first having a similar density

to the 600 g/m² fiber sheet density typically used in FRP confinement applications (525 g/m², denoted as “LDG”), and the second having a relatively high density (915 g/m², denoted as “HDG”), thus theoretically more difficult to impregnate with an inorganic matrix. The third reinforcement sheet is made of a hybrid fabric with basalt fibers, alkaline resistant (AR) glass fibers, and polyvinyl alcohol (PVA) fibers (42, 38 and 20% in weight, respectively), and has a density of 321 g/m² (denoted as “BGP”). Basalt fibers are produced from natural and readily available raw material, have mechanical properties that are similar to those of E-glass fibers, and superior thermal stability (in a range from – 260°C to 900°C), making them attractive for use as reinforcement in externally bonded composite systems [41][42].

Evaluation of Confinement Effectiveness

Compression tests on confined concrete cylinders, having diameter of 152 mm and height of 305 mm, were conducted to preliminarily evaluate the confinement effectiveness of the different fiber/matrix combinations. While this approach has limitations when enlisted to gain conclusive experimental evidence as opposed to laboratory tests on scaled or full-scale RC column specimens, it is suitable for the objectives at a material system developing stage, as reported in this study.

Test matrix

A total of 21 plain concrete cylinders were cast from a single batch of concrete, cured for 28 days, and configured per the notations in Table 3. Three unconfined cylinders, denoted as “Control”, were used as benchmark specimens. The remaining cylinders were

wrapped and identified using the “X-Y-Z” format in the first column of Table 3, where: “X” denotes the reinforcing fiber sheet (LDG, HDG or BGP); “Y” denotes the matrix (inorganic Type A, inorganic Type H, or organic Type E); and “Z” denotes the specimen number. A commercially available two-part epoxy resin (Type E) was used for the FRP confined cylinders to be used as benchmarks to the FRC cylinders. Two specimens were tested for each configuration. The organic matrix is reported to have a minimum specified tensile strength of 50 MPa, elongation of 2.5%, and compressive strength of 80 MPa, as per the manufacture’s specifications.

The mix design selected for Type H and Type A yielded inorganic matrices with adequate workability for easy application mimicking a conventional wet layup technique, and able to hold the fiber reinforcement sheets in place while curing, addressing the constructability concerns. The FRC confined cylinders were wrapped with two continuous plies of fiber reinforcement placed onto a layer of inorganic matrix that was applied over the concrete surface. A ribbed roller was used in the direction of the fibers to facilitate impregnation. After wrapping, the specimens were left to cure for 28 days at room temperature and humidity.

Test setup and instrumentation

All specimens were capped with a sulfur compound, and tested in uniaxial compression per ASTM C 39 [43] at a constant displacement rate of 0.5 mm/min. The test setup is illustrated in Figure 3. The axial load was measured continuously with a 890 kN-capacity donut-shaped load cell centered between the loading platen and a 25 mm thick

steel plate. The axial strain was measured at four locations, each at 90 degrees on the diametral plane, via PI-gauges mounted on the two yokes of a cast iron compressometer.

Results and FRC system selection

The compression test results are summarized in Table 3, including: strength (maximum stress), f_{cc} , and associated axial strain, ϵ_{cc} , where the maximum value measured with the four PI-gauges was considered; ratio of confined cylinder strength, f_{cc} , to average strength of unconfined cylinders, f_{co} , where the latter was measured at an average of 20.4 MPa; ratio of axial strain of a confined cylinder at maximum stress, ϵ_{cc} , to average axial strain of unconfined cylinders at maximum stress, ϵ_{co} , where the latter was measured at an average of 2,432 $\mu\epsilon$; ratio of average strength of two cylinders confined with a similar FRC system, $f_{cc,FRC}$, to average maximum strength of the two FRP confined counterparts, $f_{cc,FRP}$; and, ratio of average axial strain at maximum stress of two cylinders confined with a similar FRC system, $\epsilon_{cc,FRC}$, to average strain at maximum stress of the two FRP confined counterparts, $\epsilon_{cc,FRP}$. Representative axial stress-strain responses are provided in Figure 7(a), (b), and (c), for specimens confined with low density glass sheets, high density glass sheets, and hybrid basalt-glass-PVA sheets, respectively, along with that of a control specimen.

All the FRC confined cylinders experienced an increase in compressive strength and associated axial strain with respect to the control (unconfined) cylinders. When using LDG sheets with Type A and Type H matrices, strength increases up to 44 and 47%, and strain increases up to 288 and 240% were attained, respectively; with HDG sheets,

strength increases up to 23 and 56%, and strain increases up to 738 and 351% were attained, respectively; and with BGP sheets, strength increases up to 43 and 61%, and strain increases up to 12 and 213% were attained, respectively. Therefore, Type H matrix consistently resulted in larger strength increases, irrespective of the fiber reinforcement, whereas neither inorganic matrix neatly outperformed the other in terms of axial deformability.

For all the FRC confined cylinders, failure occurred because of progressive loss of compatibility in the composite jacket due to the separation between inorganic matrix and fiber reinforcement, sometimes associated with rupture of the reinforcing fibers, as shown in the photographs in Figure 4. These failure mechanisms result in axial stress-strain curves where the axial deformation may develop past the point of maximum stress, thus differently from the typical brittle failures encountered when using FRP jackets. Failure resulting from the separation between matrix and fiber reinforcement is attributed to the poor impregnation of the fibers in the LDG, HDG and BGP sheets, as observed using a scanning electron microscope. Figure 5(a) and Figure 5(b) show representative SEM images taken from failed concrete cylinders confined using LDG fiber sheets with Type A and Type H matrix, respectively. It is evident that the inorganic matrices did not effectively penetrate and impregnate the fiber reinforcement, resulting in distinguishable fiber sheet and matrix layers, whereas good compatibility was achieved between inorganic matrices and concrete substrate, as illustrated in the SEM image in Figure 6, where a sound concrete-FRC interface developed. The ineffective fiber impregnation justifies the weaker performance of the high density glass (HDG) fiber sheets compared

to the lower density glass (LDG) and basalt/glass/PVA (BGP) sheets, since higher axial strength levels should be expected as a result of the larger amount of reinforcing fibers in the hoop direction.

For all cylinders confined using epoxy-based (Type E matrix) FRP laminates, a higher level of confinement effectiveness was reached with respect to the Type A and Type H counterparts, as seen from the values of both the maximum stress ratio ($f_{cc,FRC}/f_{cc,FRP}$) and the corresponding strain ratio ($\epsilon_{cc,FRC}/\epsilon_{cc,FRP}$) reported in Table 3. The superior strength and deformability attained with the FRP jacket is attributed to the higher tensile strength and ultimate strain of Type E matrix (50 MPa and 2.5%, respectively), coupled with an optimal fiber impregnation. In fact, the FRP confined cylinders exhibited greater axial stiffness upon engagement of the composite jacket following lateral concrete expansion (Figure 7); failure always occurred in a brittle fashion because of fiber rupture; and, on average, larger strength levels were attained when using the HDG sheets, which provided greater laminate stiffness and strength.

On average, the hydraulic cement-based (Type H) matrix allowed to attain a compressive strength of 82, 73 and 95% of that of the Type E counterparts with LDG, HDG and BGP fiber sheets, respectively. Despite the poor fiber impregnation (Figure 5(b)), this performance attests to the ability of the prototype Type H matrix to engage the reinforcing fibers, and produce significant strength increase. While the HDG sheets underperformed the LDG and the BGP sheets, the lower density of the BGP sheets did not result in a more efficient FRC system compared to the LDG sheets, which are

representative of systems with fiber density of about 600 g/m^2 typically used in FRP confinement applications. Therefore, a similar FRC composite to that with Type H matrix and LDG sheets was selected for the second part of this research, which is reported in the next section.

CHARACTERIZATION AND ASSESSMENT OF FRC SYSTEM

In this phase, the characterization of the selected FRC system was evaluated by testing FRC flat coupons in direct tension, while additional FRC confined concrete cylinders were tested in uniaxial compression to: a) determine fundamental tensile composite properties including ultimate tensile strength, strain, and tensile chord modulus of elasticity; b) provide statistically meaningful results to evaluate confinement effectiveness in terms of strength and deformability (including axial and volumetric strain); c) assess increases in strength and deformability with respect to the amount of external reinforcement increasing by using three different FRC reinforcement ratios (one, two, and four plies); and, d) investigate the feasibility of making composite jacketing reversible by introducing a bond breaker between the concrete and the FRC jacket. The candidate FRC system included Type H inorganic matrix, and a high-strength glass fiber sheet typically used in FRP confinement applications, having tensile strength of 3,399 MPa, modulus of elasticity of 76.9 GPa, ultimate elongation of 4.4%, and density of 596 g/m^2 .

Test Matrix and Setup

FRC coupons were prepared according to ASTM D 3039 [44] following a wet-layup technique on a flat horizontal plane, using a two-part sandwich panel mold with non-stick surfaces with overall dimensions 500 mm width by 330 mm length (in the fiber direction). The FRC panel was release from the mold after curing for 7 days and a total of 15 flat coupons, five individual coupons for each reinforcement ratio, were cut by means of a water-lubricated precision diamond circular saw to the final dimensions specified in Figure 8. The overall coupon thickness, t , as seen in Figure 9 was controlled with shim stock equivalent to 3.81, 6.35 and 11.43 mm corresponding to one, two, and four plies, respectively. All coupons were bonded with aluminum tabs using a two-part epoxy to ensure even stress distribution during testing. Direct tensile testing of flat coupons was undertaken according to ASTM D3039 [44] at a constant head displacement rate of 0.025 mm/min using a servo hydraulic MTS testing machine. A constant pressure of 5.2 MPa was applied onto the aluminum tabs with wedge-type hydraulic grips, and the load was constantly measured via an internal 100 kN capacity load cell. Strains were obtained using an extensometer with gage length of 40 mm; Figure 10 illustrates the test setup.

A total of 22 plain concrete cylinders having diameter of 152 mm and height of 305 mm were cast from a single batch of concrete, and cured for 28 days. Four cylinders were used as control specimens. Three cylinders were confined using the selected FRC system with one ply of reinforcing fibers (ensuring an overlap length of 100 mm), six cylinders with two plies, and three cylinders with four plies. The remaining six cylinders were

confined with two plies of reinforcing fibers, where the FRC jacket was applied onto a wax-based bond breaker to facilitate removal, aiming at ensuring reversibility. All specimens were capped with a sulfur compound, and tested in uniaxial compression per ASTM C 39 [43] at a constant displacement rate of 0.5 mm/min. In order to enable estimating the volumetric strain, in addition to the setup implemented in the previous phase of this research, in-plane (radial) deformations were measured at the mid-height section of each specimen at four points, each at 90 degrees on the diametral plane, using high-accuracy displacement transducers mounted on the bottom yoke of the compressometer using aluminum L-brackets, as shown in Figure 3.

Results and Discussion

Direct tensile characterization

The results for the direct tensile characterization of the proposed FRC system are summarized in Table 4, including the ultimate tensile strength, f_{tu} ; ultimate tensile strain, ϵ_{fu} ; and the tensile chord modulus E^{chord} computed according to ASTM 3039 between the longitudinal strain range starting and ending at 1000 and 3000 $\mu\epsilon$, respectively. The average, standard deviation (SD), and coefficient of variance (CV) for the aforementioned values based on five specimens per coupon design are also provided. Samples are labeled “2P-A to -E” and “4P-A to -E” for two- and four-ply coupons. No results were obtained for one-ply coupons since test samples failed prematurely.

Tested samples followed a bilinear trend, with the first branch finishing at approximately 500 $\mu\epsilon$, followed by the second branch with a lower gradient ending at failure, as

illustrated in Figure 11 – Axial stress–strain envelope for tensile coupon tests for:, which shows the axial stress-strain envelope (max – min) response for the coupons. It is assumed that the first segment of the graph corresponds mainly to matrix cracking, and as the axial load increases more cracks are created and existing ones propagate, hence reducing the stiffness of the composite until the a point where all the matrix is fully cracked. At this point, the fibers must carry the full tensile load of the FRC composite as observed from the constant linear slope. CV values for the stress and strain measurements varied from 9.5 to 20.4%, which are typical levels for testing of material properties [45]. While the average E^{chord} values were similar for 2- and 4-ply coupons, at 12.96 to 11.87 GPa, respectively, the predominant lateral failure type was not valid as it was located inside the grip/tap (LIT or LIB failure mode codes per ASTM D3039) as seen in Figure 12. Fiber rupture was never reached indicative that FRC samples were partially loaded to similar levels for different number of plies, not engaging to ultimate capacity. This was probably caused in part due to the poor fiber impregnation, nonetheless the limited load transfer from the hydraulic grips to the fibers through the cracked matrix also seems to be an important factor during the test procedure to determine the material properties.

Therefore, the method by which the coupon samples were tested [44] is oriented towards composites where the strain capacity of the matrix is much higher than that of the reinforcing fibers, allowing for good load transfer through the hydraulic wedge-grips. This is not the case for brittle inorganic-based composites, such as the FRC system, where the contribution of the matrix in tension is negligible, and cracks create a non-

direct load path to the fibers. Based on the consistent non valid failure mode, the existing characterization methodology as a means to determine ultimate tensile capacity of FRC coupons is inconclusive.

Confinement tests

The results of the compression tests are summarized in Table 5. The specimens with one-, two-, and four-ply of bonded FRC reinforcement are labeled as “1B-1 to -3”, “2B-1 to -6”, and “4B-1 to -3”, respectively. The specimens with two plies of unbonded FRC reinforcement are labeled as “2U-1 to -6”. The following data is provided: compressive strength (maximum stress), f_{cc} ; associated axial strain, ϵ_{cc} , where the maximum value measured with the four PI-gauges was considered; ratio of confined cylinder strength, f_{cc} , to average strength of plain concrete cylinders, f_{co} , where the latter was measured at an average of 21.7 MPa; and, ratio of axial strain of a confined cylinder at maximum stress, ϵ_{cc} , to average axial strain of plain concrete cylinders at maximum stress, ϵ_{co} , where the latter was measured at an average of 2,540 $\mu\epsilon$. The strain measurements for specimens 2B-5, 4B-1 and 4B-2 are not included since the compressometer apparently moved during the tests, making the deformation measurements invalid. The experimental results in Table 5 are discussed in the next three sections with respect to the influence of the amount of FRC reinforcement, the influence of a bond breaker at the concrete-FRC interface, and the failure mode and reversibility.

Influence of amount of FRC reinforcement

Concrete confinement with a bonded FRC jacket produced an average axial strength

increase ranging from 21% with one ply of fiber reinforcement, to 64% with two plies, to 121% with four plies, respectively. The axial strength enhancement increased linearly with the amount of FRC reinforcement, and thus confinement effectiveness was not reduced when using four plies of reinforcing fibers. This is shown in Figure 13 (a), where the values of the strengthening ratio, f_{cc} / f_{co} , are plotted for the bonded specimens with respect to a measure of the stiffness of the confinement system, given by the product of the longitudinal elastic modulus of the fiber reinforcement, E_f (equal to 76.9 GPa), times the FRC reinforcement ratio, ρ_f , determined as:

$$\rho_f = \frac{4n_p t_f}{D} \quad (1)$$

where n_p is the number of plies of fiber reinforcement, t_f is the thickness of one ply of fiber reinforcement (0.246 mm), and D is the diameter of the concrete cylinder. The value of $E_f \rho_f$ is 496.5, 993.0, and 1,986.1 MPa for the one-, two-, and four-ply system, respectively. The linear trend is marked by the dashed line in Figure 13 (a), with a coefficient of determination R^2 equal to 0.93.

The average increase in axial strain at maximum stress ranged from 34% with one ply of fiber reinforcement, to 333% with two plies, to 115% with four plies (although based on specimen 4B-3 only). Figure 13 (b) shows the values of the ratio $\varepsilon_{cc} / \varepsilon_{co}$ plotted with respect to $E_f \rho_f$. The lesser consistency of confinement effectiveness in terms of deformability enhancement ($R^2 = 0.45$ for the dashed linear trend) is attributed to the

peculiar failure mechanism, consisting in all cases of progressive separation between the brittle inorganic matrix and the fiber reinforcement, similar to that noted in the feasibility study, where the location and extent of damage may significantly change among different specimens.

Influence of bond breaker at concrete-FRC interface

The use of an unbonded FRC jacket allowed the cylinders confined with 2 plies of reinforcement (specimens 2U-1 to -6) to reach a strength increase ranging from 41 to 81%, similar to the bonded counterparts (specimens 2B-1 to -6). The associated axial strain increased between 44 and 278%, thus significantly higher than the unconfined cylinders, but substantially below the level of the bonded counterparts.

Representative axial stress-strain responses are provided in Figure 14 (a) for confined cylinders with bonded (B) and unbonded (U) FRC jacket, along with that of a control specimen. While similar strength levels were attained, the deformability response was different. Stiffness loss occurred gradually in the bonded specimens, reflecting a progressive engagement of the FRC jacket as a result of concrete cracking and volume expansion. The unbonded specimens showed earlier stiffness loss, which was recovered upon engagement of the composite jacket as the axial stress approached its maximum value, accompanied by volume expansion. This behavior indicates that the presence of a sound, bonded concrete-FRC interface (as seen in Figure 6) ensures better contact between substrate and jacket, and results in a more efficient and reliable transfer of the hoop stresses and improved deformability. In fact, as reported in Table 5, the bonded

specimens reached the maximum stress on average at an axial strain of 11,018 $\mu\epsilon$, which is about 74% larger than the average of 6,324 $\mu\epsilon$ for the unbonded specimens. Yet, despite such difference in axial strain at maximum stress, the standard deviation of the values for the six unbonded specimens exceeds that for the six bonded counterparts. The lesser deformability performance in unbonded specimens is relevant and warrants additional research, particularly when investigating FRC systems for seismic retrofit applications, since deformability enhancement under lateral loads depends on the ability to develop greater axial strains in the concrete before compressive failure [10].

Confinement effectiveness in enhancing deformability was also assessed by analyzing the volumetric strain response, where volumetric strain is computed as the sum of the axial strain measured with the PI-gauges, and the two transverse (in-plane) strains measured with the four displacement transducers shown in Figure 3. Unconfined concrete under uniaxial load contracts in volume up to about 90% of the compressive strength; past this level, volume change reverses resulting in inelastic expansion till compressive strength is reached, followed by more rapid volume expansion as the softening branch develops and failure occurs [46]. Effective confinement curtails unstable crack growth by constraining volume expansion, thereby allowing larger deformations [47]. For the case of FRC confinement, this is illustrated in Figure 14 (b), which provides representative axial strain-volumetric strain responses of a bonded and an unbonded specimen. The initial slope of the curves is similar to $(1-2\nu)$, where a value of 0.20 is assumed for the Poisson's ratio of the concrete, indicating an elastic response. As the maximum axial stress is reached, the curves deviate from linearity till volume change reverses, which

occurs under larger deformations for the bonded specimens, for which the volumetric strain is consistently larger than that of the unbonded specimens at similar axial strain levels. In both cases, the development of the curve past the volumetric strain peak indicates the effect of the FRC confinement in delaying unstable crack growth, with a superior performance of the bonded configuration.

Failure mode and reversibility

For all specimens, failure occurred due to separation between glass fibers and Type H matrix, typically combined with tearing of fibers by concrete fragments as the concrete cylinder expanded in volume. The photographs in Figure 15 show an FRC jacket removed from a specimen where a bond breaker was used. It can be seen that the FRC system could be completely detached from the concrete core, making the use of a bond breaker a promising approach to ensure reversibility. However, post failure examination of all bonded and unbonded specimens also confirmed that the cement-based matrix did not effectively penetrate the glass fibers, resulting in a clean separation between reinforcing fibers and layers of inorganic matrix, as shown in Figure 15 (b). Fiber impregnation needs to be addressed to improve fiber-matrix compatibility, with the objective to more efficiently use the FRC constituent materials, and enable larger increases in strength and deformability.

SEMI-EMPIRICAL AXIAL STRENGTH-STRAIN MODEL

The axial strength, f_{cc} , and associated axial strain, ε_{cc} , of confined concrete are typically modeled as functions of the confining pressure exerted by the external jacket, f_{lu} , using the following model algorithms [36][48]:

$$\frac{f_{cc}}{f_{co}} = 1 + k_1 \left(\frac{f_{lu}}{f_{co}} \right)^m \quad (2)$$

$$\varepsilon_{cc} = \varepsilon_{co} + k_2 \left(\frac{f_{lu}}{f_{co}} \right)^n \quad (3)$$

where k_1 , k_2 , m , and n are empirical constants, and f_{lu} is given as

$$f_{lu} = \frac{2E_f \varepsilon_{lu} t_f n_p}{D} \quad (4)$$

where ε_{lu} is the average hoop strain in the external reinforcement associated with the maximum compressive stress in the confined concrete.

For the bonded specimens in Table 5 (except 2B-5, 4B-1 and 4B-2, for which deformation measurements are not available), the values of strengthening ratio, f_{cc} / f_{co} , and axial strain at maximum axial stress, ε_{cc} , are plotted in Figure 16 and Figure 17, respectively, against the ratio of confining pressure, f_{lu} , to compressive strength of unconfined concrete, f_{co} . The confining pressure is computed per Equation (4), where the average hoop strain in the FRC reinforcement is determined based on the larger radial deformations measured along the two in-plane orthogonal directions. Assuming linear relations in Equations (2) and (3), and thus having $m = n = 1$ as often proposed in the literature [48], the empirical constants k_1 and k_2 are determined via best fitting as 3.34 (R^2

= 0.65) and 0.031 ($R^2 = 0.18$), respectively, reflecting the more variable strain results as previously discussed. While the values of the empirical constant are based on a limited number of experiments, especially for the four-ply configuration, it is noted that they are in good agreement with preliminary estimates proposed for a different fiber reinforced composite system with a cement-based matrix ($k_1 = 3.45$ and $k_2 = 0.026$, respectively) [38].

The model accuracy may be improved assuming nonlinear relations in Equations (2) and (3), with $m = n \neq 1$. Numerical optimization of the empirical constants yields the nonlinear curves in Figure 16 and Figure 17, where $m = n = 0.775$, and k_1 and k_2 are determined via best fitting as 2.87 ($R^2 = 0.90$) and 0.046 ($R^2 = 0.56$), respectively, with a good correlation with the axial strength results. It is emphasized that the semi-empirical models presented are supported by a limited number of experimental results, and further research is needed to refine and verify their formulations.

CONCLUSIONS

In the first part of this study, the experimental research led to the selection of a candidate FRC composite system made of glass fiber sheets with density of 600 g/m^2 as in standard FRP confinement applications, and a hydraulic cement-based matrix, for use in fire-resistant concrete confinement applications. The confinement effectiveness of six different inorganic matrix composites was evaluated based on the results of uniaxial compression tests on confined concrete cylinders, which concluded the following:

1. The selected configurations allowed attaining substantial increases in axial strength and deformability with respect to unconfined cylinders.
2. Poor fiber impregnation was achieved, as documented in scanning electron microscope images of specimens, leading to premature failure because of fiber-matrix separation.
3. The results support the feasibility of using basalt fibers as reinforcement in composite jackets.

The direct tensile characterization and additional compression tests on plain concrete cylinders were conducted in the second part of this study, using the selected inorganic matrix-glass fiber composite system. The objectives were to determine fundamental FRC material properties; provide statistically meaningful results to evaluate confinement effectiveness, to study the influence of the amount of external reinforcement; and to investigate the use of a bond breaker for reversibility. Based on the results, the following conclusions were reached:

1. Composites with brittle matrices were not adequately characterized with the existing direct tensile flat coupon test methodology.
2. Strength increased linearly throughout the entire range of reinforcement amount tested.
3. Full reversibility was achieved using a wax-based bond breaker prior installation of the FRC jacket.

4. FRC bonded and unbonded specimens reached similar strength levels suitable for concrete confinement.
5. The bonded interface was more effective in ensuring intimate contact between concrete substrate and composite jacket, resulting in a superior and more reliable increase in deformability.
6. The predominant failure mode for the bonded and unbonded specimens was loss of compatibility in the external reinforcement due to fiber-matrix separation.

Semi-empirical models to estimate axial strength and deformation increase for confinement of concrete were also evaluated, showing good agreement with a model previously proposed for an inorganic-matrix fiber reinforced confinement system [38].

FURTHER RESEARCH

While the proposed approach to ensure reversibility of the FRP system is effective, further research is needed to investigate reversible systems that minimize tradeoffs in deformability, particularly for seismic retrofit applications. Additionally, though the FRC candidate system shows promise based on strength and deformability enhancement when compared to a FRP counterpart, it is recognized that fiber impregnation needs to be improved to more efficiently use the constituent materials.

The models presented to estimate axial strength and deformation increase from confinement are based on a limited number of test results, and further research is needed

for their refinement and verification. Moreover, tensile characterization of the developed FRC composite is fundamental to develop more accurate models. Given that current test methods provide inconclusive material properties, new test methods should be investigated to characterize composites with brittle-matrices, where a plausible test methodology is presented and discussed in Study 3.

Table 1 – Mechanical properties of inorganic cement-based matrices.

Matrix type	Average* splitting tensile strength, σ_t (MPa)	Standard deviation* for σ_t (MPa)	Average* cube compressive strength, f_m (MPa)	Standard deviation* for f_m (MPa)
Type H	1.36	0.17	31.1	2.1
Type A	0.20	0.01	2.49	0.20

* Based on results from five samples per matrix type.

Table 2 – Reinforcing fiber sheet properties used for preliminary FRC material selection.

Fiber sheet type	LDG	HDG	BGP (basalt/glass/PVA)
Tensile strength* (MPa)	3240	3240	4840 / 3400 / 1600
Tensile modulus* (GPa)	72.4	72.4	89.0 / 77.0 / 40.0
Ultimate elongation* (%)	4.5	4.5	5.4 / 4.4 / 4.0
Density (g/m ²)	525	915	321

* Property of dry fiber.

Table 3 – Results of compression tests for preliminary evaluation
of confinement effectiveness.

Specimen ID	f_{cc} (MPa)	ϵ_{cc} ($\mu\epsilon$)	$\frac{f_{cc}}{f_{co}}$	$\frac{\epsilon_{cc}}{\epsilon_{co}}$	$\frac{f_{cc,FRC}}{f_{cc,FRP}}$	$\frac{\epsilon_{cc,FRC}}{\epsilon_{cc,FRP}}$
Control*	20.4*	2,432*	1.00	1.00	-	-
LDG-A-1	29.4	9,446	1.44	3.88	0.73	0.37
LDG-A-2	24.3	8,510	1.19	3.50		
LDG-H-1	30.0	8,265	1.47	3.40	0.82	0.35
LDG-H-2	30.0	7,457	1.47	3.07		
LDG-E-1	34.1	20,340	1.67	8.36	1.00	1.00
LDG-E-2	39.3	25,170	1.93	10.35		
HDG-A-1	25.1	6,597	1.23	2.71	0.60	0.86
HDG-A-2	23.9	20,373	1.17	8.38		
HDG-H-1	31.9	4,111	1.56	1.69	0.73	0.48
HDG-H-2	28.1	10,974	1.38	4.51		
HDG-E-1	37.6	13,711	1.85	5.64	1.00	1.00
HDG-E-2	44.0	17,749	2.16	7.30		
BGP-A-1	28.5	N/A**	1.40	N/A**	0.86	0.15
BGP-A-2	29.1	2,718	1.43	1.12		
BGP-H-1	32.9	7,608	1.61	3.13	0.95	0.38
BGP-H-2	30.7	5,998	1.50	2.47		
BGP-E-1	36.6	17,022	1.80	7.00	1.00	1.00
BGP-E-2	30.4	18,390	1.49	7.56		

* For unconfined (Control) specimens, value of maximum stress, f_{co} , and associated strain, ϵ_{co} , are average of three specimens.

** Measurement not available (N/A); values from specimen BGP-A-2 only were considered.

Table 4 – Results of direct tensile characterization of FRC flat coupons.

Coupon ID	f_{fu} (MPa)	ε_{fu} ($\mu\varepsilon$)	E^{chord} (GPa)
2 plies			
2P-A	61.94	4838	16.49
2P-B	60.95	6718	10.17
2P-C	62.65	5348	14.48
2P-D	50.57	4809	12.52
2P-E	53.43	5187	11.16
AVERAGE	57.91	5380	12.96
SD	5.52	782	2.55
CV (%)	9.53	14.54	19.64
4 plies			
4P-A	38.25	3978	11.11
4P-B	60.45	5726	12.06
4P-C	55.06	4630	13.34
4P-D	47.14	4508	11.46
4P-E	38.92	3629	11.38
AVERAGE	47.97	4494	11.87
SD	9.79	799	0.89
CV (%)	20.40	17.77	7.51

Table 5 – Results of compression tests for assessment of bonded
and unbonded FRC system.

Specimen ID	f_{cc} (MPa)	ϵ_{cc} ($\mu\epsilon$)	$\frac{f_{cc}}{f_{co}}$	$\frac{\epsilon_{cc}}{\epsilon_{co}}$
1 ply, bonded				
1B-1	26.8	3,307	1.24	1.30
1B-2	24.5	3,305	1.13	1.30
1B-3	27.6	3,603	1.27	1.42
Average	26.3	3,404	1.21	1.34
2 plies, bonded				
2B-1	33.1	11,451	1.53	4.50
2B-2	36.9	8,558	1.70	3.37
2B-3	33.0	14,441	1.52	5.68
2B-4	32.3	8,900	1.49	3.50
2B-5	40.4	N/A	1.86	N/A
2B-6	37.4	11,739	1.72	4.62
Average	35.5	11,018	1.64	4.33
Standard deviation	3.2	2,396	0.15	0.94
2 plies, unbonded				
2U-1	35.0	4,024	1.61	1.58
2U-2	33.1	3,652	1.53	1.44
2U-3	31.5	6,035	1.45	2.38
2U-4	39.2	9,592	1.81	3.78
2U-5	34.1	9,246	1.57	3.64
2U-6	30.7	5,397	1.41	2.12
Average	33.9	6,324	1.56	2.49
Standard deviation	3.0	2,553	0.14	1.01
4 plies, bonded				
4B-1	48.6	N/A	2.24	N/A
4B-2	47.9	N/A	2.21	N/A
4B-3	47.2	9,798	2.18	3.86
Average	47.9	9,798	2.21	2.15



(a)



(b)

Figure 2 – Failed inorganic matrix cube compression specimens:

Type A (a) and Type H (b).



Figure 3 – Setup for concrete cylinder compression tests.

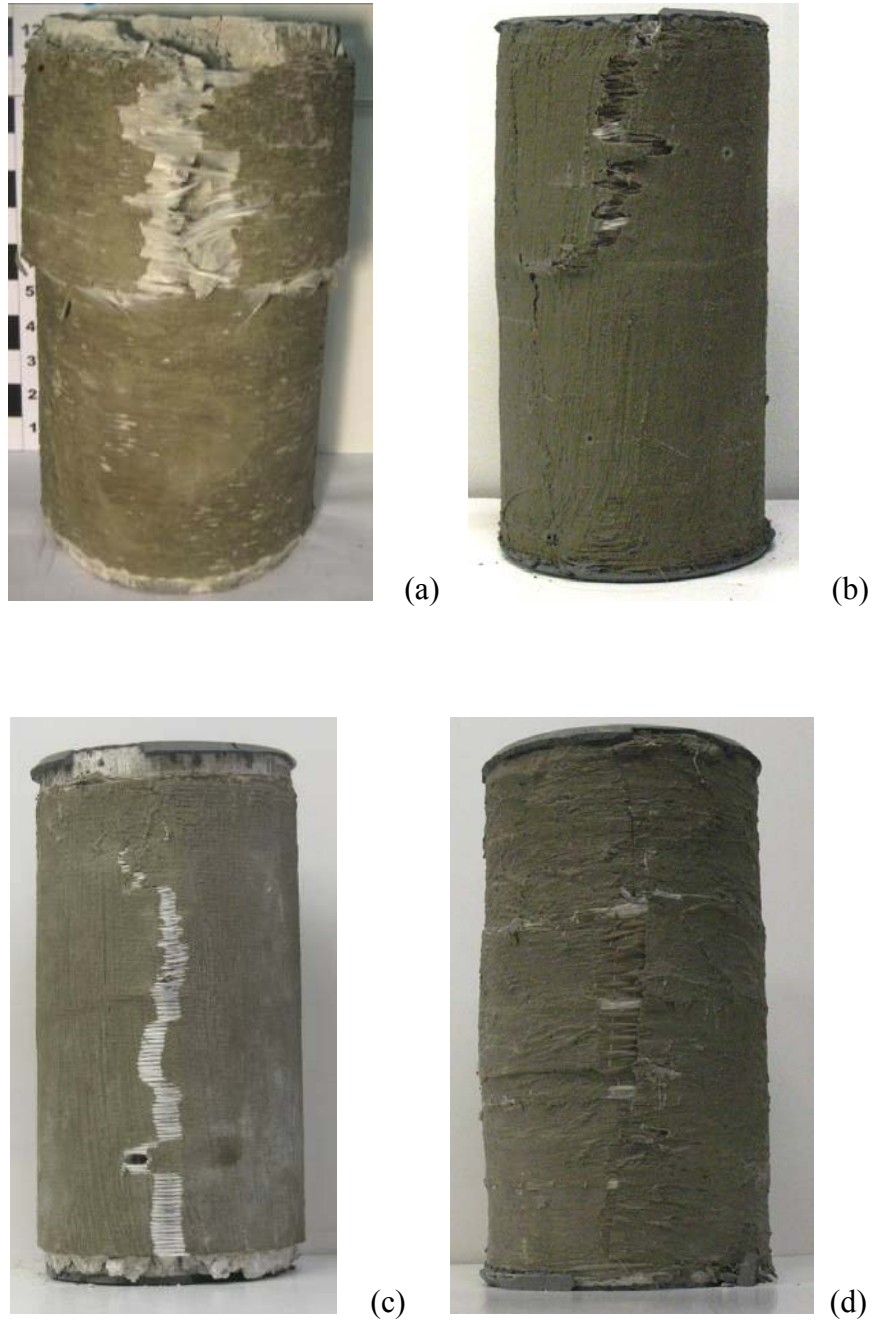


Figure 4 – Failure mode of FRC confined cylinders: predominant fiber rupture in specimen HDG-H-2 (a) and BGP-A-1 (b); and predominant fiber-matrix separation in specimen LDG-A-1 (c) and BGP-H-1 (d).

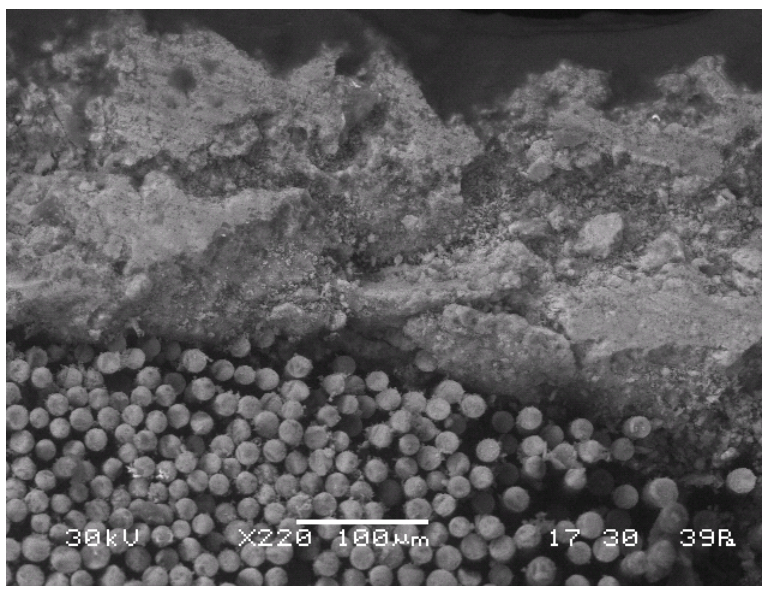
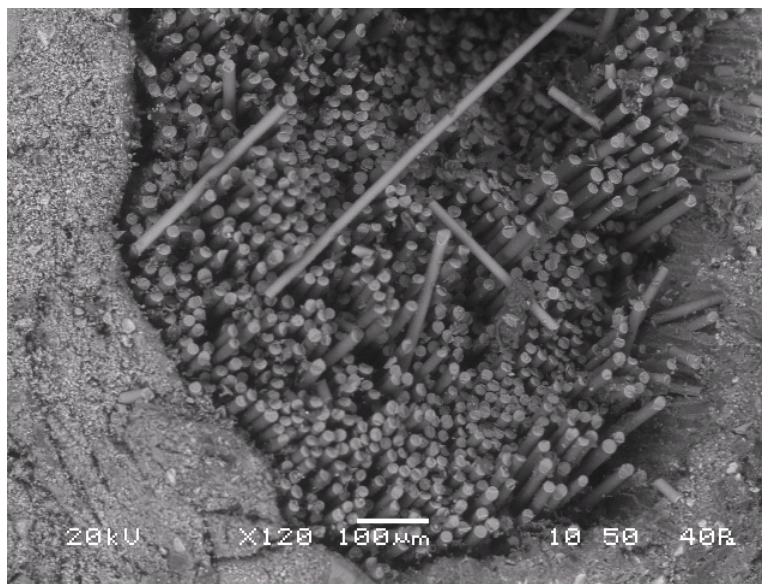


Figure 5 – Representative SEM image of FRC composite in failed concrete cylinder confined using LDG fiber sheets with Type A (a) and Type H (b) matrix.

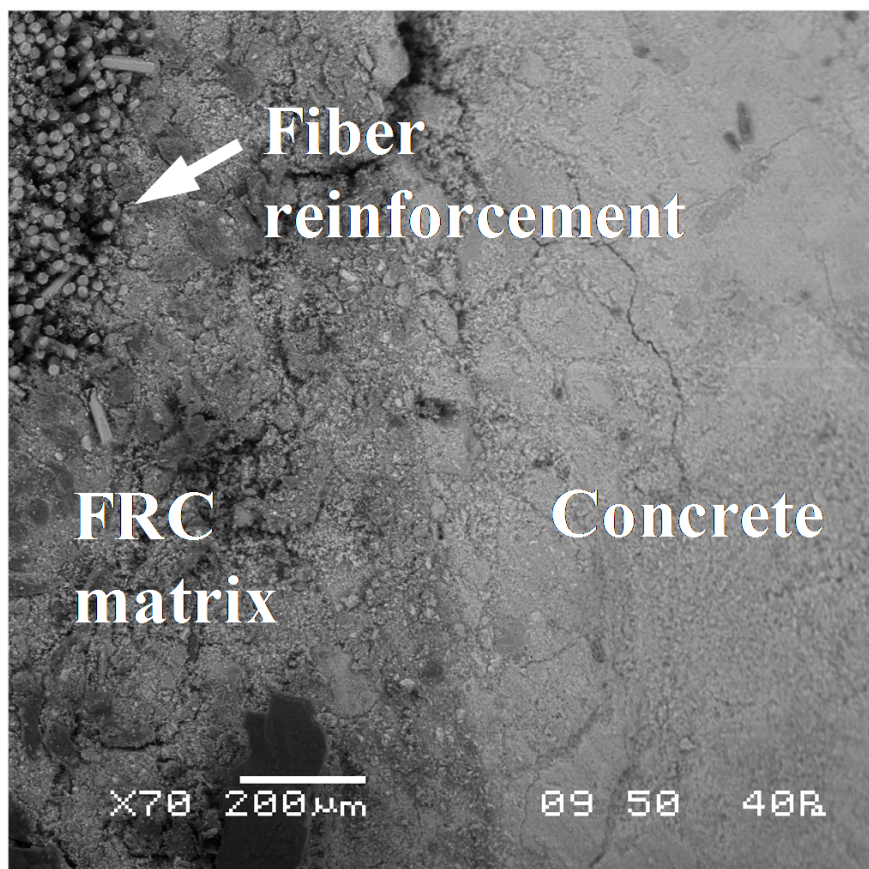
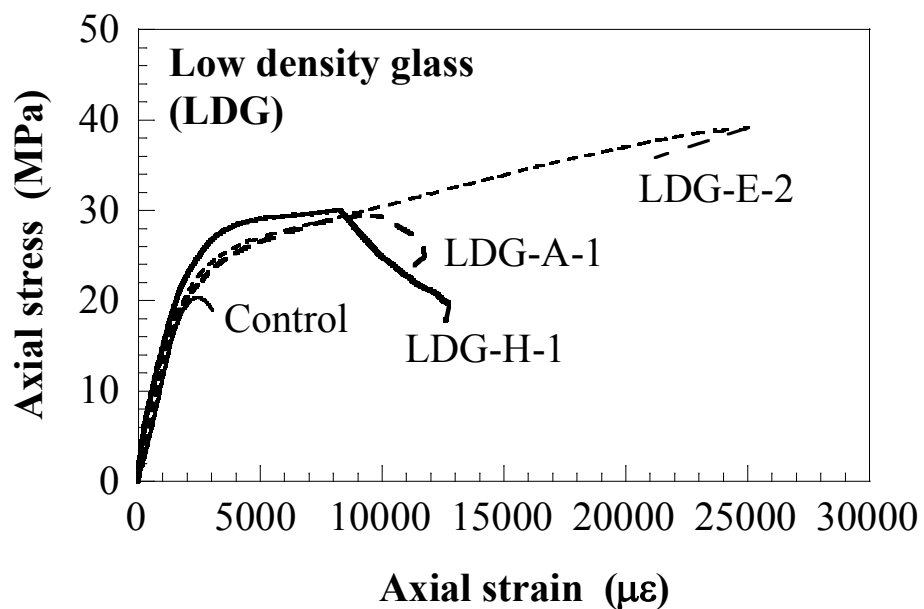
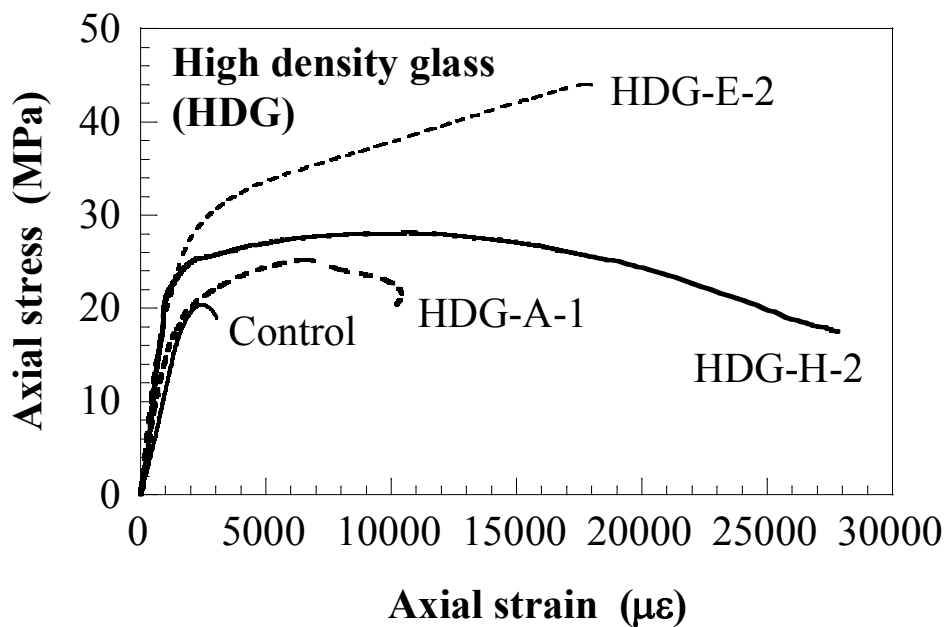


Figure 6 – Representative SEM image of interface between inorganic matrix Type A (left) and concrete substrate (right) in failed confined concrete cylinder.



(a)



(b)

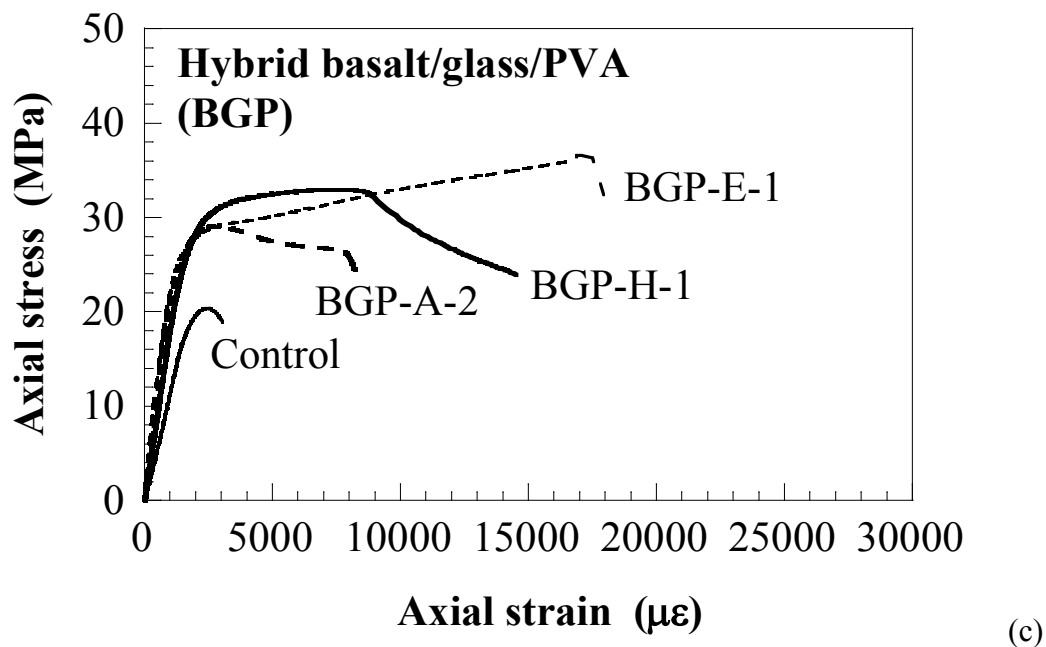


Figure 7 – Axial stress-strain response of representative concrete cylinder specimens in compression: confined with low density glass (LGD) sheets (a); confined with high density glass (HDG) sheets (b); and confined with hybrid basalt/glass/PVA sheets (c).

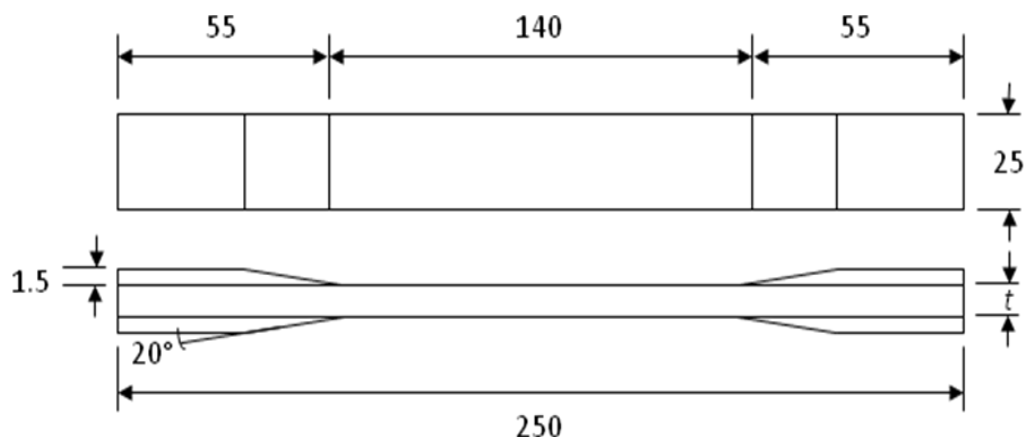


Figure 8 – FRC flat coupon drawing (dimensions in mm).

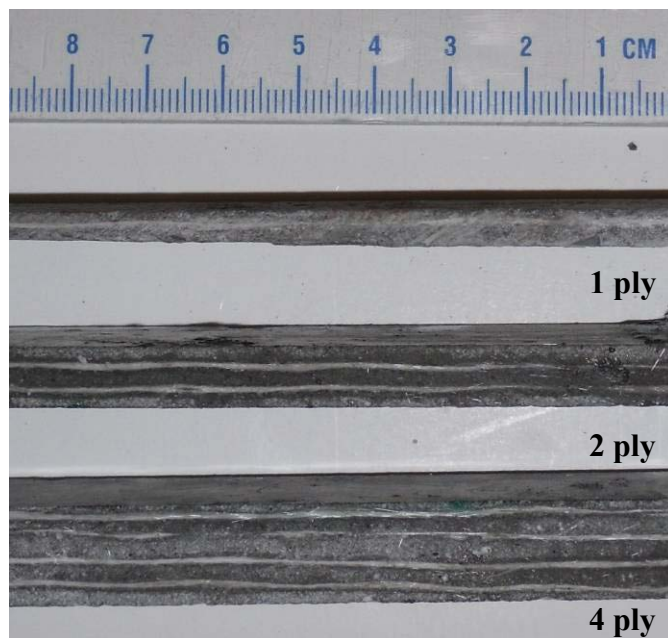


Figure 9 – FRC coupon longitudinal section, showing thickness and fiber/matrix layers for different number of plies.

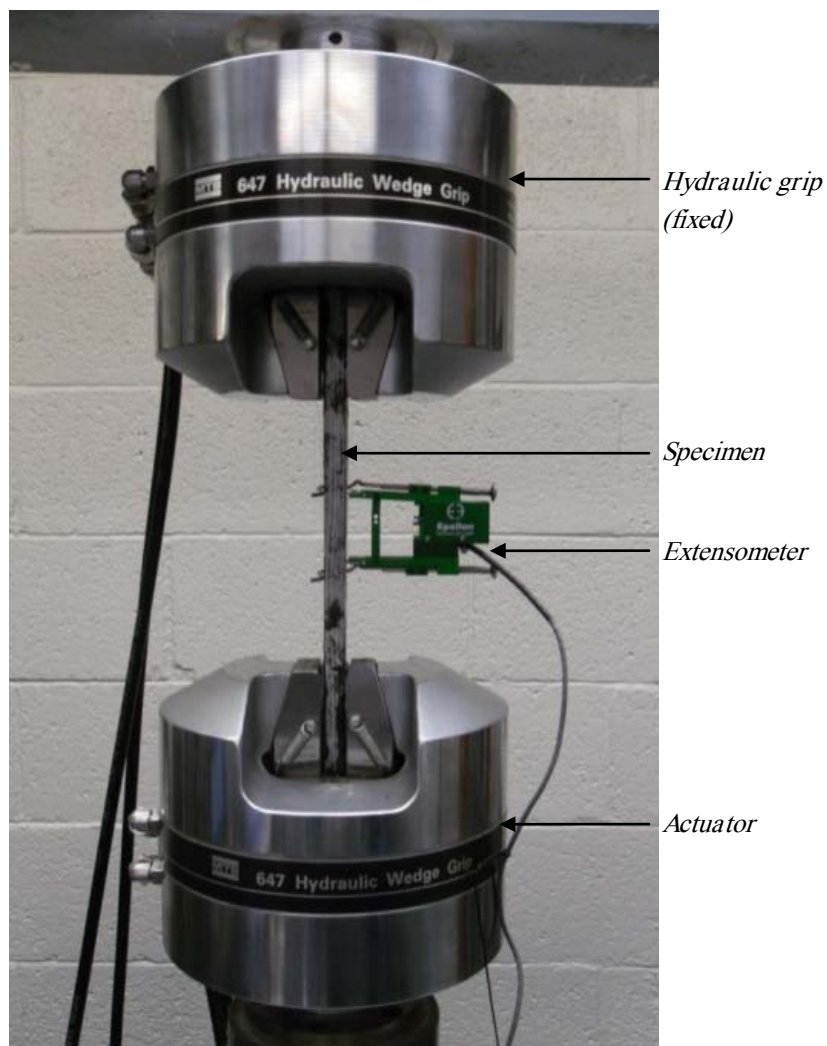


Figure 10 – Test set up for direct tensile testing of flat FRC coupons.

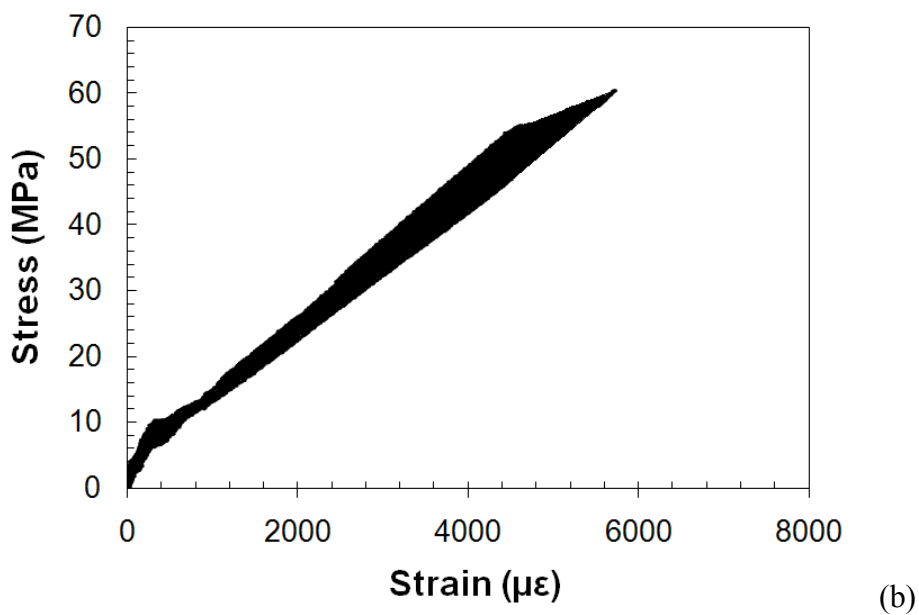
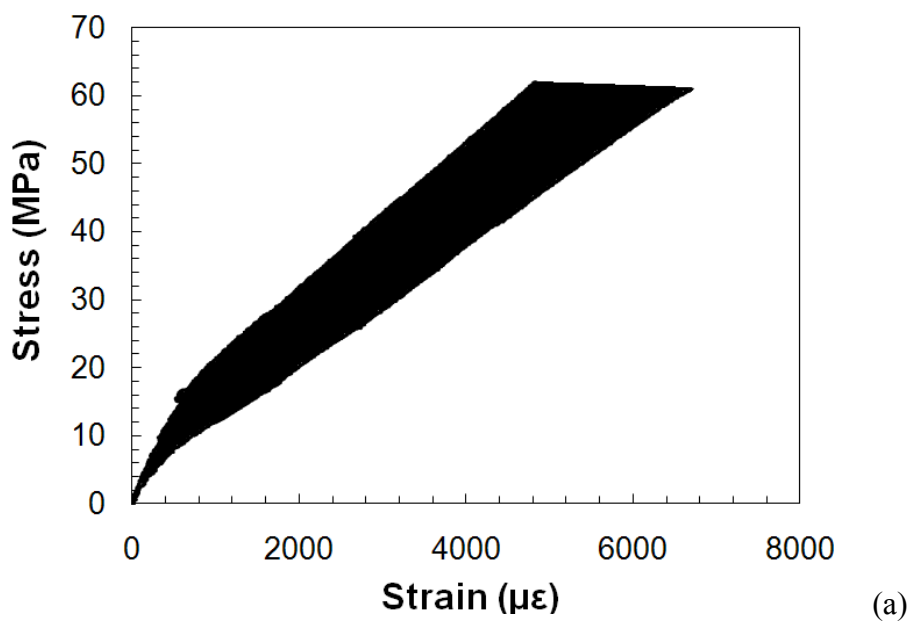


Figure 11 – Axial stress–strain envelope for tensile coupon tests for:
2 plies (a) and 4 plies (b).

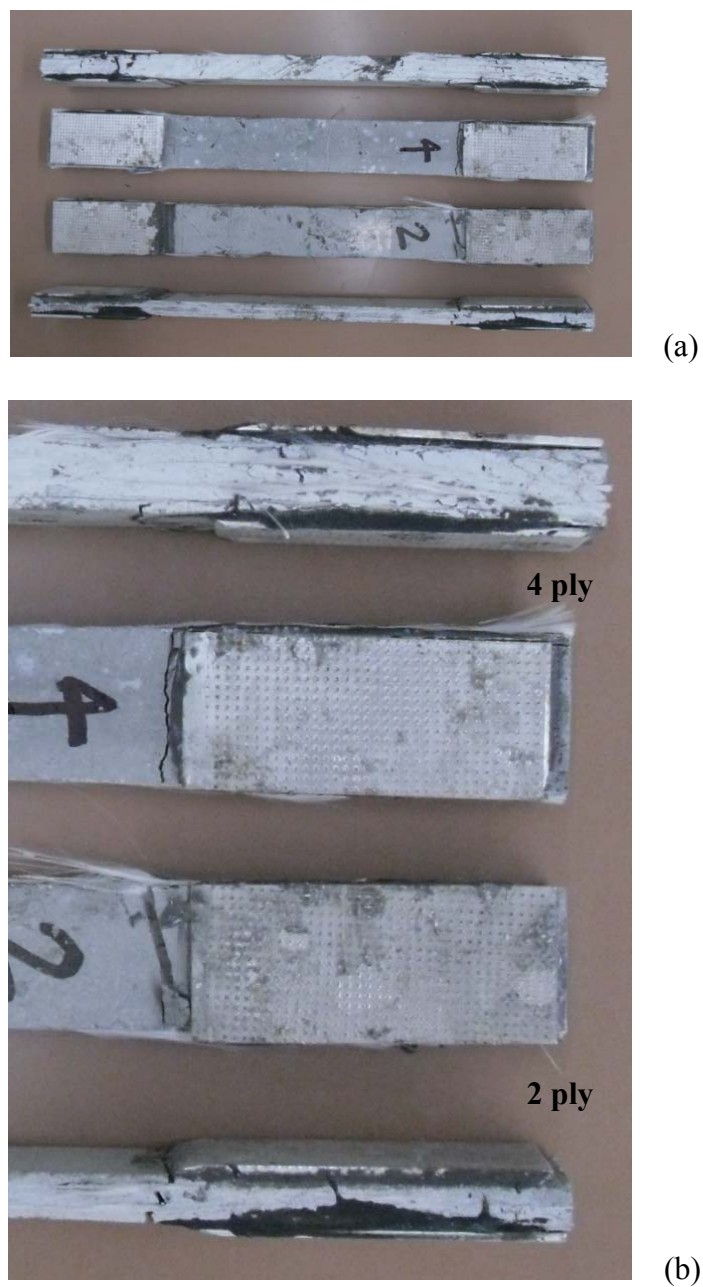
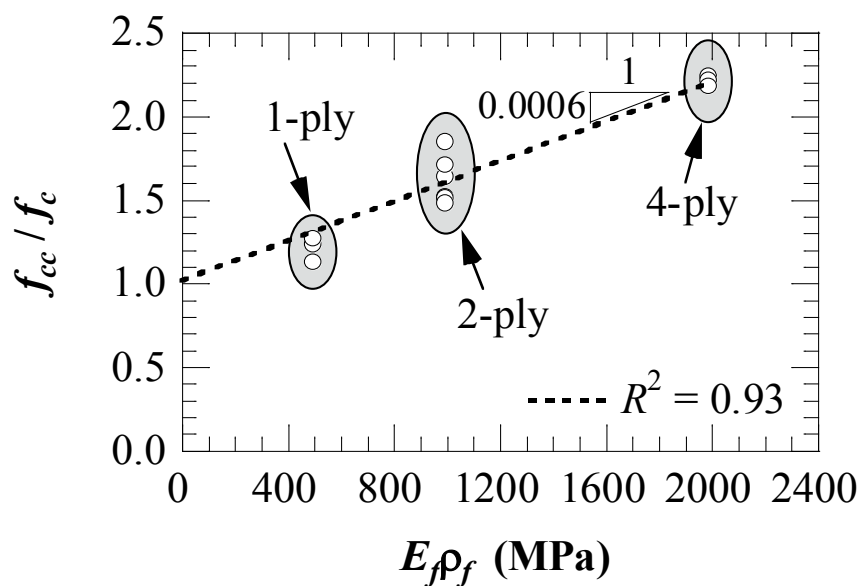
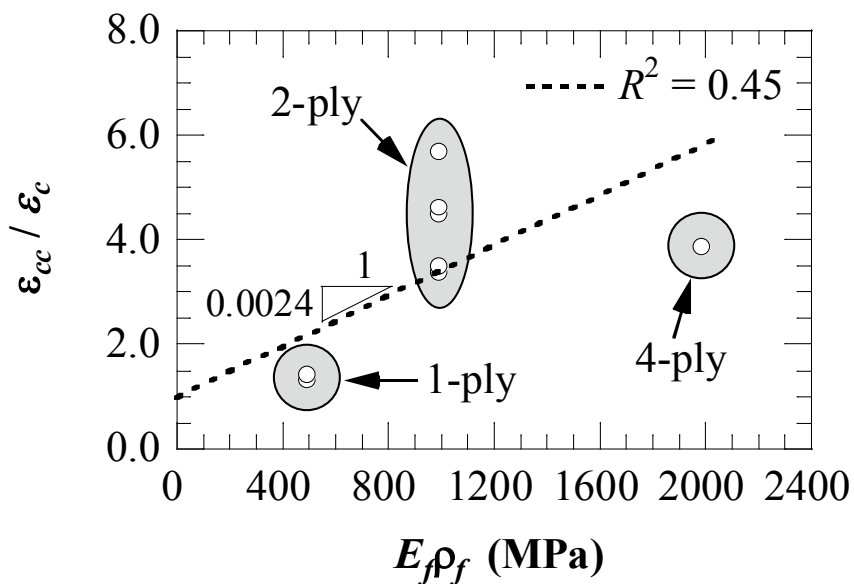


Figure 12 – Failure of representative two- and four-ply FRC flat coupon samples (a);
and failure close-up at tab location (b).



(a)



(b)

Figure 13 – Influence of amount of FRC reinforcement: experimental points and best fitting line for strengthening ratio (a) and $\epsilon_{cc} / \epsilon_c$ ratio (b) with respect to stiffness of confinement system.

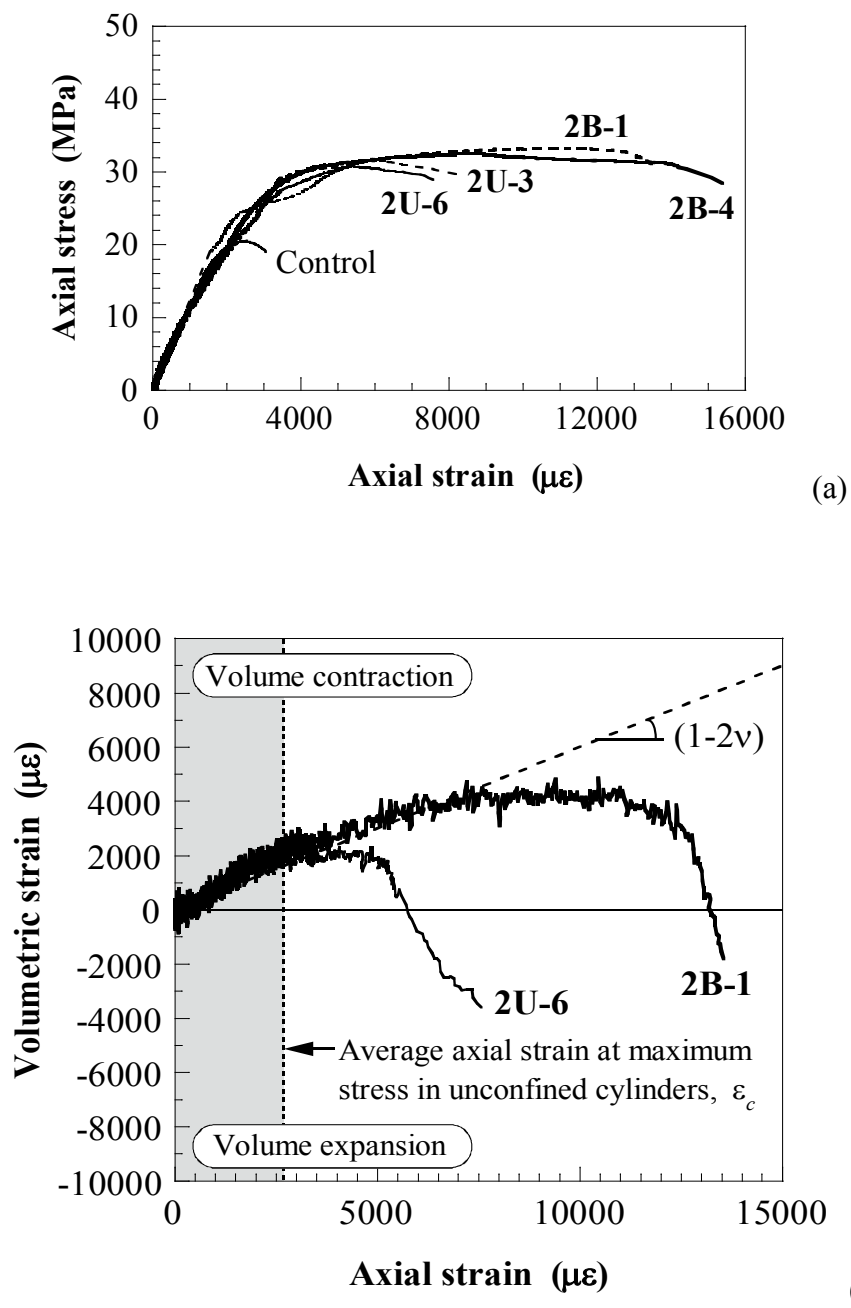


Figure 14 – Response of representative 2-ply bonded (B) and unbonded (U) FRC confined concrete cylinders in compression: axial stress-axial strain (a); volumetric strain-axial strain (b).



(a)



(b)

Figure 15 – FRC jacket removed from failed unbonded specimen (2U-3): top view, illustrating the inner surface of the FRC jacket (a); and side view, showing separation between fibers and inorganic matrix (b).

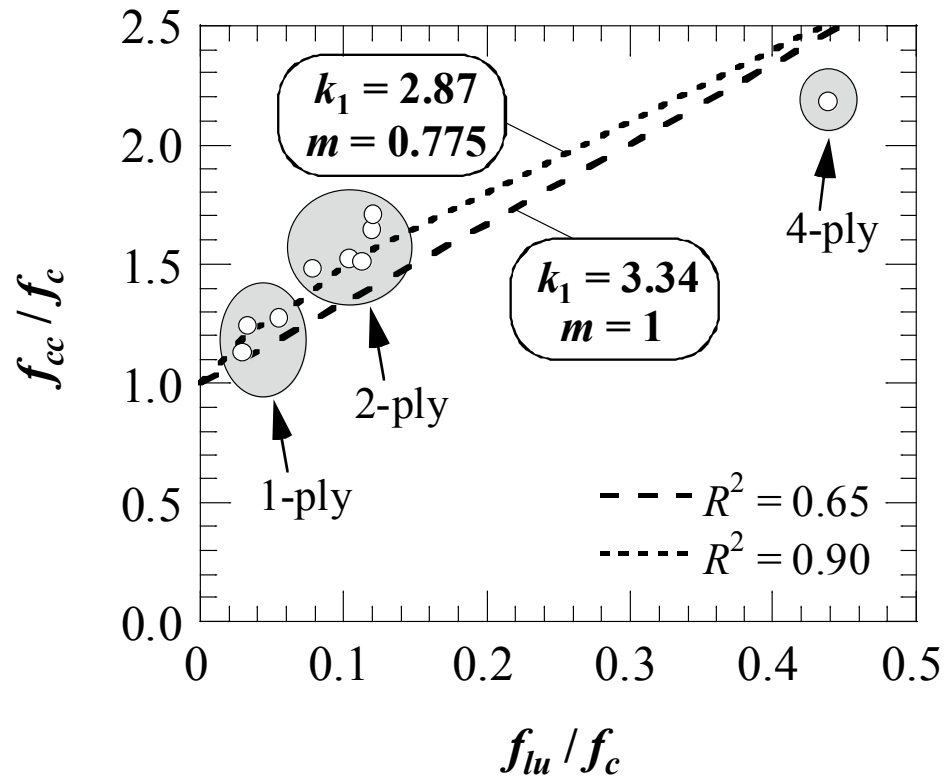


Figure 16 – Experimental points and semi-empirical linear and nonlinear model for strengthening ratio as function of confining stress for FRC bonded specimens.

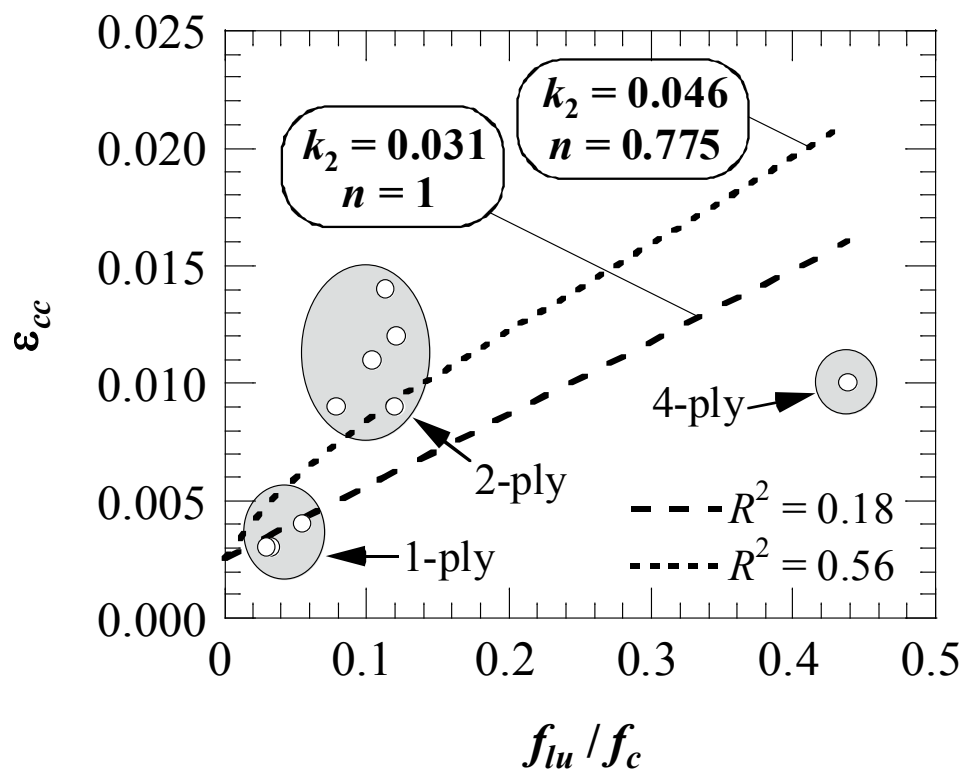


Figure 17 – Experimental points and semi-empirical linear and nonlinear model for axial strain at maximum axial stress as function confining stress for FRC bonded specimens.

CHAPTER III

STUDY 2_ SUSTAINABLE COMPOSITE STRENGTHENING SYSTEM: QUALITATIVE AND QUANTITATIVE ENVIRONMENTAL IMPACT ANALYSIS

The increasing concerns regarding environmental and health impacts of construction materials in the last decade has incentivized the development of alternative environmentally-benign material systems; where the material selection has become a critical component in the decision making process during the design stage of a construction project [21][49]. Within the rehabilitation of existing buildings and infrastructure, which represents 47 percent of the construction industry in the US alone [18], the use of FRP has been considered sustainable in part due to its durability and the aspect of structural preservation preferred to new construction. However, concerns exist due to the limited information available on FRP material system's recyclability, environmental- and health-impacts from a cradle-to-grave approach. With respect to fibers, while the production process requires high levels of energy, European directives [50] have introduced some limitations concerning the use of glass fibers when having an alkaline metal-content lower than 18 percent in weight. These fibers are considered

hazardous to workers and have been classified as a potential carcinogen when, along with a low alkaline metal content, they exhibit a small aspect ratio. Regarding the organic resins, the high energy required for their production relies on hazardous toxic constituents and intermediaries. In addition, surplus un-reacted resin material is a hazardous waste, where limited information is accessible within the construction industry for their recycling or disposal.

Therefore, there is a need to assess the environmental and health effects of externally applied FRP systems, while developing alternative composites made from components with a low influence on life cycle performance. To this end, an inorganic matrix coupled with basalt fibers might be a potential candidate composite addressing certain sustainable aspects of existing FRP systems. Inorganic binders are of interest as potential matrices due to their relative low embodied energy [51], odor and toxic emissions when processed, installed or removed [52], thus capable of minimizing related health and environmental concerns. In addition, fairly well established practices and processes exist for the safe and correct use of cement-based construction materials, as well as for their disposal and recycling [53]. Further, while the commercial applications of basalt have been well known in the past, basalt has recently been formed into continuous fibers made from natural basalt rock, an abundant and readily available raw material. Basalt fibers, which have similar properties to glass fibers, are known to be environmentally safe, non-toxic, requiring less energy to produce than glass fibers, and have been suggested as a new reinforcing material for composites [41][42], and as concluded from Study 1.

This study qualitatively and quantitatively evaluates through a life cycle assessment (LCA) framework two externally applied strengthening systems used for concrete confinement. The first retrofitting system consists of a conventional Glass FRP (GFRP), while the second uses the fiber reinforcement embedded in a cement-based matrix candidate system presented in Study 1, with basalt fibers (BFRC). The LCA comparison based on a functional unit applied to both systems, takes into account three different impact indicators consisting of: i) experimental Volatile Organic Compound (VOC) emission measurements, ii) embodied energy, and iii) carbon foot print data.

BACKGROUND

Life Cycle Assessment (LCA)

LCA is an analytical framework used to measure the transfer of environmental and social impacts associated to a product, technology or system [54]. This is achieved by providing an evaluation of the inputs and outputs throughout the entire life cycle of a given material system: starting from the material extraction, production, transportation, installation, use, maintenance, to final disposal or recycling, as depicted in Figure 18 [55]. Established LCA guidelines are well documented [56][57], following a four-stage process:

- (1) “Goal and Scope Definition” defines the extent of analysis and the system boundaries;
- (2) “Inventory Analysis” documents material and energy flows which occur within the system boundaries, also called the life cycle inventory (LCI);

- (3) “Impact Assessment or Life Cycle Impact Assessment (LCIA)”, characterizes and assesses the environmental effects using the data obtained from the inventory; and
- (4) “Interpretation and Improvement” compares and identifies opportunities to reduce the environmental burden throughout the product’s life.

Numerous studies on life cycle cost analysis of FRP composites for construction have been previously undertaken identifying their long term cost-effectiveness when compared to conventional materials such as steel and concrete, due to their durability, low maintenance, and ease of application [58][59][60][61]. However, only until recently researchers have started to focus on the broader environmental factors of FRP composites [62][63], recognizing that the environmental impact of FRP composites might be lower than traditional construction systems mainly due to lower maintenance. Simultaneously such LCAs have revealed to be incomplete, not making the cradle-to-crave connection [16].

Energy and Carbon

The embodied energy and carbon foot print of a construction material, refers to the necessary amount of consumed energy and released carbon over its life cycle (Figure 18). Conservation of energy is therefore important in the context of limiting green-house gas emissions into the atmosphere, while indirectly reducing the material life cycle costs.

Thermoset polymers, such as epoxies traditionally used in FRP systems, are known to have high embodied energy as reflected in Table 6 due to polymer’s high durability based

on their permanent irreversible cross-link structure [64]. As the use of FRP composites increases exponentially, so will the material waste and scrap; hence, disposal or recycling becomes a critical part of the embodied energy and carbon. Limited efforts have been undertaken to utilize scrap produced during the manufacture of fibers, FRP composites, and recovery from post-applied composites, where to date no acceptable FRP recycling procedure exists [65].

Volatile Organic Compounds

VOCs refer to organic chemical compounds having high vapor pressures making them dissolve in air, thus affecting the environment and air quality. In closed or semi-closed spaces, VOCs related to construction materials have shown to have adverse health effects on humans depending on their level of concentration and period of exposure [66]. The medical and lost productivity costs from health conditions due to exposure to VOCs have shown to be significant. Thus, building owners and the construction industry are moving towards products with lower VOC emissions [22].

Environmental and health issues are of direct concern during the manufacture of the composite constituents, and installation of externally-bonded FRP systems where VOCs concentration and exposure levels are believed to be considerable, but have not been measured. Indirectly, VOCs post-installation of FRP systems may produce detrimental health effects to installation workers and building occupants, as indoor air quality may be affected, inducing the sick building syndrome symptoms [67]. Additionally a number of common polymers found in FRP rely on hazardous toxic constituents and intermediaries

such as plasticizers, for example phthalates used in manufacturing epoxy. Many of these are being investigated for both carcinogenic and hormone disruption effects (e.g., formaldehyde a suspected human carcinogen, and bisphenol-A, a possible hormone disrupter) [66]. To date no VOC emission measurements of wet-layup FRP applications have been undertaken to provide quantitative data to determine their possible life cycle environmental and health effects.

METHODS AND APPROACH

Retrofitting Strategy

An externally-bonded confining retrofitting design strategy was defined to ensure adequate comparison amongst the different properties of either strengthening system, summarized in Table 7. Each strengthening system: BFRC and GFRP, was designed based on attaining equivalent reinforcement ratios, ρ_f (determined by equation (1)), to provide a 20% increase in ultimate axial strength capacity, f_{cc} , over the strength of unconfined concrete, f_{co} , assume to equal 21.5 MPa; to achieve this design, guidelines were followed [11]:

$$f_{cc} = f_{co} \left[2.25 \sqrt{1 + 7.9 \left(\frac{f_{lu}}{f_{co}} \right)} - 2 \frac{f_{lu}}{f_{co}} - 1.25 \right] \quad (5)$$

where the concrete column diameter was taken as 0.55 m, and f_{lu} is the confining pressure determined through the equilibrium condition and deformation compatibility in the circular cross-section given by equation (4). Additionally, due to the novelty of inorganic-based composite system and its relative confining effectiveness to the organic counterpart, a contrast with respect to the design model (equation (5)) was provided by

two analytical non-linear models to determine f_{cc} ; where a well established model was used for the GFRP system [8] presented in equation 6, and the proposed model evaluated and calibrated in Study 1 is used for the BFRC as seen in equation 7, which are as follows:

$$\text{GFRP: } \frac{f_{cc}}{f_{co}} = 1 + 3.5 \left(\frac{f_{lu}}{f_{co}} \right)^{0.85} \quad (6)$$

$$\text{BFRC: } \frac{f_{cc}}{f_{co}} = 1 + 2.85 \left(\frac{f_{lu}}{f_{co}} \right)^{0.778} \quad (7)$$

LCA Methodology

To evaluate and compare the environment and health impacts of the proposed strengthening composite systems, guidelines ASTM E1991 [56] and ISO 14040 [57] were implemented following the recommended four-stage process described previously.

Goal and scope definition

The time and geographic region in this study for the data set considered in the LCA corresponds to 2009 and the United States, respectively. The evaluation range for either composite system is summarized in Figure 19, where the stages considered in this study include: the “extraction”, “production”, and “installation”. Both composite systems are assumed to last the same period of time post-installation, with equal levels of maintenance needed during the “using” stage. After the use stage, the current available options for the GFRP composite includes landfill or incineration; while for the BFRC composite full recycling is possible, consisting of crushing for aggregate. Nonetheless,

accurate values have not been reported previously and therefore the “using” and “dispose/recycle” stages are not evaluated herein.

Since the properties, energy requirements, and emissions from the constituent materials of each composite system on a per-mass (*unit/kg*) basis is different as reflected on Table 7, a proposed functional unit based on the per-ply (*unit/ply*) basis for either composite is used to provide a reliable and equivalent assessment to contrast both strengthening systems.

Inventory analysis

The life cycle inventory (LCI) is treated as a flow diagram of the different processes involved during each of the stages within the evaluation range, where all materials, energy inputs, by-products and production process, are considered as depicted in Figure 20. The LCI follows recommendations made by the Tool for the Reduction and Assessment of Chemical and other environmental Impacts (TRACI) [68], consistent with the Environmental Protection Agency’s (EPA) policies and regulations.

The inventory is based on three parameters: i) embodied energy, in mega-joules per kilogram of material (MJ/kg); ii) carbon emissions of fossil fuel depletion, in kilograms of carbon dioxide per kilogram of material (kgCO₂/kg); and iii) VOC concentration emissions, in particles per million (ppm).

Impact assessment

The life cycle impact assessment (LCIA) considers only mid-point-factors (impact potential), which although codified in guidelines [57], are still undergoing modifications with several approaches discussed critically [69][70]. By following TRACI's guidelines [68], the mid-point-factors reflect the relative potency of the stressors (a set of conditions that may lead to an impact) at a common mid-point within the cause-effect chain of any of the processes throughout the evaluation range for both composite systems. Mid-point calculations can be summarized as follows [71]:

$$I_i = \sum_{xmn} F_{xmn}^i P_{xn}^i M_{xm} \quad (8)$$

where, I_i is the total potential impact of chemicals and substances x which have been released to all medias m , with all modeled exposure routes n , for a specific indicator i ; F_{xmn}^i is the fate and exposure pathway of chemicals and substances x ; P_{xn}^i is the potency of the chemicals and substances x ; and M_{xm} is the mass of the chemicals and substances x .

This study focuses on three mid-point indicators: i) primary energy (PE), measured in mega-joules per ply (MJ/ply); ii) global warming potential (GWP), measured in kilograms of carbon dioxide per ply (kgCO₂/ply); and iii) air quality (AQ), measured in particles per million per ply (ppm/ply). The first two indicators are well researched with consensus at this level of characterization [72][73], while the last is an initial attempt to develop an indicator supported with new experimental data.

Interpretation and improvement

The life cycle interpretation phase as recommended by the guidelines [57] consists of: identifying significant differences in the results; evaluating information from the LCI and LCIA ensuring completeness and reliability; while providing conclusions and recommendations for further research.

Energy and Carbon Approach

Total energy consumption, and carbon emissions for the processes involved at each stage in the evaluation range for either composite system is considered separately for each constituent, namely the fibers (basalt or glass), matrix (cement-mortar or two part epoxy-resin), and primer (only for GFRP). This last component is used when applying FRP systems to prepare the concrete surface prior installation. The inventory data and assessment corresponding to energy and carbon was derived from TRACI databases [74], and supplemented with the Inventory of Carbon & Energy [51].

Embodied energy data has been readily available and researched in foreign sources tending to use worldwide averages, and thus adopted over US based sources. This introduces a sensitive issue based on the differences in fuel mixes and electricity generation that each country might have. Nonetheless, due to the average nature of the databases, it is assumed that influence will be negligible over the results. In the case of the production stage for basalt fibers no specific data was found; nevertheless, since the overall production is comparable to that of continuous E-glass, based on a single-stage

process by melting natural basalt rock (Figure 19), it was assumed that basalt fibers underwent the same production process with respect to life cycle energy and carbon data.

Volatile Organic Compounds Approach

The VOCs were determined using an environmental chamber methodology and photoionization detection (PID) employing a modified version of standard ASTM D5116 [75].

Specimen preparation

Plain concrete cylinders cast from a single batch of concrete with a diameter and height equal to 152 and 305 mm, respectively, were strengthened using a manual lay-up technique with four- and two-ply for the BFRC and GFRP composite systems, respectively. The reinforcement level was selected based on the results of the retrofitting design discussed in the next section. Five cylinders were wrapped with each composite system following a traditional manual wet lay-up technique illustrated in Figure 21.

Test setup and instrumentation

The environmental chamber was cleaned with a generic laboratory detergent prior each test and then pre-conditioned for 2 hours to reach desirable room humidity and temperature level conditions of 65% and 23°C, respectively. A background measurement was recorded as a benchmark, and after concrete cylinders were wrapped with either composite system, specimens were introduced horizontally in the chamber. Monitoring and collection of VOCs was undertaken using a PID with a 10.6 eV gas-discharge lamp,

where the instrument and sensor module are depicted in Figure 22. The test gas used for calibration was isobutylene, with a reading accuracy of $\pm 3\%$. Air samples were collected at 15 min intervals for 2 min for a period of 180 min, at constant flow rate of 450 cc per min. The minimum, average, and peak ppm were recorded as recommended by literature [76]; Figure 23 shows the test setup.

RESULTS AND DISCUSSION

The retrofitting design strategy, the results for energy, carbon, VOC concentration emissions and their life cycle impact assessment are discussed in the following four sections.

Retrofitting Strategy

The retrofitting design strategy is summarized in Table 8, where a 20% increase in f_{cc} over unconfined concrete corresponding to 25.60 MPa was achieved. Though the design-model (equation (5)) provided a slightly higher level of f_{cc} when compared to the analytical-models, (equations (6) and (7)) the ratio $f_{cc\text{-BFRC}}$ to $f_{cc\text{-GFRP}}$ was equal to 1.0 using both modeling techniques. Based on the design, the BFRC system needed double the number of plies (and matrix) than its counterpart GFRP to provide equivalent levels of f_{cc} .

Energy and Carbon

The results from the inventory for the embodied energy in terms of MJ/kg, and carbon in terms of kgCO_2/kg , related to the extraction, production, and installation of the BFRC

and GFRP systems is summarized in Table 9. Based on this, the GFRP system requires nearly 700% increase in MJ/kg of embodied energy, while almost releasing 350% more carbon emissions in kgCO₂/kg than its counterpart BFRP. When comparing the individual contribution towards energy and carbon of the system's components, BFRC's fiber reinforcement (basalt) is the main contributor; while the matrix (polymer) is in the GFRP system. This result is expected given the large magnitude of energy required to produce polymeric resins as seen from Table 6 [64].

VOC Emissions

The environmental chamber test results are summarized in Table 10, which includes the BFRC and GFRP average VOC emissions based on five specimens, the minimum, average, and maximum emitted concentration of particles per million (ppm) are reported. The level of concentration versus the time, T , for representative samples can be seen in Figure 24. Overall average VOC concentration levels from the GFRP strengthening system followed a bilinear trend where the first branch ($T = 0$ to 30 min) increased steeply reaching a peak level of 152.6 ppm. Only at this instance the difference between the minimum, average and maximum recorded emission levels diverged to its highest difference, converging before and after this peak as seen in Figure 24 (a). The second branch ($T = 30$ to 150 min) gradually decays leveling at around 100.0 ppm there after.

The trend of VOC concentration levels of the BFRC strengthening system was significantly different from its counterpart, with a first ascending branch ($T = 0$ to 15 min) followed by a second lower gradient rising branch ($T = 15$ to 45 min). Thereafter

the emissions remain semi-constant until $T = 100$ min, where emissions oscillate sinusoidally reaching a peak of 1.2 ppm at $T = 150$ min, illustrated in Figure 24 (b).

Emissions from BFRC specimens are comparable to background-concentration levels typically found in inorganic water-based products and the environment, as defined by the EPA National Ambient Air Quality Standards (NAAQS) [77]; providing an explanation to the oscillating pattern after $T = 100$ min in Figure 24 (b). The GFRP system emitted peak concentrations levels 180 times higher than the BFRC system, remaining over 100 times higher after $T = 150$ min, as represented by the comparison average ppm versus T response for representative specimens in Figure 25.

Impact Assessment and Interpretation

LCIA results are summarized in Table 11 and includes the three mid-point indicators, I_i : primary energy (PE), global warming potential (GWP), and air quality (AQ).

Potential energy and global warming potential

The bar charts in Figure 26 (a) and (b) represent the LCIA results for the PE and GWP, respectively. For every installed ply of BFRC, approximately 3.5 times more primary energy is needed, and 3.7 times more carbon is emitted to install an equivalent GFRP ply. This corresponds to 250 and 270% increase in primary energy consumption leading to a corresponding increase in fossil fuel depletion and risk of global warming.

The assessment for the fiber component for both strengthening systems represents less than a 0.01%, while the matrix component more than 99.98% of its total PE and GWP. From a structural perspective, the fiber reinforcement is the key component of a composite systems as it is the load carrying medium, while the matrix transfers the load. Thus, it is reasonable to assume in terms of impact assessment that the fiber component ought to be the highest source of PE and GWP within the composite system. However, since mid-point indicators for the matrices within the composite systems are higher than the reinforcement fibers there will be an inherent environmental trade-off. When comparing system components, both BFRC's matrix and reinforcement fibers have a lower life cycle impact over GFRP's components as illustrated in Figure 27 (a) and (b); which represents the PE and GWP indicators for system components, normalized with respect to each strengthening system. Hence the GFRP- is quantitatively detrimental to the environmental in terms of energy and carbon when compared with the BFRC-system.

There are two additional qualitatively items not considered which may provide the BFRC system with an additional life cycle advantage over GFRP. Firstly is addressing the disposal/recycling stage, not considered in this study. After the use stage, the GFRP system may need to be incinerated or deposited in a landfill, increasing its contributions towards PE and GWP, while the BFRC can be fully recyclable as discussed previously. Secondly, polymer based systems, which are combustible, when used inside buildings are required to be insulated against fire with an additional component. Cement-based matrices may not need fire insulation, especially when coupled with basalt fibers which

have a high degree of thermal stability in comparison to glass fibers [41]; accounting for fire insulation may modify the total PE and GWP contributions of the GFRP system.

Air quality

The mid-point impact potency of the air quality for the peak, and average (2.5 hours post-installation) concentration levels of emitted VOCs from the composite's matrices is summarized in the last two rows of Table 11. The results are based on equation (6) where, F_{xm}^{AQ} pathways were obtained from existing *Tracking and Analysis Framework* (TAF) model database [78], and set equal to 1.000 and 1.073 kg⁻¹ for the BFRC and GFRP matrices respectively; P_{xm}^{AQ} was taken from the environmental chamber peak, and average (2.5 hrs post-installation) ppm emissions (Table 10); and M_{xm} was determined from the matrix properties provided in Table 7 for a single installed ply. The results show that for every installed ply of GFRP, there is 33 times more potential for the air quality to immediately deteriorate after installation with VOCs, and 24 times more 2.5 hours post-installation, than when installing a BFRC composite system.

The difference in magnitude of VOC levels between the strengthening systems is significant, where exposure to concentration emission levels recorded in the GFRP system over a period of one hour can lead to detrimental health effects ranging from chest pain, coughing, throat irritation, congestion/bronchitis, to asthma as determined by the NAAQS [77]. Such exposure periods can be reached and exceed during the application of manual layup FRP strengthening systems in closed, semi-closed environments, or when handling the product at a short distance from the source of emissions. Over long

exposure or cumulative periods, certain VOCs emitted from polymer based resins have shown to be human carcinogen, and possible hormone disrupter [66]. Furthermore, the rate of ozone formation in the troposphere, which is governed by complex chemical reactions, has been found to be influenced by VOC concentrations similar to those emitted from the production and installation of epoxy resins [79]. Therefore BFRC systems have a significant lower impact on the surrounding air quality where installed, reducing health related effects of individuals handling or present near the system.

CONCLUSIONS

This study provides qualitative and quantitative data to evaluate through a life cycle assessment (LCA) method two externally-bonded strengthening systems used for concrete confinement. The first retrofitting system consists of a conventional Glass FRP (GFRP), while the second uses the fiber reinforcement embedded in a cement-based matrix candidate system presented in Study 1, with basalt fibers (BFRC). The LCA includes three life cycle mid-point indicators derived from experimental Volatile Organic Compound (VOC) emissions, embodied energy, and carbon foot print data for each system. The main conclusions reached in this study are as follows:

1. For every installed ply of BFRC, approximately 3.5 times more primary energy is needed, and 3.7 times more carbon is emitted to install an equivalent GFRP ply.

2. The matrix was the component for both strengthening systems which contributed towards most of the energy consumption and carbon emissions, leading to increase of fossil fuel depletion and risk of global warming.
3. Based on the environmental chamber tests, for every installed ply of GFRP, there is 33 times more potential for the air quality to immediately deteriorate after installation with VOCs, and 24 times more 2.5 hrs post-installation, than when selecting a BFRC composite system.
4. Overall, based on the life cycle assessment method the BFRC- provides an environmentally-benign alternative over the GFRP-composite system.

The LCA information presented herein may provide understanding of the environmental and health impacts, similar to the exiting economic-cost methods, to the decision-making process of design that traditionally has not been considered when selecting composite strengthening systems. Therefore this study implements the LCA methodology as a tool to determine engineering trade-offs between composite systems based on the economic, technical, environmental, and health challenges currently faced by the construction industry.

FURTHER RESEARCH

While the presented LCA analyzes the environmental and health impacts based on the energy, carbon, and VOC emissions for a broad evaluation range using a functional unit, the recycling and/or disposal for current polymeric based composite strengthening systems is not considered. Therefore, there needs to be further research to quantitatively

determine the environmental effects of recycling and/or disposing each of the investigated composite systems in order to achieve a full LCA evaluation. Additionally, supplementary components for strengthening composite systems applied inside occupied buildings, such as fire insulation, should be accounted within a LCA to have a better comparison between both composite systems.

The initial effort to quantify the effects from VOC emissions may be further developed by implementing thermal gas chromatography to identify the components and relative concentrations within the composite's VOC emissions. Such research may potentially provide data to assess end-point and damage potential indicators as part of an LCA to determine relative long term environmental and health impacts caused by the use of composite strengthening systems.

Table 6 – Embodied energy of selected thermoplastic and thermoset polymers [64].

Type of Polymer	Embodied Energy (MJ/kg)
Low-density polyethylene	80.5
High-density polyethylene	79.9
Polystyrene expandable	83.7
Polyvinyl chloride	65.2
Acrylonitrile butadiene styrene	95.0
Polycarbonate	116.8
Epoxies	140.7

Table 7 – Reinforcement and matrix/primer properties*

Composite system		GFRP	BFRC
<i>Reinforcement properties</i>			
Young Modulus (MPa)	E_f	76900	80900
Tensile Strength (MPa)	f_f	3399	3882
Tensile strain	ε_f	0.047	0.042
Design strength (MPa)	f_{fu}	2889	3299
Design strain	ε_{fu}	0.03995	0.03553
Sheet thickness (m)	t_f	0.00025	0.00012
Weight fiber sheet (kg/m ²)	ρ_r	0.596	0.325
<i>Matrix/Primer properties</i>			
Thickness matrix (m)	t_m	0.001	0.003
Thickness primer (m)	t_p	0.00007	n/a**
Density of Matrix (kg/m ³)	ρ_m	1056.7	1562.5
Density of Primer (kg/m ³)	ρ_p	1056.7	n/a**

* provided by manufacturer

**Not applicable (n/a) to BFRC system.

Table 8 – Externally-bonded confining retrofit design.

Composite System		GFRP	BFRC
<i>Design Parameters</i>			
Plain concrete compressive strength (MPa)	f_{co}	21.50	
Column Diameter (m)	D	0.55	
Reinforcement ratio	ρ_f	0.00537	0.00524
Confining pressure (MPa)	f_l	0.825	0.847
Number of plies	n_p	3	6
<i>Design Model</i>			
$f_{co} \left[2.25 \sqrt{1 + 7.9 \left(\frac{f_l}{f_{co}} \right)} - 2 \frac{f_l}{f_{co}} - 1.25 \right]$ (MPa)	f_{cc-ACI}	26.70	26.83
<i>Analytical Model</i>			
$f_{co} \left[3.5 \left(\frac{f_l}{f_{co}} \right)^{0.85} + 1 \right]$ (MPa)	$f_{cc-GFRP}$	26.21	n/a*
$f_{co} \left[2.85 \left(\frac{f_l}{f_{co}} \right)^{0.778} + 1 \right]$ (MPa)	$f_{cc-BFRC}$	n/a*	26.49

* Not applicable (n/a)

Table 9 – Energy and Carbon inventory data.

System	Composite Component	Energy (MJ/kg)	Carbon (kgCO ₂ /kg)
GFRP	Glass fibers (reinforcement)	28.00	1.53
	Primer (surface preparation)	78.20	2.26
	Epoxy resin (matrix)	139.32	5.91
	TOTAL	245.52	9.70
BFRC	Basalt fibers (reinforcement)	26.24	1.35
	Cement mortar* (matrix)	4.60	0.18
	TOTAL	30.84	1.53

*Hydraulic mortar with no added sand or aggregate

Table 10 – Minimum, maximum and average concentration of emitted VOCs for BFRC and GFRP strengthening systems, based on an average of five specimens.

System	GFRP			BFRC		
Time (min)	VOC concentration emissions (ppm)					
	Min.	Avg.	Max.	Min.	Avg.	Max.
Background	0.000	0.000	0.000	0.000	0.000	0.000
0	4.005	10.186	18.384	0.086	0.133	0.190
6	74.947	80.046	83.882	0.384	0.454	0.502
15	125.871	127.952	129.352	0.624	0.703	0.750
30	138.900	145.750	152.600	0.759	0.849	0.914
45	139.536	143.279	147.080	0.912	1.000	1.072
60	140.172	140.808	141.560	0.834	0.987	1.090
75	128.209	128.510	128.829	0.828	0.994	1.107
90	126.229	126.528	126.814	0.833	1.002	1.111
105	118.108	118.428	118.715	0.803	0.945	1.053
120	114.407	114.685	115.026	0.906	1.063	1.147
135	107.402	107.821	108.288	0.786	0.953	1.058
150	100.439	100.807	101.216	1.050	1.110	1.155
165	99.776	100.099	100.426	0.814	0.923	1.001
180	100.002	100.179	100.378	0.742	0.909	1.017

Table 11 – LCIA summary results.

Mid-point Indicator, I_i	System component	GFRP	BFRC
PE (MJ/ply)	Reinforcement	0.0071	0.0035
	Primer	0.0400	n/a*
	Matrix	260.3475	74.4769
	Total	260.3945	74.4804
GWP (kgCO ₂ /ply)	Reinforcement	0.0004	0.0002
	Primer	0.0004	n/a*
	Matrix	11.0440	2.9629
	Total	11.0448	2.9631
AQ (ppm/ply)	Peak	306.0	9.35
	Average (2.5hrs post-installation)	201.9	8.56

* Not applicable (n/a)

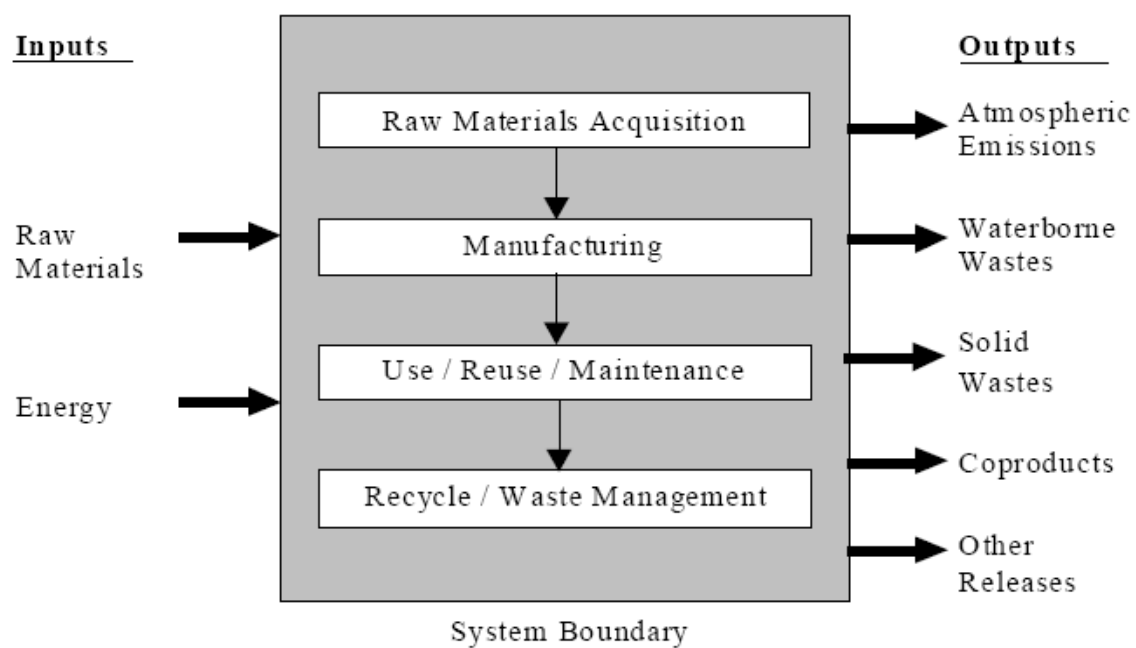


Figure 18 – Life Cycle Stages [55].

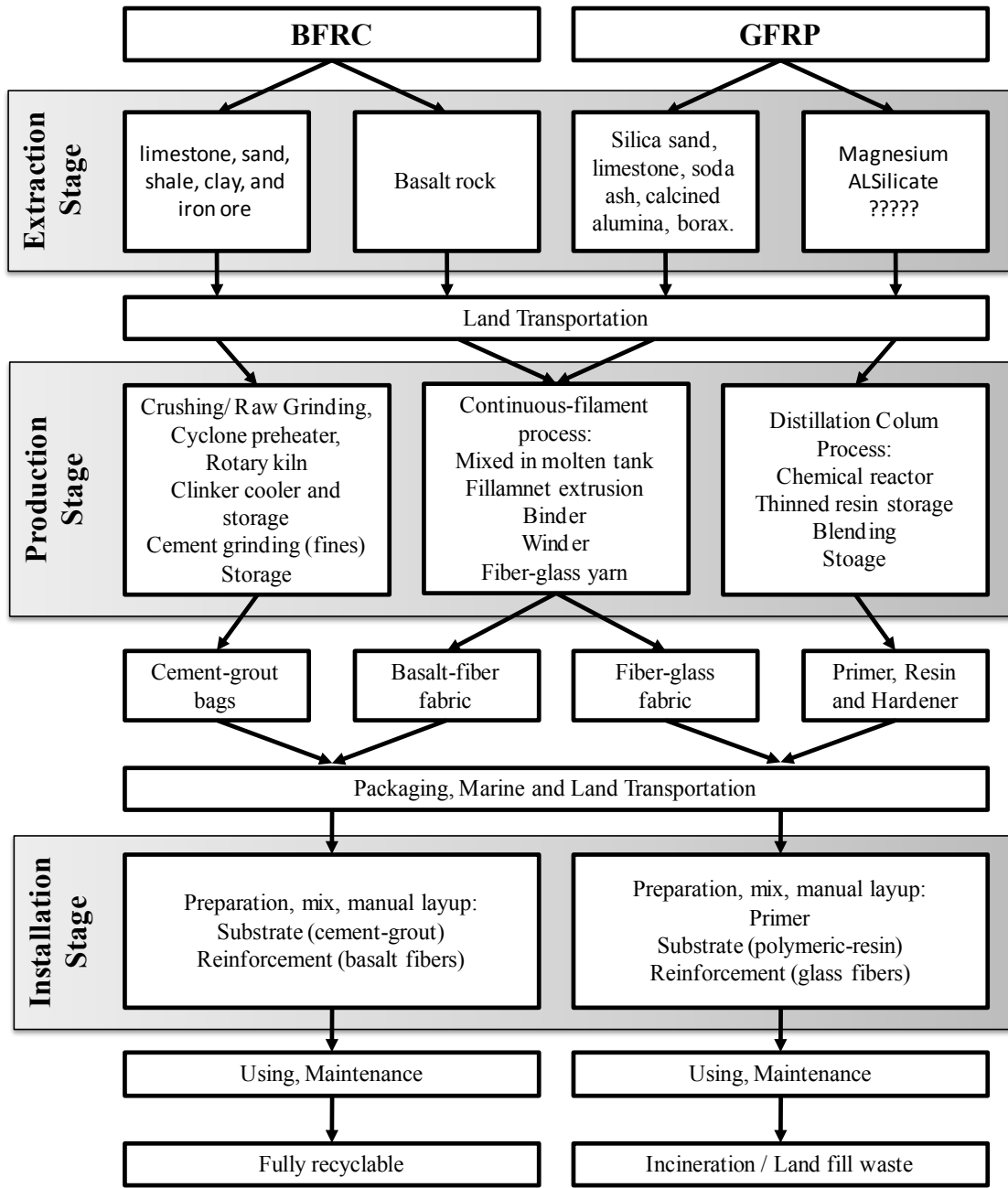


Figure 19 – Summary of the evaluation range for BFRC and GFRP composites.

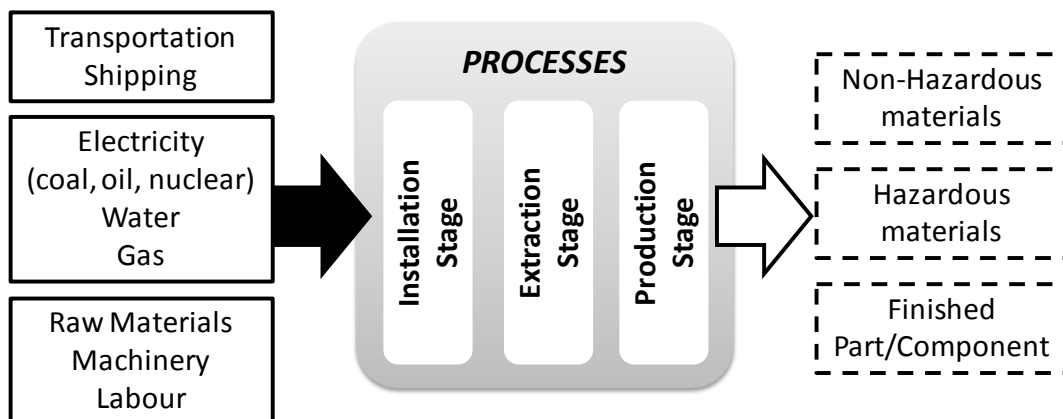


Figure 20 – Processes within the LCI of BFRC and GFRP composites.



Figure 21 – Sample preparation following the wet lay-up technique.

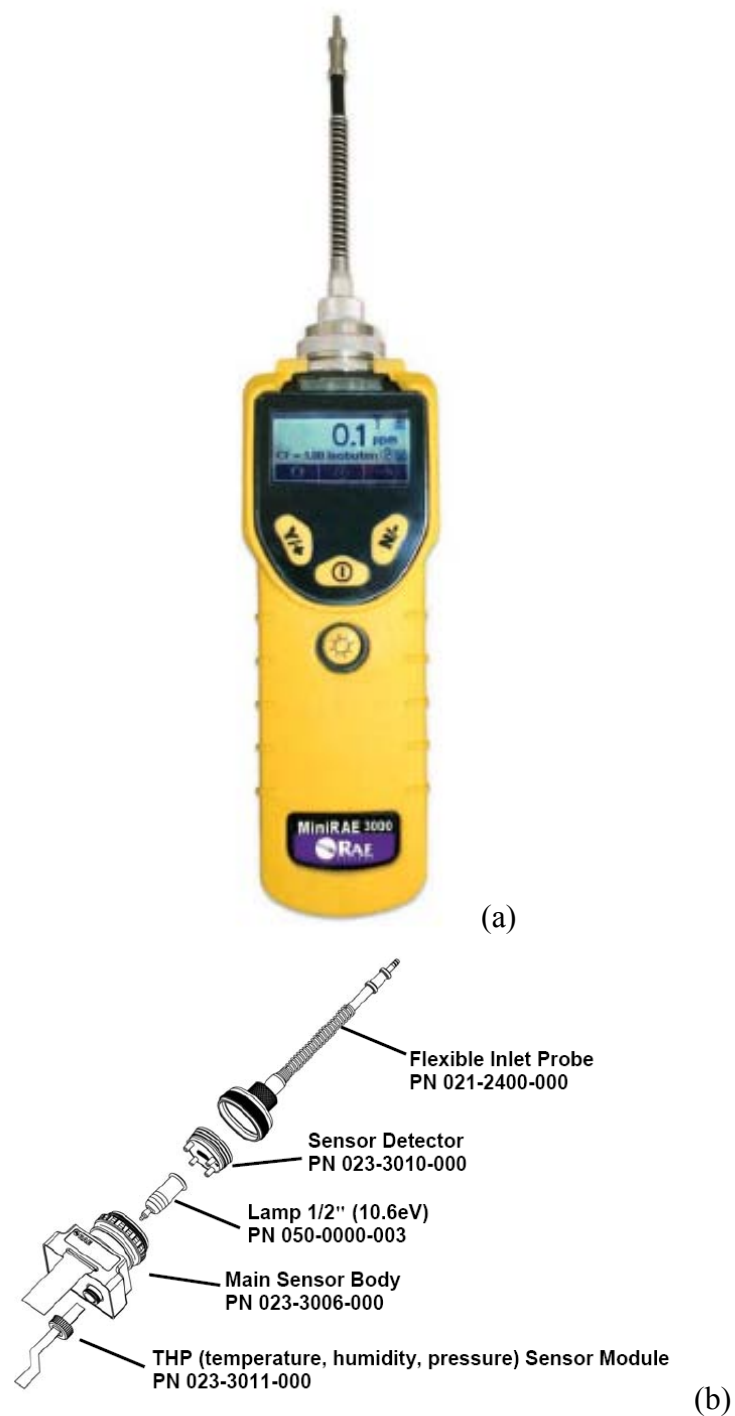
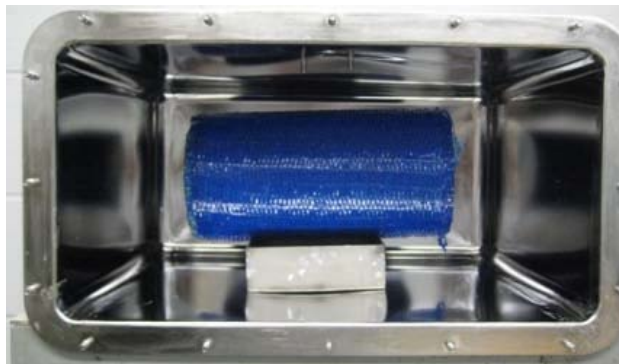


Figure 22 – PID instrument (a); and PID sensor module and components (b).

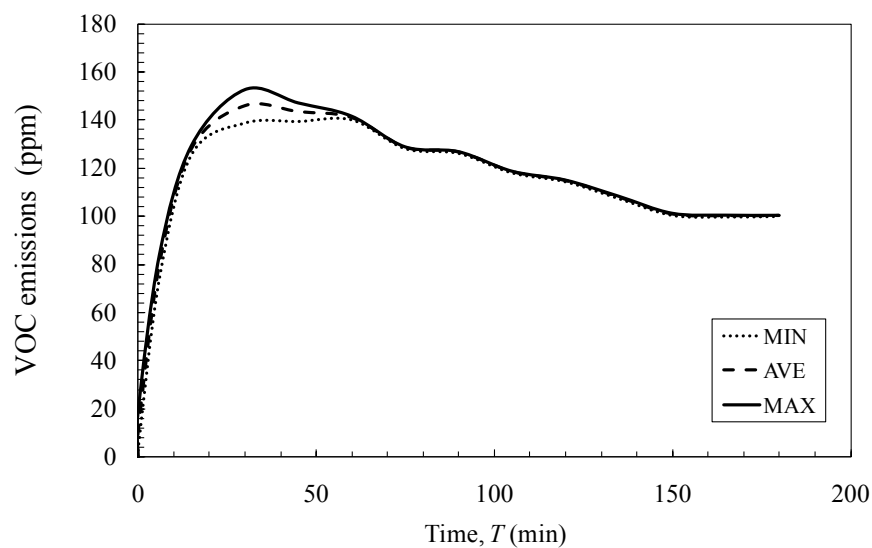


(a)

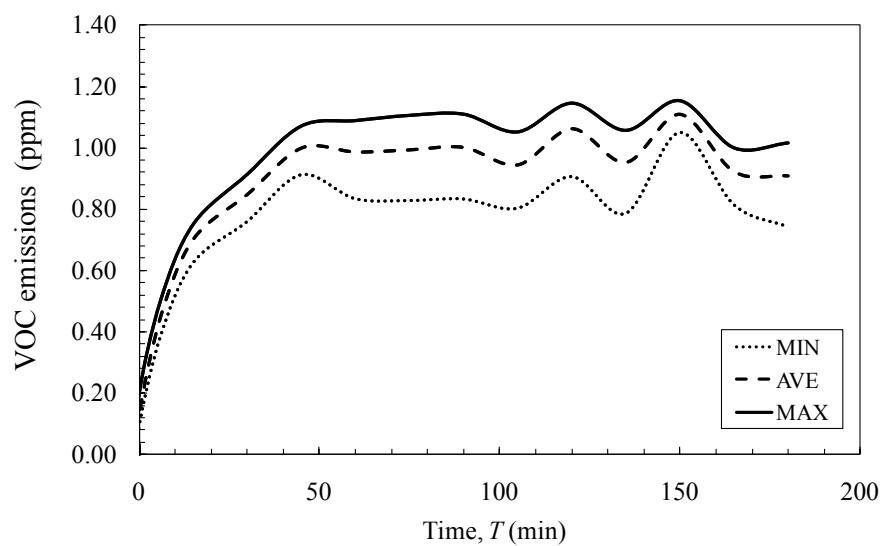


(b)

Figure 23 – Environmental chamber test setup (a);
and specimen within environmental chamber (b).



(a)



(b)

Figure 24 – Minimum, average and maximum concentration levels of emitted VOCs for representative: GFRP- (a); and BFRC-strengthening system (b).

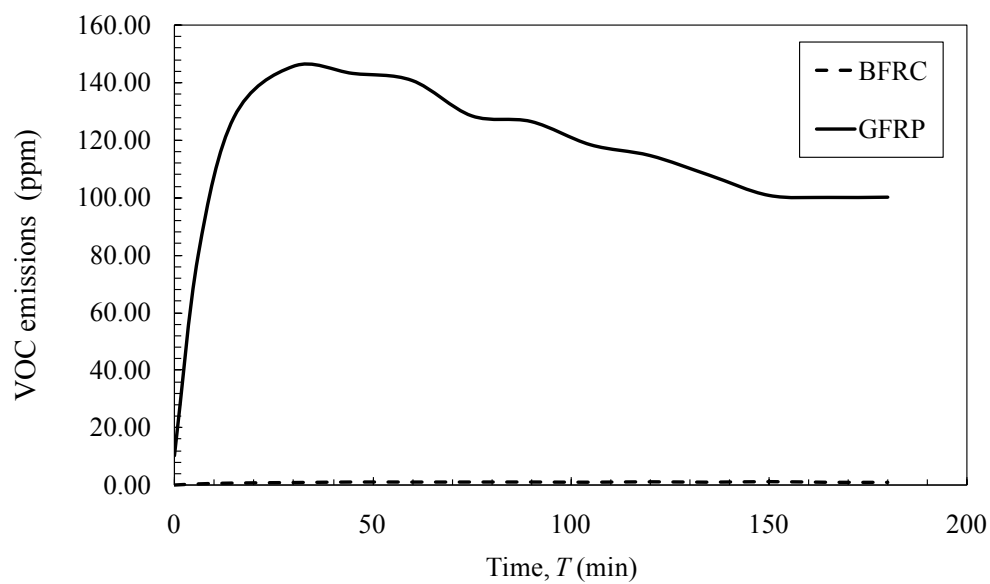


Figure 25 – Comparison of average concentration of emitted VOCs of representative BFRC and GFRP strengthening systems.

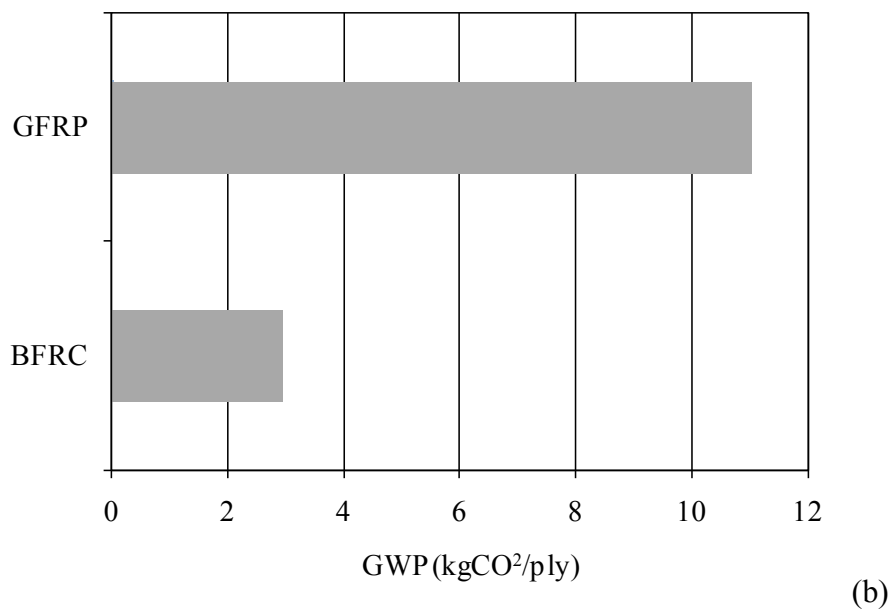
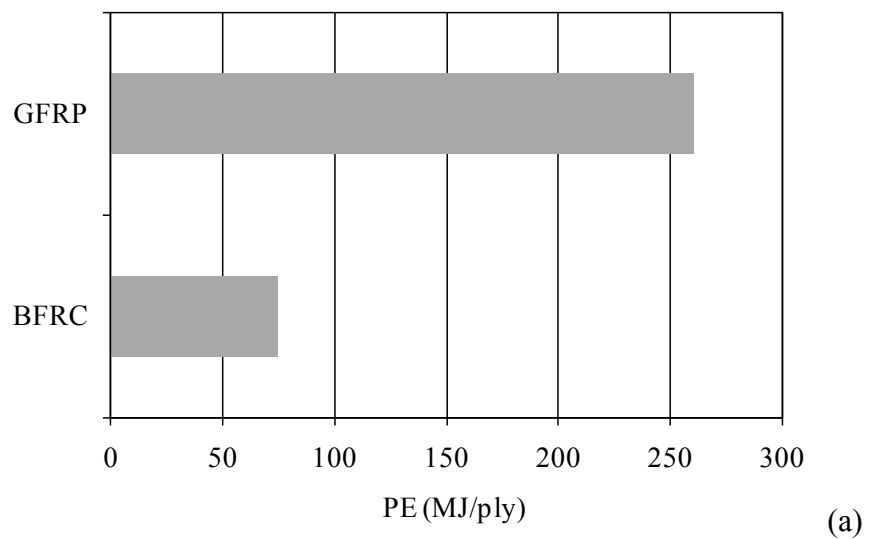


Figure 26 – LCIA results for each composite system: Potential Energy (a); and Global Warming Potential (b).

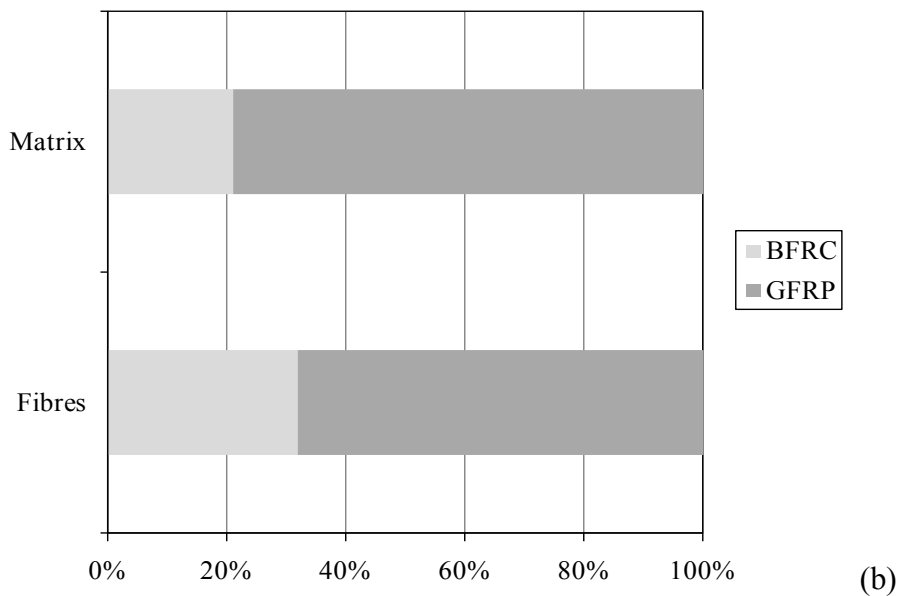
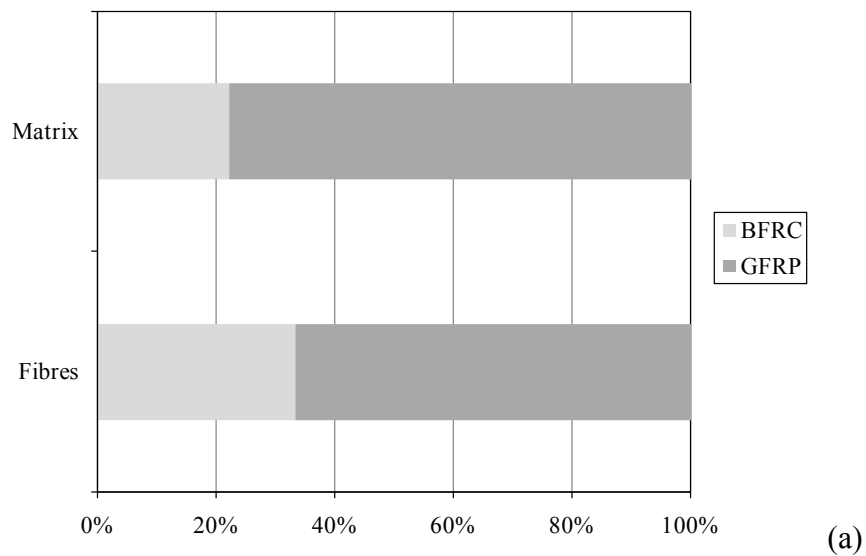


Figure 27 – LCIA normalized results for each system component:

Potential Energy (a); and Global Warming Potential (b).

CHAPTER IV

STUDY 3_ICE METHODOLOGY

Acceptance of FRP laminate characterization is currently based solely on tests methods using flat coupon specimens as determined by ASTM standards [44] and ACI guidelines [80]. The motivation to propose a unique and novel Investigation of Circumferential-strain Experimental, herein referred to as ICE, methodology for FRP characterization arises from the fact that:

Based on the research presented in Study 1, which develops and characterizes a new type of fiber reinforced cement-based matrix (FRC) composite system for confinement applications, it is concluded that composites with brittle matrices are not adequately characterize with the existing tensile flat coupon test method, and the ICE methodology presented herein is developed as a candidate test method to engage brittle matrix composite systems, such as the FRC system [81].

The existing theoretical models and design guidelines available to predict the effects of FRP confinement on concrete rely on the common assumption that FRP fails when

circumferential strain in the jacket reaches its ultimate tensile strain and ruptures. The value for such critical parameter, the ultimate FRP tensile strain, is determined from material flat coupon tensile tests. Extensive research [23][24][25] has suggested that ultimate FRP tensile strain determined experimentally according to flat coupon tests, could not be reached at the circumferential rupture of FRP jackets confining concrete cylinders. Available experimental data has shown that the strain efficiency factor of externally applied FRP jackets, κ_e , expressed as the ratio of the tensile circumferential strain in the FRP at failure to the average failure strain observed in FRP uniaxial tensile flat coupons tests, varies substantially from 0.58 to 0.91[26]. The causes for such differences are probably due to the effect of the radius of curvature, the multi-state of stress, or the uneven pressure exerted by the concrete resulting from its cracking.

The first part of this study, Part A, reports on a newly developed test method aimed at providing an efficient and reliable experimental technique to measure the ultimate circumferential (hoop) strain of FRP laminates, including specimens with different jacket diameters and laminate thicknesses. The ICE methodology uses the unique property of water that expands when it changes state of matter from liquid to solid, as a medium to apply a uniform internal hydrostatic pressure. The method was first assessed on different circular metal containers to assess its feasibility, and then validated on cylindrical hand lay-up manufactured Glass FRP (GFRP) specimens.

The second part of this study, Part B, explicitly evaluates the experimental data reported in Part A and compares it with GFRP flat coupon direct tensile tests used as a benchmark, to determine the effect of GFRP jacket curvature (diameter) and laminate thickness (number of plies) on the strain efficiency. The outcome of these findings over current design guidelines for FRP confined concrete is also discussed.

PART A: ICE METHODOLOGY FOR FRP CHARACTERIZATION

BACKGROUND

Standardized tests such as the split disk method [82], or the inactive tension testing of filament-wound pressure vessels [83], and other test methods which use fixtures such as poly-tetrafluoroethylene (PTFE) rings [84][85], expandable bladder systems [86][87], or mechanical quadrant rings [88], have been previously proposed to characterize the circumferential (hoop) strength and strain properties of composite laminates for various applications, including FRP for concrete confinement. Even though these test methods provide specific circumferential properties for composite laminates, none has been adopted in part due to limitations including: a) complex testing layouts, fixtures, or specimens with high machining tolerances; b) seal related problems, resulting in non-uniform radial loading conditions due to frictional effects; c) test fixture configuration, which introduces undesirable bending stresses, change in stiffness or additional costly components; d) size and boundary condition effects, leading to complicated result

interpretations due to gauge lengths or specimen dimensions; or e) high cost, related to the equipment needed to apply high hydraulic pressures or specimen fabrication.

The ICE methodology proposed herein possesses compelling features, including simplicity of test configuration in terms of machining and minimum number of parts, no undesirable end conditions, readily available equipment, and capability to test large scale specimens without added difficulties or cost. Its novelty originates from the lack of moving parts or complex fixtures to transfer load to the specimen, and simultaneously has the ability to apply a truly hydrostatic load. This last feature is consequent of the unique property of water that expands when it changes state of matter from liquid to solid, resulting on an applied load to test specimens.

Ordinary ice I_h , one of the 15 known crystalline phases of water as seen from the phase diagram in Figure 28, reduces its density upon freezing [89]. This negative thermal expansion is attributed to the inherent strong intermolecular interactions. The crystal structure of I_h is composed of tessellating oriented hexagonal rings, with an oxygen atom on each vertex and the edges of the rings formed by hydrogen bonds as represented in Figure 29 (a) [90]. While the hydrogen bonds are shorter in the crystal than in the liquid structure, this locking effect reduces the average coordination number of molecules as the liquid approaches nucleation forming spacious crystal lattices with tetrahedral coordination [91], which can expand in volume up to 9% as depicted in before and after freezing sequence in Figure 29 (b) and (c), respectively. In the presence of restraints, this expansion leads to considerable hydrostatic pressures caused by the molecular forces as

manifested by bursting pipes in winter and concrete cracking due to freeze-thaw cycles. The magnitude of such pressures varies on the crystal structure dependent on the temperature (and density), and can be calculated from the adiabatic bulk modulus, K , which for I_h at -13°C is 7.81×10^{10} dyne/cm², or 7810 MPa [92], this multiplied by its volume change (9%), is equivalent to more than 700 MPa. The ICE methodology discussed herein, builds on these properties to develop a new test method for FRP characterization.

ICE METHODOLOGY FEASIBILITY

First, the research evaluated the feasibility of the proposed ICE method as a test technique by testing small scale cylindrical specimens made from an isotropic material on the basis of: test behavior, cost of testing fixtures, strain magnitude, strain distribution (both longitudinally and diametrically), and failure mode of specimens. For this purpose, cylindrical open-top unlined electrolytic tin plated steel cans with similar aspect ratios, properties summarized in Table 12, were selected from a standard container manufacture to ensure consistency of the product, in terms of constant material properties, and geometric dimensions.

ICE Fixture Design

The ICE methodology rig, illustrated in Figure 30, is configured from two aluminum square end-plates with concentric grooves machined in the inner surface of each plate to accommodate open-ended cylindrical specimens of varying thickness and an O-ring used as an end seal. Plates were drilled with aligned circular holes at each corner and joined

with four high -strength and -stiffness steel studs with threaded ends. The ICE fixture formed a frame designed to restrict movement in the longitudinal direction, allowing displacement only in the radial direction. In addition, the designated top-plate was drilled with a 3 mm diameter hole so as to insert thermocouples to record the internal temperature of the specimen during testing. Given the relative simplicity of the ICE method rig, multiple rigs were manufactured for different specimen diameters and to allow for simultaneous testing.

The assembled rigs were introduced in an environmental chamber to cool the water within the specimen and allow the change of state of matter from liquid to solid. A commercially available vertical-type top-freezer with a 20 liter compressor and -18°C temperature capacity with auto control was selected. This choice was made based on: a) dimensions of internal environmental chamber; b) availability; c) compressor capacity, to provide the required amount of thermal energy in terms of specific heat and enthalpy of fusion; d) internal air temperature system control, since specimens could not be exposed to temperatures lower than the prescribed -15°C ; and e) system precision, to reduce fluctuations and maintain a steady air temperature during testing.

Test Matrix and Setup

A total of 12 cans were tested with two different diameters, namely small “S” and large “L” labeled as “S-1 to -6” and “L-1 to -6” summarized in the first column of Table 13. All specimens were instrumented with three adhesively bonded uniaxial foil strain gauges (SG) applied in the horizontal direction to record circumferential strains with two

different configurations. The first was a cross-sectional configuration, intended to measure the cross-sectional strain distribution at mid section ($\frac{1}{2}$ height of cylinder); three SG were installed at 120° apart from the center of the specimen as seen in Figure 31 (a). The second was a longitudinal layout, aimed to assess the influence of boundary-effects of the ICE methodology rig; three SG were installed and aligned at $\frac{1}{4}$, $\frac{1}{2}$ and $\frac{3}{4}$ of cylinder height as depicted in Figure 31 (b).

Cylindrical can specimens were oriented vertically with the closed bottom-end inserted into the groove of the corresponding ICE method rig plate and filled with regular tap water. The top rig plate, fitted with the thermocouple and an O-ring seal, was then placed on the upper-end of the specimen to then insert the high-strength studs, bolted with equal amounts of torque. Bolts were torqued in a specific diagonal order to guarantee a uniform and symmetric compression of the seal. Subsequent to securing all bolts, the specimen was placed inside the environmental chamber on wooden supports as means to insulate and allow air circulation around the entire test rig. The internal temperature of the specimen, now filled with water, and the air temperature of the environmental chamber were recorded using J-type thermocouples.

Feasibility Results and Recommendations

Feasibility test results are summarized in Table 13 which provides the internal specimen temperature at failure, T_s , and the ultimate tensile circumferential strains at the different locations of the specimen as per notation referred to in Figure 31. The average, standard

deviation (SD), and coefficient of variation (CV) based on three specimens for each strain configuration for the small and samples are also provided.

Test behavior

The loading process using the ICE methodology begins when the specimen's inside temperature reaches an average of -2.99°C , after which, the pressure increases as illustrated in Figure 32, showing the strain-time-temperature response for representative specimens. The rate of strain increase (slope) measured for three different strain gauges located at mid-section of a specimen vary throughout the test, merging towards failure when the strain remains constant. The changes in slope throughout the test appear to coincide with the start- and end-cycles of the chamber's air temperature. Additionally, the non-linear behavior for the measured strain, at any point in time, observed during the tests might be attributed to the material properties of the metal cans as it yields past its elastic zone. Nonetheless, all ICE methodology tests followed the same strain pattern and behavior.

The large recorded air temperature oscillations are most likely due to the performance of the environmental chamber compressor and the automatic control system; this is also reflected in the high CV values for the specimen's internal temperature shown in the last column of Table 13. This poor consistency temperature, may inhibit the speed of ice nucleation and growth, thus changing the internal pressure acting on the specimens. Based on these observations a modified ICE methodology environmental chamber with

higher precision and control systems was selected for the second part of this research, reported in the next section.

Failure mode and strains

The failure mode reflected in Figure 33 was reproduced by all test specimens, where for the smaller diameter cans the metal cracked in shear at mid height, and larger cans experienced extreme plastic deformation as expected from high internal hydrostatic force. The CV for the ultimate strains varied from 0.11% to 5.10% which are low in comparison with typical CV magnitude levels for testing of material properties [45], this reflects the repeatability of the readings, and provides initial evidence for the reliability of the ICE methodology. The circumferential strain measurements from the different stain gauges corresponding to the cross-sectional layout were uniform for both small and large diameter specimens (Figure 32 (a)), where CV values ranged only from 0.16% to 0.62% showing high consistency of ultimate strain measurements. The circumferential strain measurements from the different stain gauges corresponding to the longitudinal configuration followed a similar distribution to the deformation of failed specimens (Figure 33), with a maximum strain at the mid cross-section and significant lower equivalent strains at the $\frac{1}{4}$ and $\frac{3}{4}$ heights cross-section (Figure 32 (b)), where the CV ultimate strain values varies from 0.11% to 5.10%. This distribution appears to be due to the influence of boundary conditions (end plates), hence a prescribe 2:1 aspect ratio for specimens is recommended for the next part of this study in order to avoid boundary conditions affecting strain readings longitudinally, specially at mid-height.

ICE METHODOLOGY FOR FRP CHARACTERIZATION

Cylindrical hand lay-up manufactured GFRP specimens were tested using the ICE methodology configuration described previously, to assess the reliability of the proposed test technique as a method to determine the ultimate circumferential strain of the FRP laminates. The main parameters considered in this part of the research included the internal specimen diameter and laminate thicknesses (based on the number of plies). In this phase, 54 GFRP specimens cast from a single batch of epoxy resin, were hand manufactured with three different reinforcement ratios, namely one-, two-, and three-ply; and three internal diameters, namely 60, 115 and 171 mm. Specimens are identified throughout the study using the “X-Y-Z” format, where: “X” denotes the number of plies (1P, 2P or 3P); “Y” denotes the diameter (60, 115 or 171); and “Z” denotes the specimen number, where a total of five specimens were manufactured with the same number of plies and diameter.

Materials and Specimen Fabrication

The GFRP specimens were manufactured with a commercially available two-part epoxy resin with a minimum specified tensile strength of 50 MPa, elongation of 2.5%, and compressive strength of 80 MPa. The matrix was coupled with high-strength unidirectional sheet density of 596 g/m² typically used in confinement applications made of a glass fiber with a tensile strength of 3,399 MPa, modulus of elasticity of 76.9 GPa, and ultimate elongation of 4.4%, as per manufacture specifications.

The fabrication of open ended GFRP cylinder specimens initiated by placing horizontally the continuous dry glass fiber sheet to then impregnate it manually following a wet-layup technique. Subsequently a PVC-pipe used as a mold with a longitudinal slot and fitted with a removable wedge, was placed on top of one end of the impregnated fiber sheet and rotated circularly so the full length of the fiber sheet coiled around the mold. A ribbed roller was used throughout the process to improve fiber impregnation; Figure 34 summarizes the manufacturing stages. After fabrication, the specimens were placed horizontally on a frame in the air to cure for a period of 48 hours. The molds were released after the curing process by removing the wedges; GFRP cylinders were cut to length using a high precision horizontal band saw. The length of the cylindrical specimens was established using the prescribed aspect ratio of 1:2 from the feasibility section to avoid boundary condition effects from the end plates of the test rig.

The length of the glass fiber sheet reinforcement was equal to the external circumference of the PVC-mold, multiplied by the number of designated plies (1, 2 or 3), plus an additional half circumference. The two fold purpose of the selected specimen design was: i) to force failure on the “no-lap” zone of the specimen (covering half the circumference) with the designated number of plies; and ii) to provide a comparison of strain distribution based on the laminate thickness at a given diametric cross-section between the “no-lap” region and the opposite “lap” region, as illustrated in Figure 35 (a).

Instrumentation and Test setup

The GFRP cylinders were instrumented with horizontally oriented adhesively bonded SG to measure the circumferential strain in two different configurations; the first layout used two SG at mid-section ($\frac{1}{2}$ cylinder height) 180° apart, each 90° from the end of the fiber sheet (overlap), one located in the no-lap and the other in the lap region, as seen from Figure 35 (b). The second configuration (used in only one specimen per design) included six SG: three located at $\frac{3}{4}$, $\frac{1}{2}$ and $\frac{1}{4}$ of cylinder height (H) at the no-lap region, and the other three in the lap zone at the same height locations shown in Figure 35 (c).

Circumferential strain was the only measurement recorded since the no displacement could be permitted in the longitudinal direction based on the design of the ICE fixture. If axial displacements were to occur, since fibers are only in the circumferential direction, it is reasonable to assume that negligible load transfer would occur in the axial direction through the matrix. Additionally in hydrostatic loading conditions, when comparing the tensile radial stress, f_r , with the circumferential, f_θ , based on Equations 9 and 10, it is reasonable to assume the f_r is negligible (hence no radial displacements recorded) in comparison to the f_θ based on the R/t ratio, where p is the internal radial pressure.

$$f_\theta = \frac{pR}{t} \quad (9)$$

$$f_r = p \quad (10)$$

Test specimens were setup similar to the metal cans describe in the previous section, where one end of the GFRP specimen was adhered with waterproof silicon into the groove of the bottom plate and left to cure for 24 hours, due to the double open-end design of the GFRP cylinders. After verifying possible leaks thought the bottom seal or the GFRP jacket, the cylinder was filled with regular water and the setup process continued as prescribed earlier, with the addition of steel stiffening plates to reinforce the exiting aluminum end plates. Note that if leaks were found, a repair was made by either re-doing the bottom seal, or adhering a compatible peel-and-stick 25 mm diameter patch over the leak location on the GFRP jacket. A commercially available chest-type freezer with a 50 liter compressor and -30°C temperature capacity controlled through a high precision thermostat set at a control setting of 3-units to provide an internal air temperature of -15°C , was selected as an alternative environmental chamber due to need of higher precision controls to reduce the previous large fluctuations in air temperature. Temperature inside the specimens was not recorded in this phase due to the presence of the stiffing plates; however it is reasonable to assume that the temperature behavior inside the specimen is similar to that of the metal cans, with the difference that the process might be slower due to the size of the specimens and the insulation provided by the FRP jacket. Additionally, a selected number of tests were recorded with video and audio footage to further understand the test procedure, especially at the failure point.

RESULTS AND DISCUSSION

The results of the GFRP cylindrical specimens are summarized in Table 14, which include the average peak circumferential strain values at the mid cross-section in the no-

lap, ε_{90} , and lap region, ε_{270} ; standard deviation (*SD*); coefficient of variation (*CV*) based on five specimens per design; the average circumferential equivalent lap strain, ε_{e90} , calculated as the product between ε_{270} and the normalized thickness ratio, t_n ; and the ratio ε_{90} to ε_{e90} . Where t_n is the ratio of, the number of plies at the lap zone (where ε_{270} is recorded) to the number of plies at the no-lap zone (where ε_{90} is recorded). The ICE methodology and the experimental results are discussed in the next three sections with respect to: the circumferential strain in terms of variance, distribution and behavior; the failure modes of GFRP cylindrical specimens; and, the evaluation of the test methodology.

Circumferential Strain

The ε_{90} and ε_{270} values increased with increasing diameter, while for 3-ply specimens lower values were recorded than the 1- and 2-ply counterparts with equal diameter. On the other hand, the ε_{90} and ε_{e90} readings were consistently lower when compared to flat coupon specimens of the same GFRP constitutive materials under the same environmental conditions, as seen from the average ultimate strain results based on three samples for 1-, 2- and 3-ply flat coupon tensile tests at -15°C equal to 19271, 17968, and 19238 $\mu\varepsilon$ respectively, as reported in Part B of this study (Table 17), where the mechanical properties of flat GFRP coupons were investigated.

Strain variance

The range of *CV* for the ε_{90} and ε_{270} readings varied from 2.7 to 15.4% (for the 2P-171, and 1P-115 specimens respectively), which are typical *CV* magnitude levels for testing of

material properties [45]. Though it is possible to observe a pattern in the CV values depending on the laminate thickness and diameter, this statistical parameter alone cannot differentiate for possible statistical variances across the different tested specimen designs. A multiple-factor analysis of variance (ANOVA) reported in Table 15, was undertaken assuming a normal distribution with a confidence level of 95% ($\alpha=0.05$) to test for the reliability of the ICE methodology as an experiment method based on the possible statistical significant differences between the recorded ε_{90} values. ANOVA compares the variance due to the ‘between-groups variability’ (*Mean Square Effect, or MS_{effect}*) with the ‘within-group variability’ (*Mean Square Error, or MS_{error}*) via the F test, which tests whether the ratio of the two variance estimates is significantly greater than a critical value, F_{crit} , extracted from the distribution of statistical tables based on the number of degrees of freedom, df , where:

$$F = \frac{MS_{effect}}{MS_{error}} \quad (11)$$

The outcome of ANOVA is to either reject or accept the null hypothesis, which states that there are no mean differences between groups in the results, while still expecting minor random fluctuations in the strain values of the different types of specimen designs when considering a small number of samples per design, as is the case. Under the null hypothesis, the variance estimated based on within-group variability should be about the same as the variance due to between-groups variability. The ANOVA test results in an F value that clearly exceeds the F_{crit} value for the ε_{90} variance in either diameter or laminate thickness (number of plies) groups, therefore rejecting the null hypothesis as there is indeed a significant statistical difference between specimens as their diameters or

laminate thickness change. This is a reasonable outcome, since ultimate circumferential strain levels will differ depending on the curvature (diameter) and laminate thickness (number of plies) as suggested in previous research [23][24][25], and discussed in the previous section. Furthermore, when considering the interaction between all tested specimens (regardless of diameter and laminate thickness), the F value is lower than the F -crit accepting the null hypothesis. Consequently there are no statistical significant differences between the specimen diameter and its laminate thickness, inferring that the sample design is not affected by the test methodology. Thus using the ICE methodology as a test method for characterization is reliable, since its load-to-failure method has no relationship between either or both diameter and laminate thickness of the tested specimens.

Strain distribution

The equivalence ratio $\varepsilon_{90}/\varepsilon_{c90}$, reported in last column of Table 14, varied from -12 to +10%, which assuming a hydrostatic loading condition and based on equilibrium should be equal to 1.0 (0%). The small variation in percentage might be attributed to the use of a normalized thickness, t_n , using the number of plies rather than the actual specific laminate thickness for each specimen at the location where the strain was measured. Nonetheless, it is reasonable to infer a homogeneous cross-sectional strain distribution was experienced in all specimens as determined from the equivalence ratio and as expected from a hydrostatic loading condition.

Results for the circumferential strain measurements from the longitudinal instrumentation layout are reported in Table 16. It is possible to observe that regardless of the failure location, the maximum ultimate circumferential strain was recorded by the mid-height SG, and the strains at $\frac{1}{4}$ and $\frac{3}{4}$ cylinder height were between 4 and 26% lower in magnitude. The strain-time response illustrated in Figure 36 shows a representative specimen's circumferential strain instrumented with the longitudinal layout. Hence, it is reasonable to assume that boundary-conditions are negligible for strain values recorded at the mid-height section of GFRP cylindrical shells.

Strain behavior

The strain behavior was consistently linear elastic till failure as observed from representative strain-time-temperature response provided in Figure 37 for different laminate thickness and diameters; this is in contrast to the non-linear behavior of the metal cans in the feasibility part of this study due to the plasticity of the material. The strain-time slopes differ depending either on the volume of each specimen (given that larger diameter specimens required more time for the water to freeze and consequently apply internal pressure), or on the number of samples tested simultaneously in the environmental chamber (given that more time is needed for the thermal heat transfer from the compressor to take place when numerous samples are tested together). Nonetheless, the gradient remained constant throughout the test exhibiting a linear respond until failure, at which point the strains drop suddenly.

When examining the strain behavior for the full test length starting when the specimen is introduced in the chamber until failure, a distinct singularity of relative sudden drops in strain prior reaching failure was observed. This phenomenon did not always occur, and in some cases more than one drop prior failure was recorded as depicted in Figure 38, which shows two equal specimens one with, and the other without the drops. The reason for the drops, confirmed by video footage, was due to partial leaks through the top seal, probably because the O-rings were not fitted snugly at the start of the test setup. This phenomenon had no impact on the loading or strain-behavior, given the constant parallel gradient after each drop, and with further ice nucleation the seal operated as expected, allowing the pressure to build up to failure.

Failure Mode

The observed loading and failure of the cylindrical GFRP shell specimens was comparable to the those described in the extensive available research studies on FRP-confined concrete [7][8][10]. Partial white discolorations were observed in the top and bottom thirds of some specimens, indicative of plastic flow of the resin, leaving the white glass fibers to carry the lateral load of the expanding ice until failure. Failure was marked by rupture of the GFRP within the middle third section for most specimens, and at lower reinforcement ratios, failure extended longitudinally throughout the height of the specimen, as seen from the 171 mm diameter samples in Figure 39. Shattering sounds of fibers could be heard throughout the test, but were most prominent about 90% of ultimate capacity and continued to increase sporadically till failure, at which point the GFRP jacket ruptured suddenly zipping through the cross-section and migrating longitudinally.

It was noticed that with increasing reinforcement ratio, the failure occurred through the entire cross-section, this is expected as the normalized thickness ratio, t_n , decreases with increasing number of plies resulting in a more uniform cross-sectional thickness. In all cases, the predominant tensile failure type varied between horizontal splitting or angled, codes “S” and “A” per ASTM D 3039 [44], as seen in Figure 40.

Additionally, even though ice is considered to be frictionless, under certain conditions it can stick bonding to any type of surface [90][92]. Nonetheless, it is reasonable to assume that throughout the test no bond between the GFRP jacket and the ice (as the loading medium) occurs since the inside of the specimen is still in a liquid state (water) at the instance of failure concluded from the data and supported with video footage, as discussed in the next section. Thus no bond stresses are developed, which means the GFRP shells are not under a multi-state of stress.

Evaluation of Test Methodology

Water’s ability to expand in volume upon freezing was successfully used as a medium to apply a uniform hydrostatic load on cylindrical samples based on the strain data collected. Additionally, video footage captured an immediate burst of pressurized liquid water at the instance of GFRP jacket failure. Hence at failure, the mid third of the specimen is still liquid, and therefore the top and bottom are partially solid (frozen); this can be explained by ice crystal growth, which has been critically examined [93]. Ice nucleation occurs greatly enhanced at the ends of the specimen (due to the conductive property of the metal end-plates) rather than within bulk water [94]. The nucleation of

hexagonal ice crystals begins at the ends of the specimen, due to the cold bridge formed by the end metal plates. Ice growth then continues to increase from the nuclei forming a layer in the top and bottom of the specimen. As ice grows a small amount of volume increase is generated, which in turn increasing the internal pressure of the specimen applied hydrostatically to the liquid inside of the specimen. This process continues until failure is reached. After failure some of the internal water is lost due to the opening caused by the rupture of the fibers, nonetheless due to the low temperature of the chamber, ice crystals nucleate at the walls of the specimen growing towards the central core. If allowed sufficient time (depending on the diameter of the sample), the inside of the specimen will become solid. Internal ice nucleation and growth during testing was also investigated prior- and post- failure of GFRP specimens and is illustrated in Figure 41. A section of a 171 mm diameter specimen left for a period of 24 hours is shown in Figure 41 (a), it is notable the thickness of the internal ice layer, where the core of the specimen is still a void filled with liquid water, since not sufficient time was provided for the water to freeze. Figure 41 (b) reveals the growth of ice longitudinally, from the ends towards the center of the specimen, it is possible to distinguish different contrast of ice colors, representing the layers of ice growth where the mid-third is clear (void).

The operational technique of the ICE concept results in an efficient and repeatable characterization methodology due to the lack of complex moving parts, which require no maintenance. The capacity to undertake mass-testing is plausible since fabrication of the test rig is simple and involves few parts, while large capacity industrial freezers are readily availability as environmental chambers. The lack of end grips, as those found in

flat coupon tensile tests, avoids special specimen preparation and prevents undesired end conditions influencing test outcomes. This special feature prompts this methodology to effectively and fully engage any type of composite system. The main limitations of the ICE method lie in the maximum expansion of ice, and the maximum hydrostatic pressure that can be exerted, which is dependent on the temperature (and density) of water. Both of these limitations do not prevent the ICE method as means to characterize FRP composites since I_h can expand up to 4.5% radially in 3-D, and can achieve pressures of approximate 700 MPa based on its bulk modulus at -13°C [92].

The ICE methodology is limited only to materials that are not affected by temperatures below -5°C , at which ice nucleation and growth is sufficient. An alternative limitation of the proposed method might be the test length, which is much higher than current ones. Nonetheless, the test-time might be significantly reduced by adding pre-cooled water or freezing specimens from the inside-out (this would require additional fixtures). Alternative methods to speed the required amount of thermal energy in terms of specific heat and enthalpy of fusion might be used; however the method to achieve this ought not to expose the specimen to extreme low temperatures during testing, as the mechanical properties may degrade significantly. Additionally, internal pressure measurements were not recorded as it was not part of the objectives in the development of the ICE methodology. Nevertheless, this aspect might be easily adjusted by using pressure gauges (given that at failure, the inside of the specimens is still liquid water), hence obtaining stress-strain relationships for the composite sample. Alternatively, the ICE methodology's environmental chamber could be coupled with a universal test frame, thus

being able to read the axial load (obtaining the internal pressure), but also provides the possibility to apply a bi-axial state of stress in the jacket, extending the use of this method to test FRP laminate-sheets with other fiber orientations such as $\pm 45^\circ$.

CONCLUSIONS

In the first part of the study, the feasibility of the ICE methodology as a concept to characterize the ultimate circumferential (hoop) strain in cylindrical metal cans by means of the unique property of water, that expands when it changes state of matter from liquid to solid, to apply a uniform internal hydrostatic pressure was successfully assessed. Despite the poor control systems in the environmental chamber used, cylindrical metal specimens experienced repeatable strain distributions with reproducible failure modes prompting to use the method with FRP composite specimens at a 2:1 aspect ratio.

The objectives in the second part of this study were to assess the applicability of ICE methodology for FRP characterization, understand the loading processes, strain levels and distribution, failure modes, and to provide statistically meaningful results. The evaluation of ultimate circumferential strains of different manufactured manual lay-up cylindrical GFRP shells with varying diameters and laminate thicknesses concludes the following:

1. GFRP cylinders followed a linear elastic behavior till failure, were specimens failed in the middle third section in pure tension.

2. The loading mode was hydrostatic (confirmed with video footage, as water bursted out through the GFRP jacket at the instant of failure).
3. Ultimate circumferential strain values increased with increasing diameter, while being consistently lower when compared to similar GFRP flat coupon specimens under the same environmental conditions.
4. The reliability of the proposed test method, and repeatability of recorded strain measurements was confirmed, as concluded from ANOVA test results.

The proposed ICE methodology to characterize circumferential strain of cylindrical GFRP laminates provides an effective test technique without undesired end grip conditions or complex parts that can be further developed by laboratories, manufactures, and specifiers benefiting from advancing this simple and efficient method. Additionally this characterization method opens the opportunity to test other FRP composite configurations made of different matrix materials or fiber orientations.

PART B: EXPERIMENTAL EVALUATION OF FRP STRAIN EFFICIENCY USING ICE METHODOLOGY

BACKGROUND

The confinement action of concrete provided by externally-bonded FRP laminates on circular concrete columns is based on a well-understood mechanism [8][23][95], which is a result of the lateral expansion of concrete under axial load. With increasing axial stress, corresponding lateral strain increases engaging the confining jacket, which develops a tensile circumferential (hoop) stress in the FRP jacket balanced by a uniform radial pressure reacting against the concrete lateral expansion. Through equilibrium condition and deformation compatibility in the cross-section, the confining action in the FRP-confined concrete can be schematically depicted in Figure 42, where the radial confining pressure, p , exerted by the FRP is given by:

$$p = \frac{2f_{\theta}t}{D} = \frac{2E_{frp}\varepsilon_{\theta}t}{D} \quad (12)$$

where, f_{θ} is the tensile circumferential FRP stress, proportional to the circumferential FRP strain, ε_{θ} ; t the total FRP thickness; D the diameter of the confined concrete column; and E_{frp} the young modulus of elasticity of the FRP laminate. The maximum confinement pressure exerted by the FRP is determined when the tensile circumferential strain in the FRP ruptures. This failure criterion is assumed by existing theoretical models and design guidelines to predict the ultimate capacity of FRP confined concrete, where the value for such critical parameter - the ultimate tensile strain - is commonly obtained from direct tensile tests [44][80].

However, extensive research has suggested that ultimate FRP tensile strain determined experimentally in direct tension could not be reached at the circumferential rupture of FRP jackets confining concrete cylinders [23][25]. Available experimental data has shown that the strain efficiency factor, κ_{ε} , expressed as the ratio of ultimate tensile circumferential strain in the FRP, $\varepsilon_{\theta u}$, to the failure strain observed in direct tension, ε_{fu} , varies substantially from 0.58 to 0.91 [24][26]. Design values for κ_{ε} of 0.5 and 0.7 for Carbon and Glass FRP jackets respectively, have been previously suggested [95][96]; while ACI design guidelines recommend, irrespective of material and diameter, a value of κ_{ε} equal to 0.55 [11]. These design coefficients are calibrated based on average values derived from large experimental databases of FRP using small cylinders, medium-, and large-scale columns. Several reasons for this phenomenon have been suggested [23][25][95], including: a) heterogeneity and deformations in cracked concrete that may cause local stress concentrations in the FRP jacket; b) multi-state of stresses in the FRP jacket; c) quality of the execution in terms of fiber alignment, presence of voids, or

surface imperfections; d) size effect when applying multiple layers; and e) curvature of the FRP jacket. Nonetheless, none of the aforementioned explanations has been experimentally confirmed.

APPROACH

To evaluate the strain efficiency factor, in addition to the cylindrical hand lay-up manufactured GFRP specimens tested for the validation of the ICE methodology in Part A, a total of nine GFRP flat coupon specimens with one-, two-, and three-ply, were tested with the purpose of determining the ultimate tensile strain and elastic modulus for use as a benchmark, as summarized in Table 17. Coupons were manufactured with identical constituent materials as the cylindrical GFRP shells, and tested under the same environmental conditions. Since the physical and mechanical properties of FRP resins are influenced based on their glass-transition temperature T_g [97][98]; such properties have been specifically investigated for the GFRP composite used in this study, and were found to degrade outside the temperature range from -15 to 36°C. The selected lower-bound temperature (-15°C) also used with the ICE methodology, should be representative of any type of FRP system under service temperature by assuming that both test methods are independent of the type of constituents and temperature level [99].

Specimen Preparation

Flat coupon specimens were prepared in accordance to standard ASTM D 3039 [44] using a horizontal two-part sandwich panel mold with a non-sick inner surface of overall width dimensions 500 by 330 mm length (in the fiber direction), following a wet-layup

technique. The GFRP panel was released after 72 hrs from the mold and individual coupons were cut by means of a water-lubricated precision diamond circular saw to the final dimensions specified in Figure 43. The final step in the preparation process involved bonding aluminum tabs using a commercially available high strength adhesive. Tabs were pre-stamped to create small dents on the surface to improve the mechanical grip between the tab and the sanded surface of the GFRP coupons, allowing better load transfer to engage the GFRP laminate during testing.

Test Setup and Instrumentation

GFRP coupon specimens were tested according to ASTM D 3039 [44], loaded at a displacement rate of 0.025 mm/min using a servo-hydraulic MTS810 universal test frame coupled with an environmental chamber set at average temperature of -15°C and 0% humidity; where specimens were allowed to condition for a period of five minutes prior loading. Mechanical wedge-type grips were used to engage the specimens by applying a uniform pressure on the aluminum tabs. The load was measured via an internal 50 kN capacity load cell, while strains were recorded using two uniaxial foil strain gauges (SG) protected with a plastic insulating coating and adhesively bonded at the centre of both sides of each coupon. Figure 44 (a) and (b) illustrate the test setup, and specimen instrumentation respectively.

RESULTS AND DISCUSSION

Results for the GFRP flat coupon tensile tests are summarized in Table 17 including: ultimate tensile strength, f_{tu} ; tensile chord modulus, E^{chord} ; last measured and computed

ultimate tensile strains, ε_{fu} and ε^*_{fu} , respectively; and the failure type according to ASTM D 3039, where “A” and “S” refers to angled or longitudinal splitting, respectively. The average, standard deviation (*SD*), and coefficient of variance (*CV*) for the aforementioned values based on three specimens per design are also provided. The E^{chord} value was computed according to ASTM between the longitudinal strain range starting and ending at 1000 and 3000 $\mu\varepsilon$ respectively. The strain values were based on the average of the two SG readings, which were very close to each other.

Direct Tensile Tests

The ultimate axial tensile force carried by flat coupons increased linearly with increasing number of plies; therefore no relative slip between plies occurred during testing as reflected from the average f_{fu} for one-, two- and three-ply coupons that are within a ± 48 MPa range. The average E^{chord} varied from 89.7 to 92.4 GPa, while the average last measured ε_{fu} fluctuated within a ± 652 $\mu\varepsilon$ range comparable to the average computed ε^*_{fu} values as seen from the stress-strain response in Figure 45 for representative samples. Since the reliability of the measured SG readings near to or above 20000 $\mu\varepsilon$ was reduced, the computed ultimate strain data point is used as the benchmark for the strain efficiency factor discussed in the next section. The *CV* percentages, varying from 1.9 to 11%, are typical low levels for material characterization [45]; further, the repeatability of the results is reflected in the outcome of the single factor ANOVA test summarized in Table 18, assuming a normal distribution with a confidence level of 95% ($\alpha=0.05$). The null hypothesis, which states the results for the three groups of f_{fu} data values are the same (one-, two-, and three-ply coupons), was confirmed given that the *F-value* did not exceed

the *F-critical* value at a probability of 78%, reflecting the reliability of the results provided herein. The axial stress-strain response was perfectly linear elastic to failure as expected and illustrated in Figure 45, where GFRP coupons failed suddenly rupturing in tension. The failure type was predominantly mixed between angled and/or longitudinal splitting, located for all tests within the middle of the specimen gauge length as seen in Figure 46, which shows the typical failure of representative coupon samples.

Strain Efficiency Factor

The results for strain efficiency factors are summarized in the third column of Table 19 for different diameter specimens, where κ_ϵ is expressed as the ratio of the average ultimate tensile circumferential strain in the GFRP cylinders, $\epsilon'_{\theta u}$ (Table 14), to the average computed tensile failure strain in GFRP flat coupons, ϵ'_{fu} . The relationship between κ_ϵ and the diameter, D , appears to increase logarithmically as reflected in Figure 47 where increasing curvature (diameter) yields higher κ_ϵ ratios. The change in strain efficiency is most significant at small curvatures ($D < 60$ mm), as noticed by the higher gradient in slope of the best-fit curves for different laminate thicknesses for which the R^2 values are 0.97, 0.89, and 0.86 for one-, two-, and three-ply, respectively. While at higher curvatures ($D > 171$ mm) the effect on strain efficiency is minor, as the gradient in the curves is reduced. Nonetheless, the ultimate tensile strain observed in the flat coupon GFRP specimens was never reached in the cylindrical counterparts as κ_ϵ varied from 0.45 to 0.89. The relationship between κ_ϵ and D seems unaffected by laminate thickness, as it is possible to observe the parallel trend between the different best-fit curves, even though it is clear that the higher the number of plies, the lower the κ_ϵ as discussed in next

paragraph. The overall laminate thickness is the product between the number of plies, and the fiber-sheet density; which depend on the material, strengthening design, and the FRP application [100][101]. For GFRP in confinement applications a 600 g/m^2 uni-directional sheet density is typically employed, resulting in a laminate with a fiber content ranging from 50 to 80 % by weight [102].

The relationship between the laminate thickness and κ_ε for the same diameter specimen reduces as the number of plies increase. The difference between one- and two-ply appears to be negligible, where similar changes in strength efficiency have been previously reported between one- and two-ply of CFRP laminates applied to different corner radii [103]. The reduction in κ_ε due to laminate thickness appears to be higher at three-ply, this could be attributed to the in-plane strain distribution based on the theory of curved beams [104]. As the laminate thickness increases, the FRP jacket might no longer be treated as a thin-wall cylinder where $t \ll R$ and strains are constant throughout the jacket thickness. In a thick-wall cylinder where $t < R$, the strains are higher at the inner surface than the outer, location at which the reported strain measurements are recorded. Thus, no conclusive evidence can be drawn from the possible effect that additional laminate thicknesses might have on κ_ε . Further reasons previously suggested [25][26], which might produce this reduction in ultimate strain with increasing laminate thickness include fiber misalignment, and waving caused during the specimen preparation.

Design Guidelines and Parameters

Since both thickness and diameter of FRP jacketing systems have an effect on the strain efficiency, the following ratio (equation 13) may provide a normalized parameter to capture their combined effect on κ_ϵ :

$$\frac{2t'}{D} = \frac{t'}{R} \quad (13)$$

where the laminate thickness is normalized, t' , and made equal to the number of plies (1, 2, or 3) since ply density is constant for all samples, and R is taken as the inner radius of the cylindrical GFRP shells. The same set of results is illustrated separately by specimen diameter, Figure 48 (a); number of plies, Figure 48 (b); and both combined, Figure 48 (c); where the relationship (represented by the solid curve with an R^2 value of 0.69) is non-linear, and as t'/R increases, κ_ϵ decreases. Comparable theoretical and experimental trends have been reported for different FRP materials applied to confine concrete cylinders [105].

It is possible to identify three t'/R regions as depicted in Figure 48 (c), which suggest that different κ_ϵ values might be used for design purposes depending on the externally bonded FRP application. The suggested regions are explicitly applicable to the relationship derived from the results obtained in Table 19, and based on threshold values determined conservatively from design guidelines of RC concrete and externally bonded FRP composites. The first region where $t'/R < 1/125$, covers FRP structural aspects such as

wrapping circular columns, here the effect of curvature on κ_ε is minor given that strain efficiency is higher than 0.9. The threshold value is evaluated by assuming one-ply reinforcement and the minimum diameter of a circular column, assumed to equal 250 mm. Minimum sizes for compression members were eliminated after the 1971 ACI-318 code [106], nonetheless the assumed dimension, which is in accordance with requirements set by other codes [107], can be evaluated by accounting for minimum required steel reinforcement, spacing, concrete cover and geometry design. The second region where $t'/R > 1/13$, covers FRP detailing aspects of wrapping applications where the laminate is bent around chamfers of non-circular elements, here the effect of curvature on κ_ε is major, as the strain efficiency drops to become less than 0.5. The threshold value is established assuming one-ply reinforcement and the minimum recommended chamfer radius equal to 13 mm [11]. The third region, $1/125 < t'/R < 1/13$, is transitional between the previous two and shows the non linear descending relationship between the strain efficiency and t'/R .

The κ_ε presented herein, which is valid for hydrostatic loading conditions, represents one of two components of the κ_ε used in designing FRP laminates [25]. The second component not discussed in this study, accounts for the effect of non-uniform cross-sectional strain distribution in the FRP jacket caused by cracking of the concrete. Therefore, the effect of concrete expansion on κ_ε needs to be explored to understand the absolute ultimate tensile FRP strain capacity for confined concrete applications. This effect will depend on the confining effectiveness of FRP jackets, which will vary according to column cross-section. For non-circular sections the confining effectiveness

is reduced when compared to circular sections, where the reduction is based on the aspect ratio of the cross-section [108][109]. Consequently, the proposed κ_ϵ values where $t'/R > 1/13$, may not be applicable to non-circular sections due to the non-hydrostatic load condition, as the least amount of concrete dilation occurs at the corners when it is axially compressed. Nevertheless, a reduction of 0.5 between circumferential and direct tensile strength for one-ply CFRP laminates bent around a 13 mm corner radius has been previously reported [110], comparable to the strain reductions suggested in this study. Based on the foregoing discussion it is reasonable to assume that the ultimate FRP tensile strain, ϵ_{fu} , currently reported from direct tension tests, is a function of radius of curvature, R , and laminate thickness (dependent on the number of plies, n , and the fiber sheet density, ρ):

$$\epsilon_{fu} = f(R, n, \rho) \quad (14)$$

It should be noted that in bond-critical applications, such as “U-wraps” on beams for shear strengthening, the effective strain is calculated using a bond-reduction coefficient, κ_v , where the anchorage length is considered the critical design parameter. The assumptions made here should be treated as preliminary guidance for the evaluation of κ_ϵ only.

CONCLUSIONS

In this study, the evaluation of the experimental data reported in part A, which tested cylindrical GFRP shells under hydrostatic load conditions using the ICE Methodology,

was compared to equivalent flat coupon tensile tests to determine the influence of curvature and thickness on the strain efficiency, κ_e , of GFRP composite laminates. Based on the experimental evidence, it is possible to conclude the following:

1. The ultimate FRP tensile strain, ε_{fu} , is a function of radius of curvature and laminate thickness, for a given fiber ply density and number.
2. The ultimate direct tensile strain observed in GFRP coupons was never reached by the cylindrical counterparts.
3. Larger diameter GFRP specimens, yield higher strain efficiency ratios.
4. Increasing the GFRP laminate thickness, for the same diameter specimen, reduces the strain efficiency.
5. Three regions determined by the ratio of nominal laminate thickness to radius of curvature, t'/R , are suggested for design purposes where different strain efficiency factors might be used depending on the application of the cylindrical GFRP composite tested: one region covers FRP wrapping circular columns with minor detrimental effects to strain experienced; the second region covers detailing FRP laminates bent around chamfer radii of non-circular columns and major detrimental effects to strain are experienced; and the third is the transitional region between the other two and shows the non linear descending relationship between the strain efficiency and t'/R .

FURTHER RESEARCH

The ICE methodology for FRP characterization opens a possibility of further research which can respond to numerous fundamental unanswered questions regarding the behavior of FRP composites used in infrastructure rehabilitation, such as:

- Mechanical characterization of brittle based composite matrices, such as the fiber reinforced cement-based composite (FRC) developed in Study 1.
- Characterization properties of other FRP materials, such as Carbon FRP (CFRP) or Basalt FRP (BFRP).
- Studying the behavior of FRP used for confined concrete with alternative non-circular cross-sectional shapes including: square-sections (specially evaluating the corners); and hollow sections (understand why RC hollow columns fail outwards when strengthen with FRP).
- Assessing the influence of fiber alignment and quality control, by comparing prefabricated FRP tubes with manual lay-up FRP with the same constituent materials.
- Researching the influence of circular jackets with multi-ply reinforcement, since current design values used for multi-ply confinement applications are based on single-ply coupon properties (as provided by manufactures). While developing design coefficient factors of multi-ply applications, relative to single-ply tests.

- Considering the effect that the overlap might have in externally bonded FRP by instrumenting the over-overlap zone and re-designing FRP cylinder specimens for this purpose with different overlap lengths.
- Evaluating the behavior of hybrid-fiber sheets due to the recently increase in the use of hybrid-FRP. When using different materials with significantly different properties in the same fiber sheet, currently it is unclear what design parameters ought to be used.
- Assessing the behavior of externally bonded FRP made from different fiber orientations, such as sheets with fibers in the 0, ± 45 and 90 ° directions.

Table 12 – Cylindrical metal can properties.

Specimen type	S	L
Wall thickness, t (mm)	0.267	0.267
Internal Diameter, D (mm)	53.98	103.19
Height, H (mm)	73.03	141.29
aspect ratio, D/H	0.739	0.730
t/R ratio	0.0049	0.0026

Table 13 – Results of cylindrical metal cans tested with ICE methodology.

Cross-sectional strain configuration ($\mu\epsilon$)				
Specimen ID	SG-A	SG-B	SG-C	T_s ($^{\circ}\text{C}$)
S-1	22987	23027	23096	-2.49
S-2	23106	23026	22841	-3.54
S-3	23087	22961	23082	-4.21
Average	23060	23005	23007	-3.41
SD	64	38	143	0.87
CV (%)	0.28	0.16	0.62	25.40
L-1	23085	22880	23086	-1.32
L-2	22969	22906	22975	-4.44
L-3	22856	22994	23086	-3.30
Average	22970	22927	23049	-3.02
SD	114	60	64	1.58
CV (%)	0.50	0.26	0.28	52.28
Longitudinal strain configuration ($\mu\epsilon$)				
Specimen ID	SG-1	SG-2	SG-3	T_s ($^{\circ}\text{C}$)
S-4	13270	22959	12721	-2.29
S-5	12481	23012	12364	-2.91
S-6	13801	23122	13153	-2.33
Average	13184	23031	12746	-2.51
SD	664	83	395	0.35
CV (%)	5.04	0.36	3.10	13.82
L-4	15864	22963	15819	-2.49
L-5	15760	23013	15801	-2.28
L-6	n/a	22992	14452	-4.29
Average	15812	22990	15357	-3.02
SD	73	25	784	1.10
CV (%)	0.46	0.11	5.10	36.58

Table 14 – Results of cylindrical hand lay-up manufactured GFRP specimens tested with ICE methodology, strains measured at mid-height of specimen.

Diameter, D (mm)	Statistics Parameter	ε_{90} ($\mu\varepsilon$)	E_{270} ($\mu\varepsilon$)	ε_{e90} ($\mu\varepsilon$)	$\varepsilon_{90}/\varepsilon_{e90}$
1 ply, $t_n = 2:1$					
60	AVERAGE	10529	5650	11301	0.93
	SD	1402	854	1708	
	COV (%)	13.3	15.1	--	
115	AVERAGE	14917	6756	13512	1.10
	SD	2296	966	1933	
	COV (%)	15.4	14.3	--	
171	AVERAGE	16125	7786	15573	1.04
	SD	941	1069	2138	
	COV (%)	5.8	13.7	--	
2 plies, $t_n = 3:2$					
60	AVERAGE	10987	7067	10601	1.04
	SD	462	522	784	
	COV (%)	4.2	7.4	--	
115	AVERAGE	16127	11272	16908	0.95
	SD	1473	1294	1941	
	COV (%)	9.1	11.5	--	
171	AVERAGE	16500	10103	15155	1.09
	SD	447	782	1173	
	COV (%)	2.7	7.7	--	
3 plies, $t_n = 4:3$					
60	AVERAGE	9149	7390	9854	0.93
	SD	838	1107	1476	
	COV (%)	9.2	15.0	--	
115	AVERAGE	14166	9762	13016	1.09
	SD	1619	995	1326	
	COV (%)	11.4	10.2	--	
171	AVERAGE	14136	12021	16028	0.88
	SD	509	1333	1778	
	COV (%)	3.6	11.1	--	

Table 15 – ANOVA three-factor with replication test for ultimate circumferential strains
at mid-section

Source of Variation	SS	df	MS	F	P-value	F crit
Sample (Diameter)	287671124	2	143835562	55.01	8.2E-13	3.20
Columns (Plies, laminate thickness)	49827319	2	24913659	9.53	0.000355	3.20
Interaction	16670833	4	4167708	1.59	0.192376	2.58
Within	117666501	45	2614811			
Total	471835778	53				

Table 16 – Results of cylindrical hand lay-up manufactured GFRP specimens tested with
ICE methodology, strains measured at $\frac{3}{4}$, $\frac{1}{2}$ and $\frac{1}{4}$ of cylinder height.

Specimen ID	Strain measurement ($\mu\epsilon$)					
	ϵ_{90}			ϵ_{180}		
	SG-1A	SG-2A	SG-3A	SG-1B	SG-2B	SG-3B
1P-60-1	10544	10950	10943	5945	6185	5634
1P-115-5	10970	13277	11218	5839	6661	5955
1P-171-1	13941	15622	13144	6362	8589	7728
2P-60-5	9499	10986	9178	7328	7699	6290
2P-115-1	13921	14796	13780	10855	12690	11034
2P-171-5	14105	16599	15649	n/a*	9738	8773
3P-60-1	n/a*	9069	7371	5555	6864	5079
3P-115-2	13431	15513	13627	8816	9697	8933
3P-171-5	13636	14238	12768	n/a*	13492	n/a*

*Measurement not available (n/a)

Table 17 – GFRP flat coupon tensile test results.

Specimen ID	Ultimate tensile strength f_{fu} (MPa)	Tensile chord modulus E^{chord} (GPa)	Last measure tensile strain ϵ_{fu} ($\mu\epsilon$)	Computed ultimate tensile strain $\epsilon^*_{fu} = f_{fu} / E^{chord}$ ($\mu\epsilon$)	**Failure type
1-ply					
1P-A	1899	86.1	19100	22047	A+S
1P-B	1572	93.3	n/a*	16854	S
1P-C	1769	92.9	19442	19051	S
Average	1747	90.8	19271	19316	
<i>SD</i>	165	4.0	241		
<i>CV</i> (%)	9.4	4.4	1.3		
2-ply					
2P-A	1805	90.2	18160	20005	A
2P-B	1835	93.4	18813	19659	A+S
2P-C	1496	93.5	16932	16000	A+S
Average	1712	92.4	17968	18553	
<i>SD</i>	188	1.8	955		
<i>CV</i> (%)	11.0	2.0	5.3		
3-ply					
3P-A	1663	88.4	19227	18808	S
3P-B	1913	90.0	19206	21505	A+S
3P-C	1845	91.6	19280	20145	S
Average	1807	90.0	19238	20153	
<i>SD</i>	129	1.7	38		
<i>CV</i> (%)	7.2	1.9	0.2		

* Measurement not available (n/a)

**According to ASTM D3039

Table 18 – ANOVA single factor test for flat coupon f_{fu} results.

Source of Variation	SS	df	MS	F	P-value	F crit
Between Groups	13866	2	6933	0.26	0.78	5.14
Within Groups	158062	6	26343			
Total	171929	8				

Table 19 – Average ultimate tensile strain for cylindrical specimens and flat coupons.

Nominal laminate thickness $t' = \text{no. of plies}$	Average ultimate tensile strain ($\mu\epsilon$)	Strain efficiency factor $\kappa_c = \epsilon'_{\theta u} / \epsilon'_{fu}$	t'/R
$D = 60 \text{ mm}$			
1	10529	0.57	0.033
2	10987	0.59	0.067
3	9149	0.45	0.100
$D = 115 \text{ mm}$			
1	14917	0.81	0.017
2	16127	0.87	0.035
3	14166	0.70	0.052
$D = 171 \text{ mm}$			
1	16125	0.88	0.012
2	16500	0.89	0.023
3	14136	0.70	0.035
$D = \infty \text{ mm}$			
1	19316	1.00	0.00
2	18553	1.00	0.00
3	20153	1.00	0.00

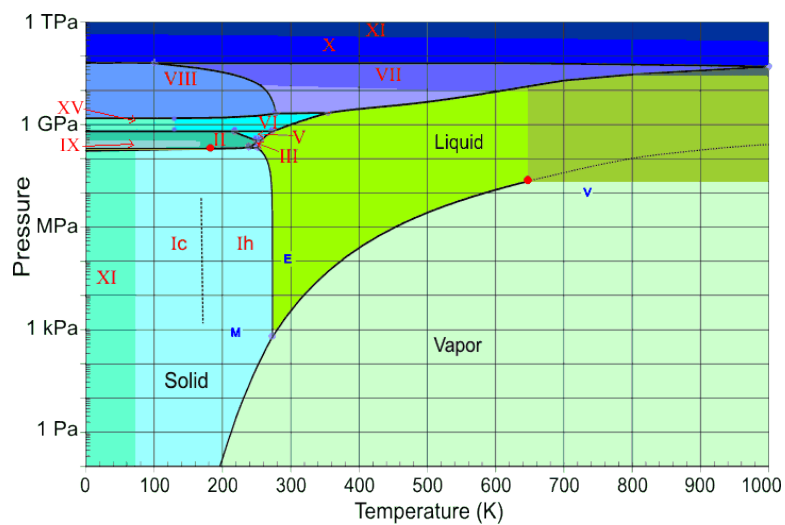


Figure 28 – Phase diagram of water. Dash line represents average working temperature of ICE methodology environmental chamber.

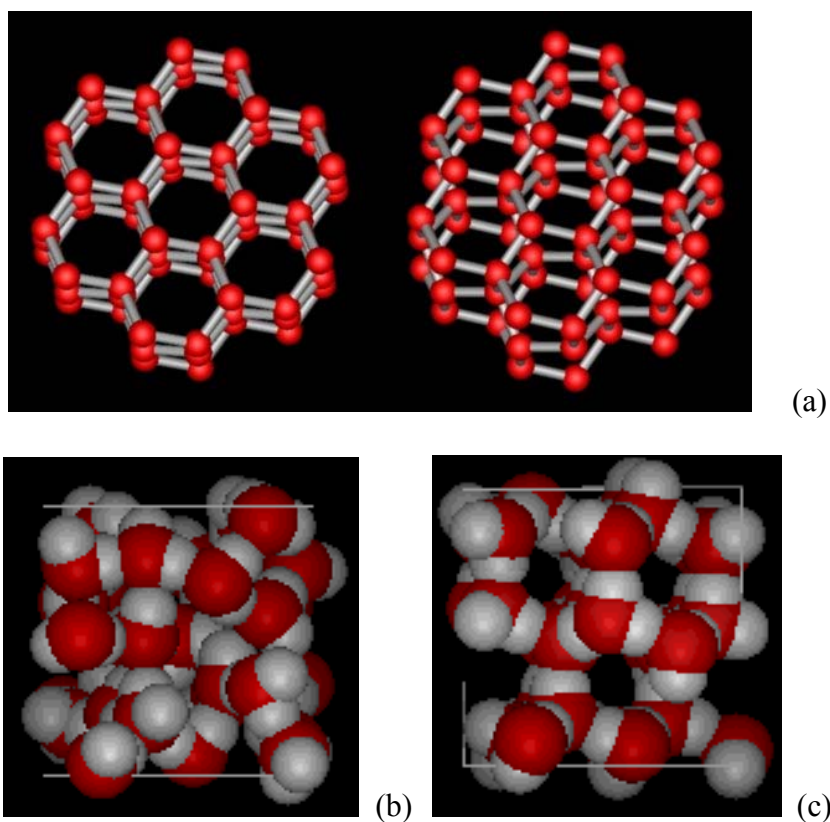


Figure 29 – General ordinary ice crystal structure (a), ice prior freezing (b), ice after freezing (c).

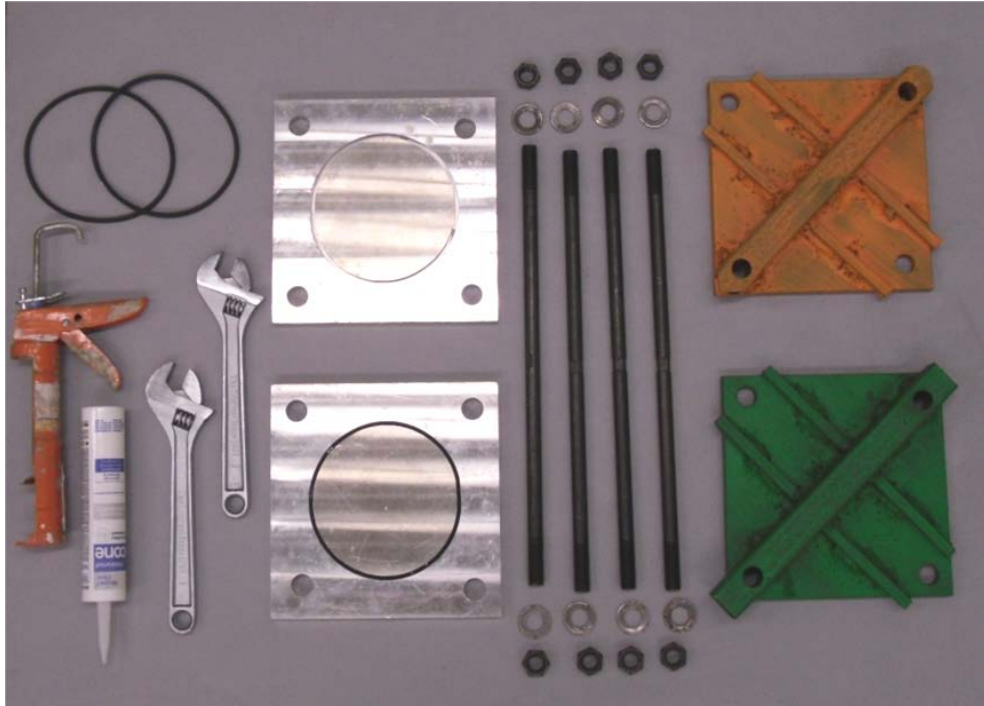


Figure 30 – ICE methodology rig components.

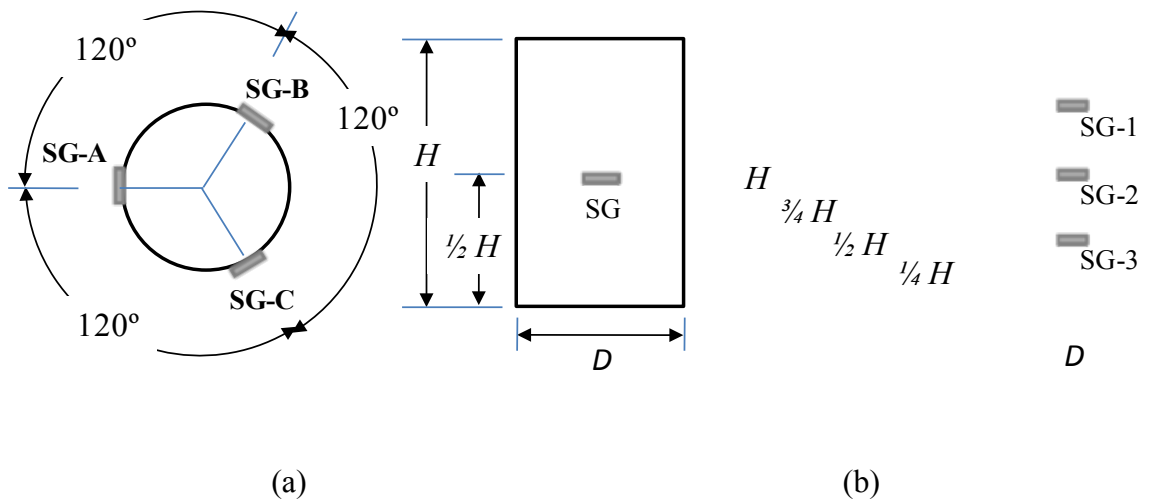


Figure 31 – Strain gauge (SG) configuration for metal can specimens: cross-sectional layout (a); longitudinal layout (b).

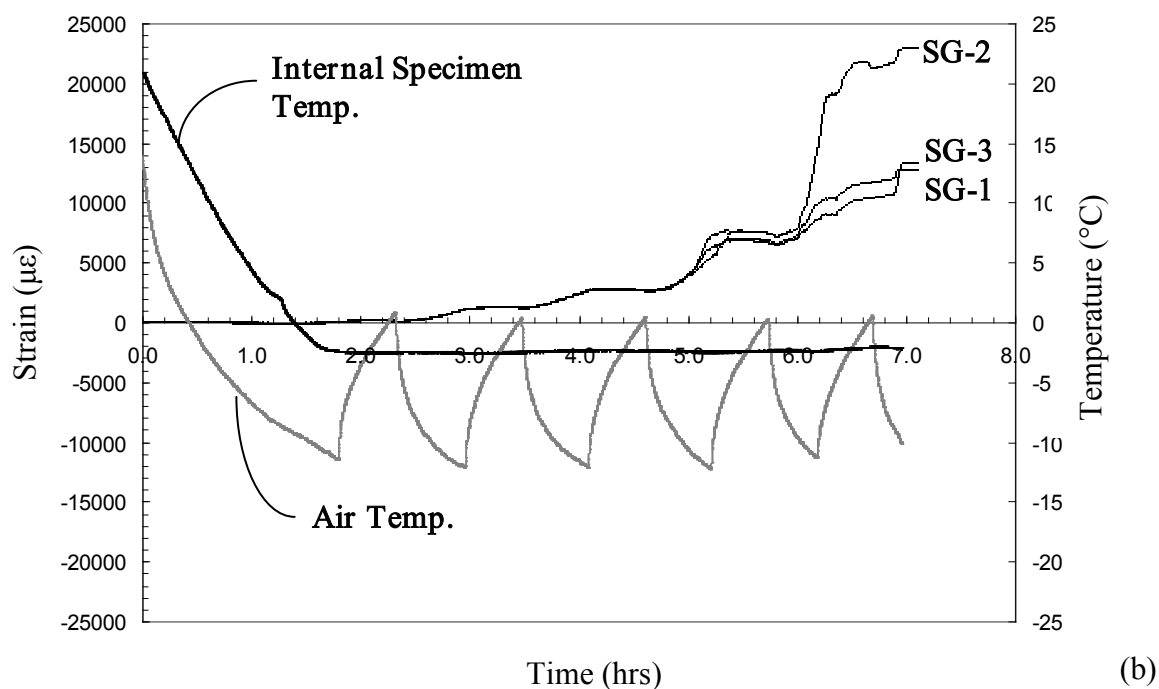
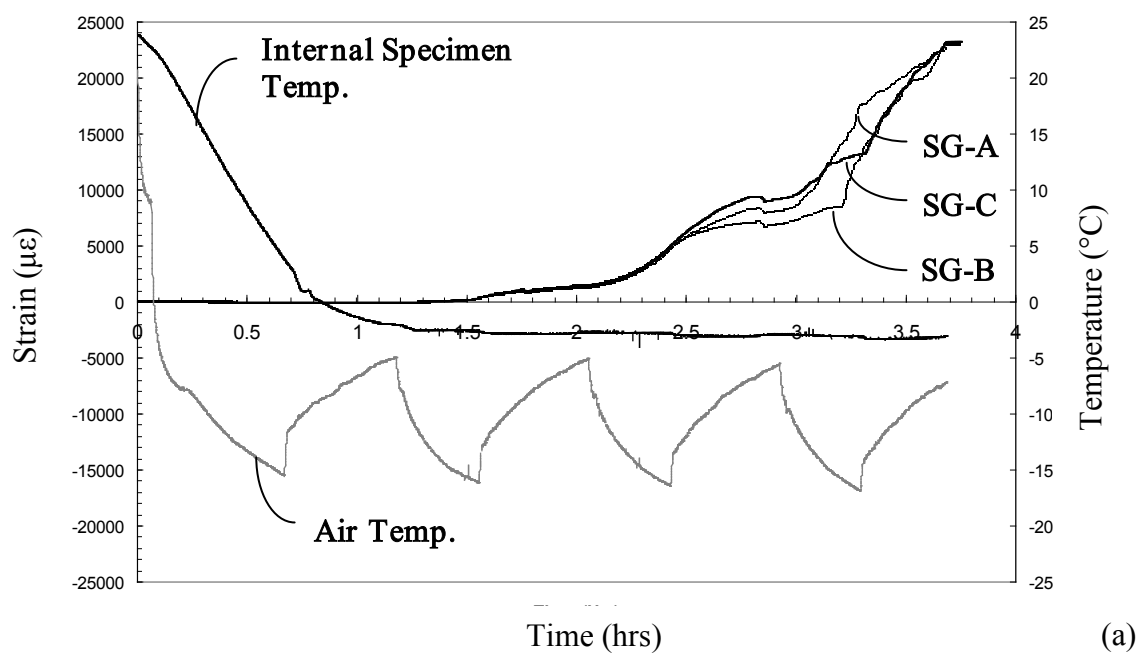


Figure 32 – Strain-time- temperature response of a representative metal can specimen, (S-2) with cross-sectional strain layout (a), and (S-4) with longitudinal strain layout (b).



(a)



(b)

Figure 33 - Representative failure mode of metal cans with large diameter (a); small diameter (b).



Figure 34 – Hand lay-up GFRP cylinder specimen fabrication process.

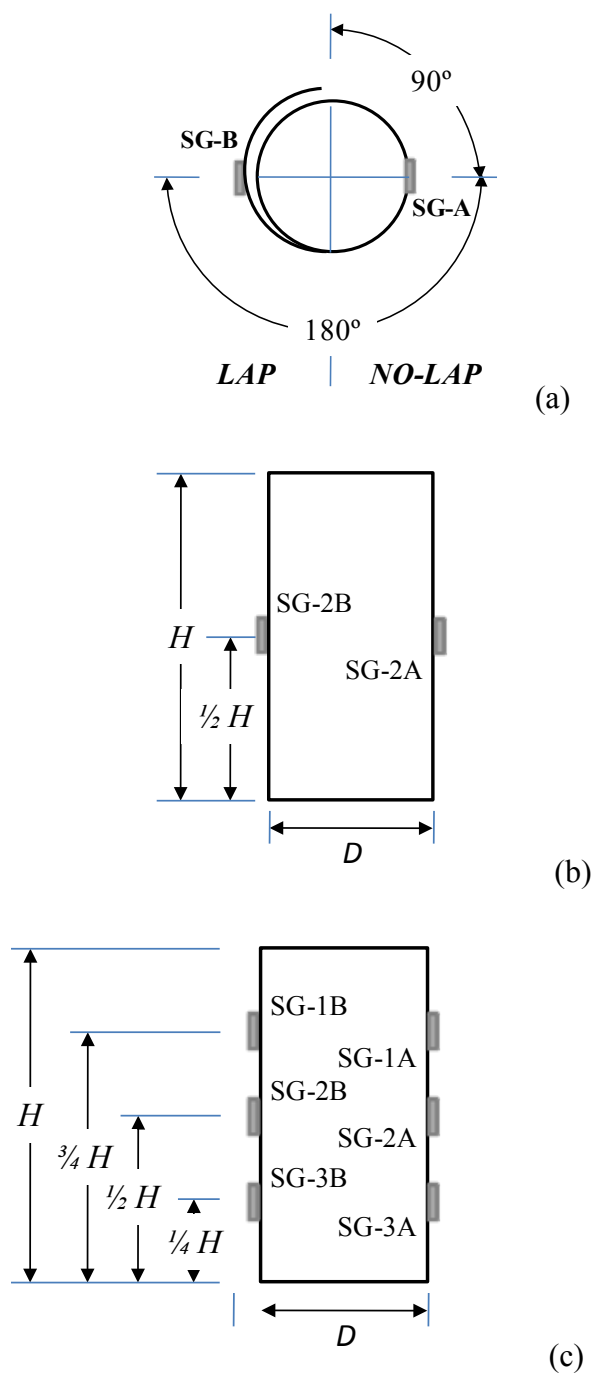


Figure 35 – Strain gauge (SG) configuration for GFRP specimens: plan view (a); front view for layout of two SG (b); and six SG (c).

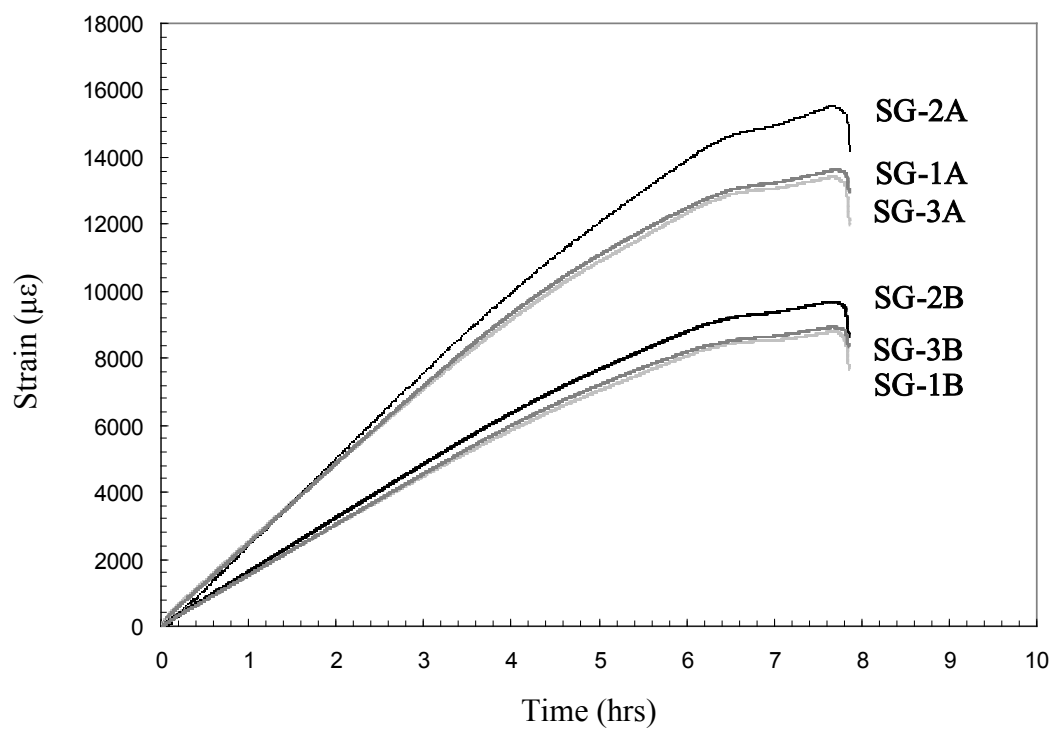
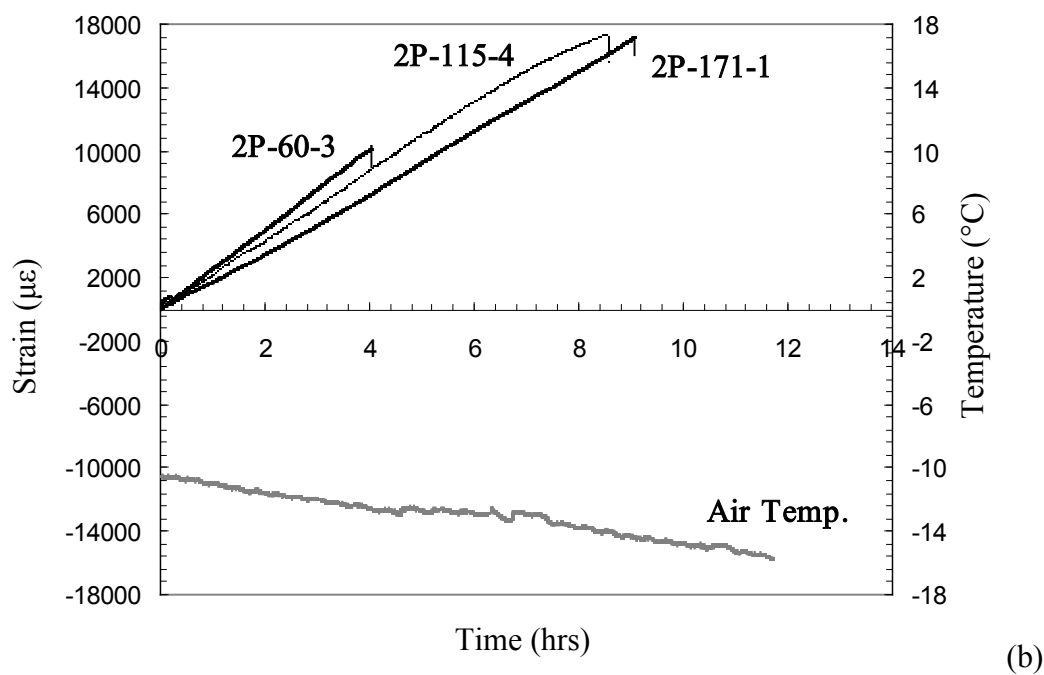
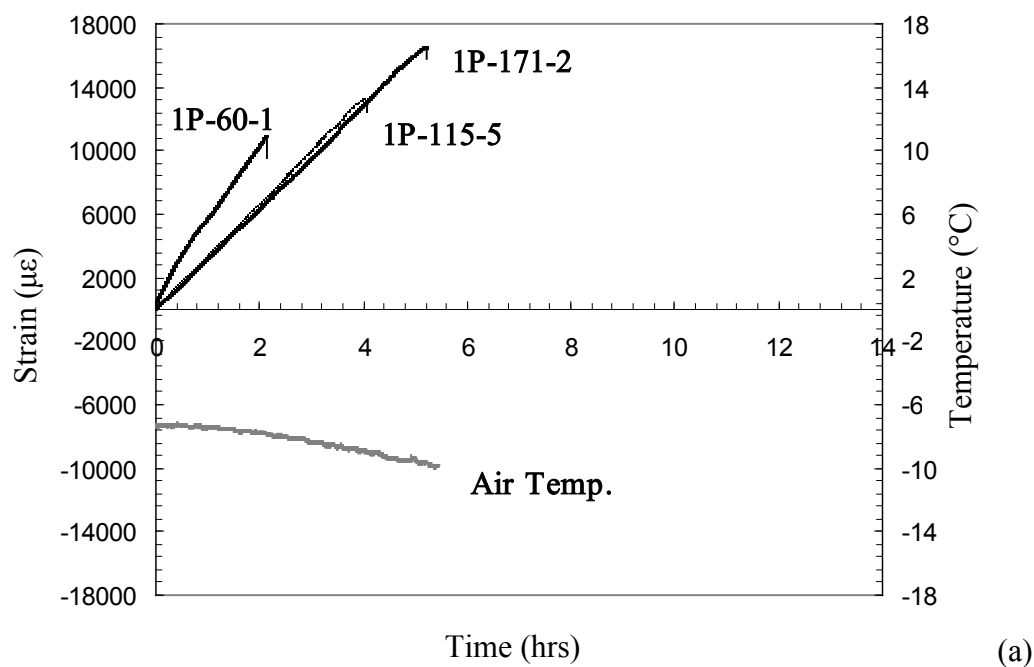


Figure 36 – Circumferential strain measurements for a representative GFRP specimen 3P-115-2 instrumented with the longitudinal layout.



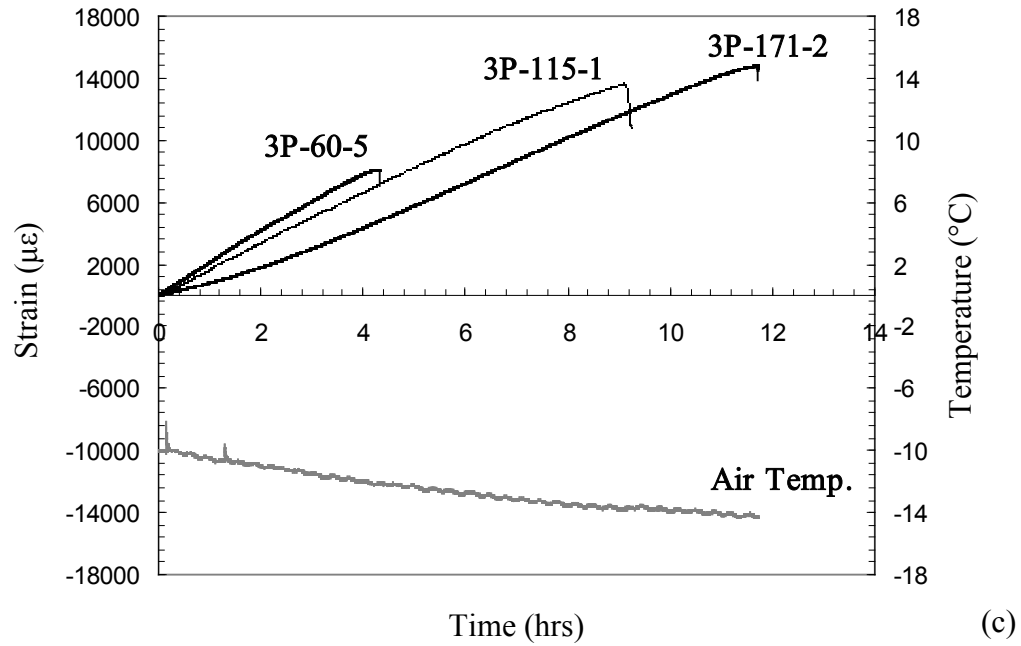


Figure 37 – Strain-time-air temperature response of representative GFRP specimens with one ply (a); two plies (b); and three plies (c).

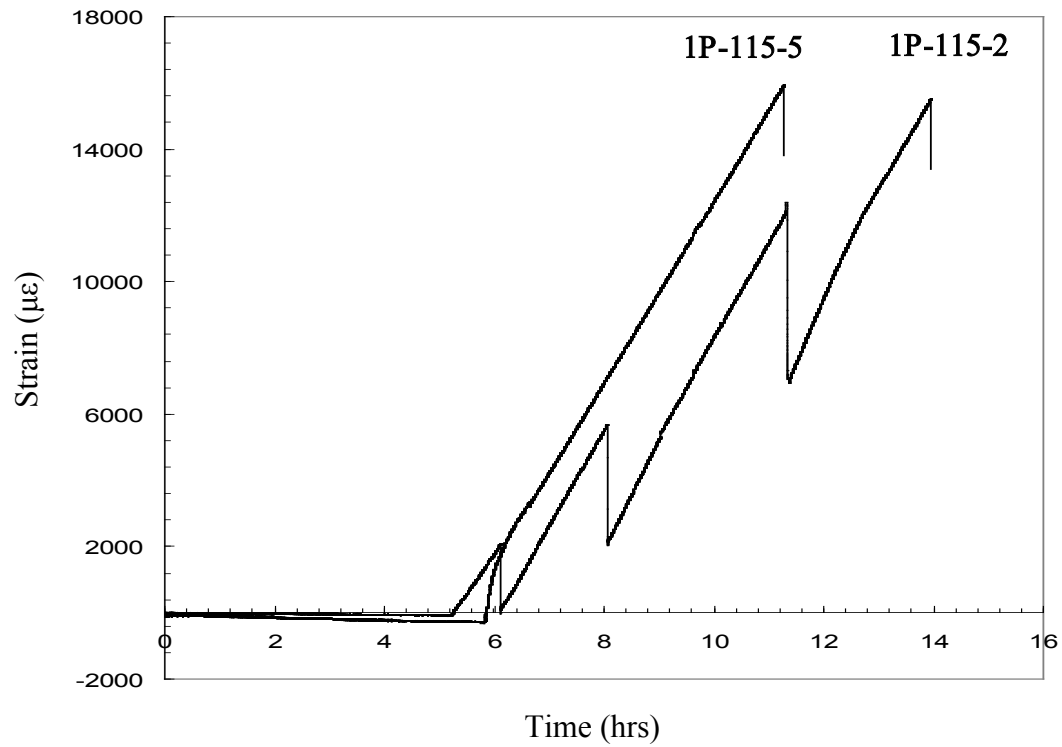


Figure 38 – Strain-time response for the entire test length showing the difference between same design specimens: 1P-115-2 showing pressure loss (due to leak), and 1P-115-5 without pressure loss (good seal).

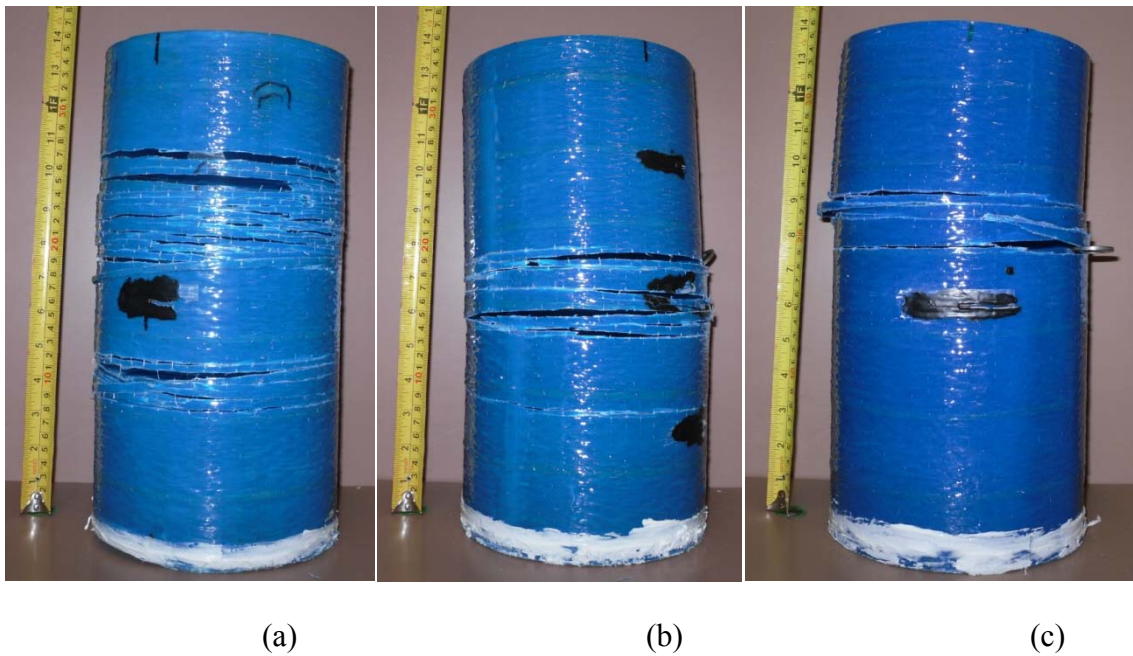


Figure 39 – Failure mode of 171 mm diameter GFRP cylindrical specimens

1P-171-2 (a); 2P-171-5 (b); and 3P-171-1 (c).



Figure 40 – Typical tensile failure observed on specimen 1P-171-2.

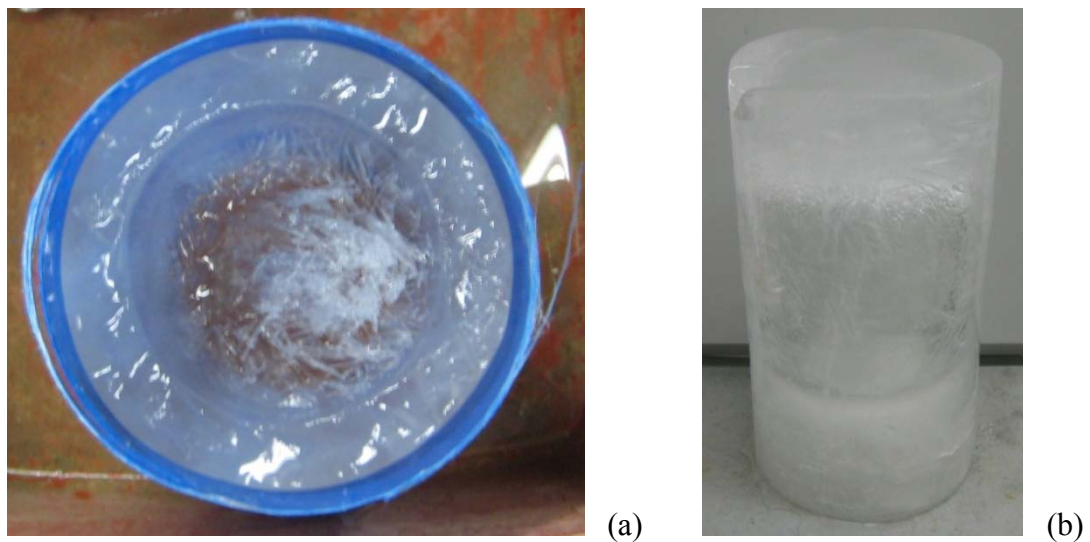


Figure 41 – Specimen 1P-171-4 failed at the mid cross-section after testing, showing the inside of the specimen with the ice layer formation (a); ice block inside specimen 2P-171-3, showing that the centre core is hollow (filled with water).

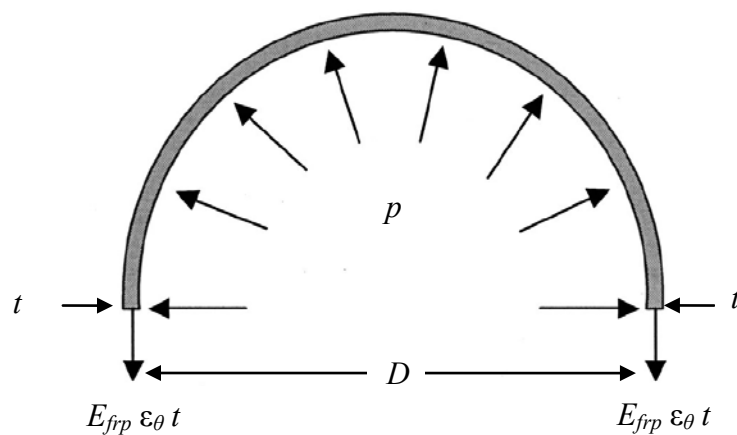


Figure 42 – Scheme of confinement action.

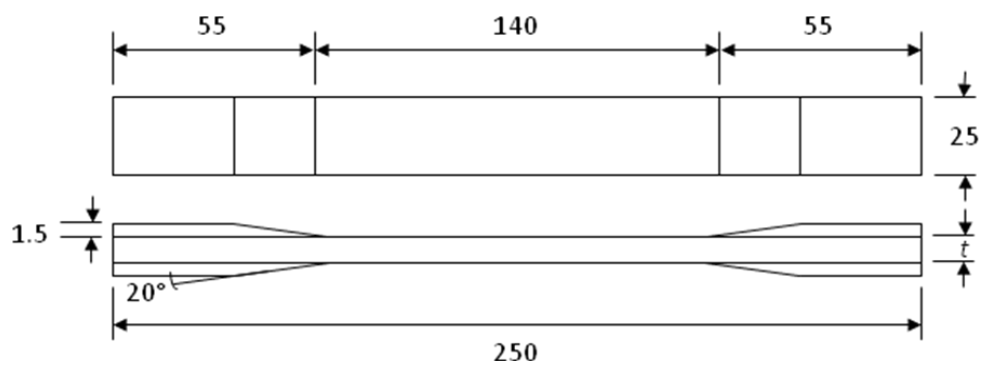


Figure 43 – GFRP flat coupon specimen drawing (dimensions in mm).

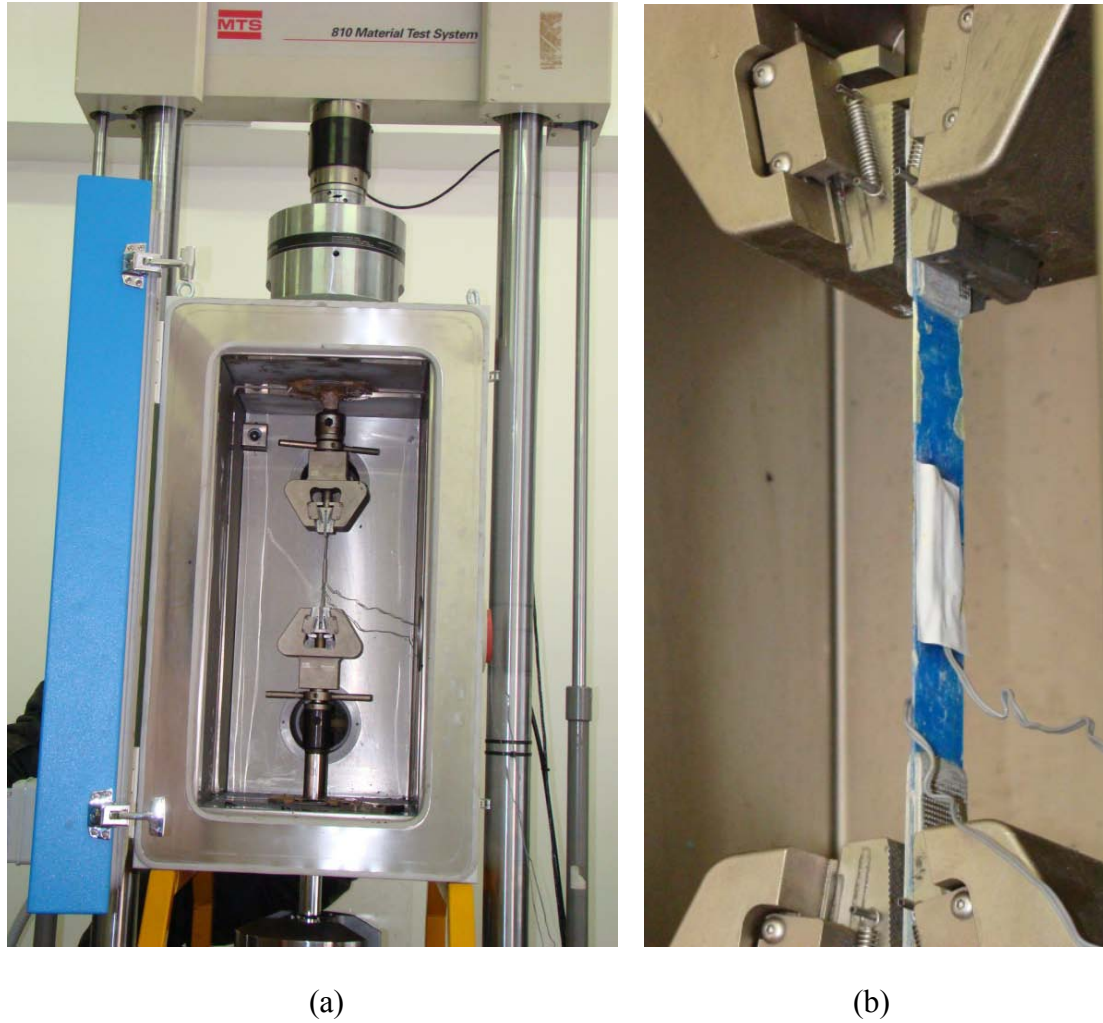


Figure 44 – Test setup for GFRP flat coupon specimen tensile (a);
and flat coupon specimen instrumentation (b).

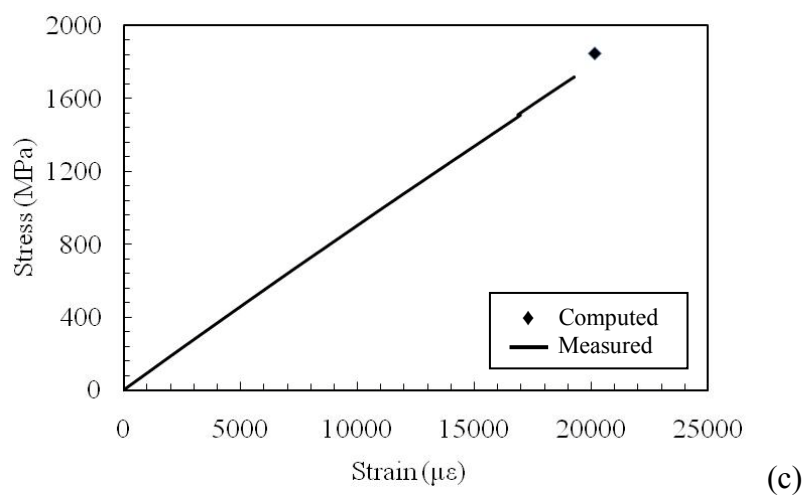
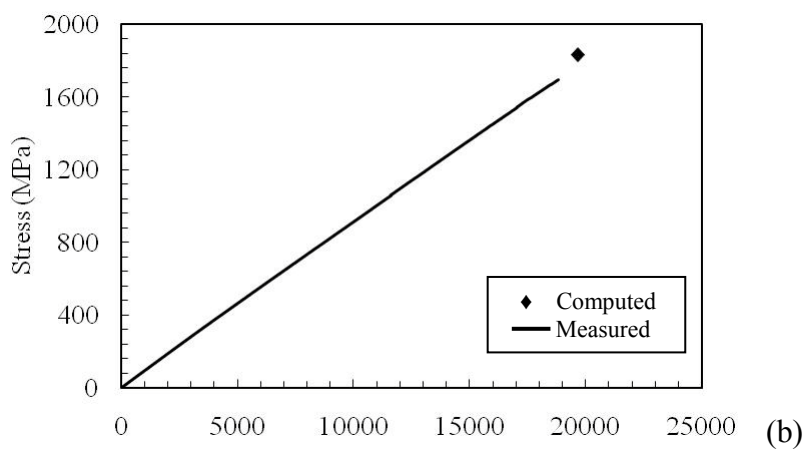
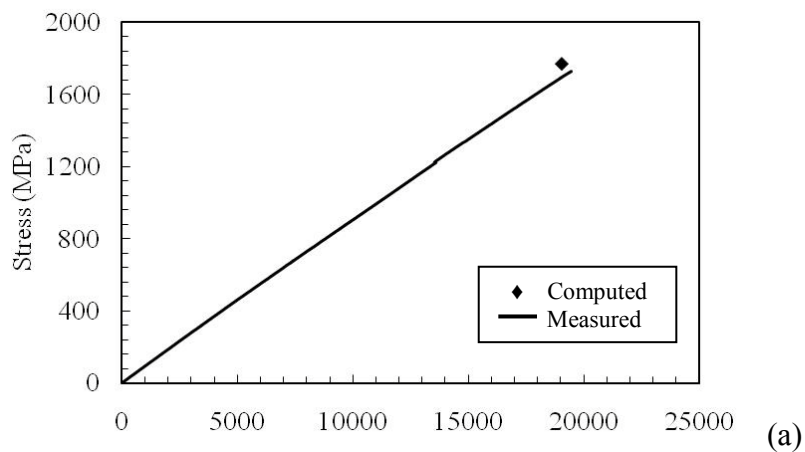


Figure 45 – Representative direct tensile axial stress-strain response for GFRP flat coupon, 1P-C (a); 2P-B (b); and 3P-C (c).



Figure 46 – Representative tensile failure experienced by flat coupons,

A type (a); and S type (b).

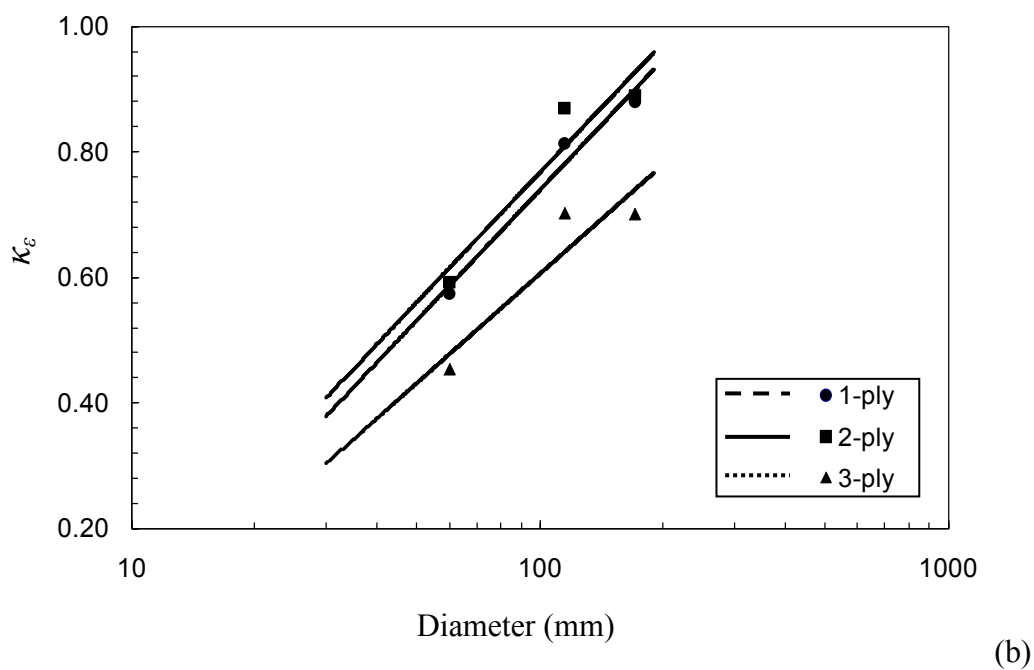
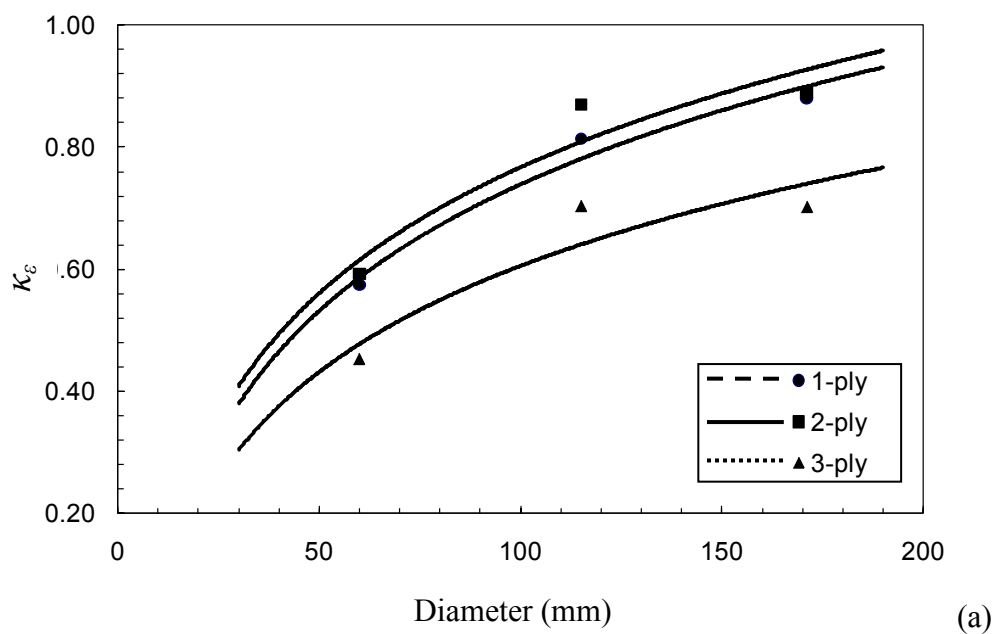


Figure 47 – Strain efficiency factor, κ_{ε} , vs cylinder diameter, D , at different number of plies; ordinary scale (a), and logarithmic scale (b).

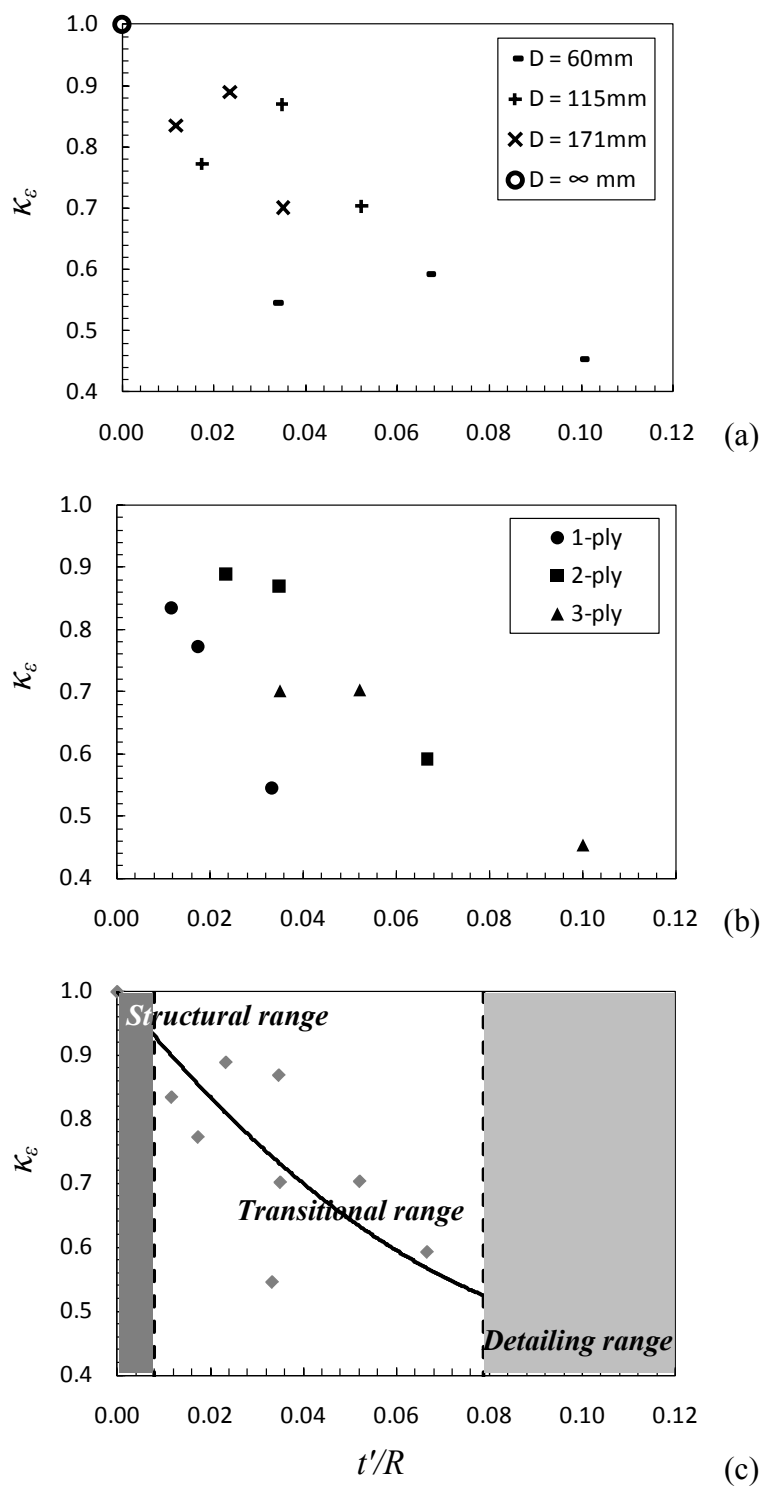


Figure 48 – Strain efficiency factor, κ_ϵ vs. t'/R ratio showing specimens by: diameter (a); number of plies (b); and combined results (c).

CHAPTER V

CONCLUSIONS

The experimental programs presented in Study 1 and Study 2, are unique activities to advance knowledge and understanding of FRC composite systems. Study 1 develops a compatible and fully reversible FRC confinement system that provides increases in axial-strength comparable to polymeric systems, with significant increases in axial strain compared to unconfined concrete. While Study 2, presents a life cycle assessment framework allowing for an integrated life cycle decision-making approach when selecting material systems for strengthening of infrastructure. Study 3 builds on the conclusions from Study 1 with a twofold purpose; on the one hand, to develop a novel test method aimed at providing an efficient and reliable experimental technique to characterize FRP composite laminates, so as to validate and later implement it on FRC composites to determine material properties. On the other, to determine the effect of jacket curvature (diameter) and thickness (number of plies) on strain efficiency of FRP laminates, so as to provide experimental evidence to explain the large scatter in strain efficiency observed in FRP confined concrete.

The conclusions derived from the experimental and analytical evidence obtained by the small scale cylinder tests, and the quantitative and qualitative environmental impact assessment for the proposed fiber reinforced cement-based composite system for concrete confinement, are herein summarized:

1. The proposed FRC prototype configuration attained substantial increases in axial strength and deformability with respect to unconfined cylinders, where strength increased linearly throughout the entire range of reinforcement amount tested; additionally the use of basalt fibers as reinforcement in organic and inorganic based composites for confinement applications was verified.
2. Full reversibility was achieved using a wax-based bond breaker, where the FRC bonded and unbonded specimens reached similar strength levels suitable for concrete confinement; however, the bonded interface was more effective in ensuring intimate contact between concrete substrate and composite jacket, resulting in a superior and more reliable increase in deformability.
3. The FRC system had poor fiber impregnation, yielding a strongly layered composite of alternating cement-matrix and dry fibers; this lead to premature failure due to the separation between the fiber and the matrix.
4. Composites with brittle matrices are not adequately characterized with existing direct tensile flat coupon standardized test methods.
5. Semi-empirical models to estimate axial strength and deformation increase for confined concrete showed good agreement with a model previously proposed for an inorganic-matrix fiber reinforced confinement system.

6. For every installed ply of BFRC, approximately 3.5 times more primary energy is needed, and 3.7 times more carbon is emitted to install an equivalent GFRP ply.
7. The matrix was the component for both strengthening systems (BFRC and GFRP) which contributed towards most of the energy consumption and carbon emissions, leading to increase of fossil fuel depletion and risk of global warming.
8. Based on the environmental chamber tests, for every installed ply of GFRP, there is 33 times more potential for the air quality to immediately deteriorate after installation with VOCs, and 24 times more 2.5 hrs post-installation, than when selecting a BFRC composite system.
9. Overall, based on the life cycle assessment method an inorganic based composite provides a significantly environmentally-benign alternative over the organic counterparts.

Understanding the strengths, weaknesses, opportunities and issues of externally-bonded FRP systems [17] reveals that to advance the use of composite systems within the construction industry it is necessary to research new combinations of materials. To this extent, Study 1 responds to this need by developing an alternative fiber reinforced cement-based composite system for concrete confinement providing new experimental evidence to understand the behavior of such composites. Additionally Study 2 implements the life cycle assessment methodology as a tool to determine engineering trade-offs between composite systems based on the economic, technical, environmental, and health challenges currently faced by the construction industry.

The following conclusions are highlighted from the experimental outcomes and evaluation of FRP strain efficiency using the ICE methodology:

1. The proposed ICE methodology to characterize circumferential strain of cylindrical GFRP laminates is simple, effective and reliable.
2. GFRP cylinders followed a linear elastic behavior till failure, with failure in the middle third section under hydrostatic loading.
3. Ultimate circumferential strain values increased with increasing cylinder diameter, while being consistently lower when compared to similar GFRP flat coupon specimens under the same environmental conditions.
4. The ultimate FRP tensile strain is a function of the radius of curvature and laminate thickness, for a given fiber ply density and number.
5. Larger diameter GFRP specimens yield higher strain efficiency ratios, while increasing the GFRP laminate thickness for the same diameter specimen, reduces the strain efficiency.
6. Three regions are established from a conservative approach using the ratio of nominal laminate thickness to radius of curvature, t'/R . They suggest that different strain efficiency factors might be used for design purposes depending on the externally bonded FRP application. The first region covers FRP wrapping circular columns, minor detrimental effects to strain are experienced in this region. The second region covers detailing of FRP laminates bent around chamfer radii of non-circular columns, major detrimental effects to strain are experienced

in this region. The third is the transition between the other two, and shows the non linear descending relationship between the strain efficiency and t'/R .

The novelty of the ICE methodology lies in the use of water that expands when it changes state of matter from liquid to solid, as a medium to apply an internal hydrostatic pressure. This yields a unique test method without complex configurations of moving parts, while being able to apply safely high hydrostatic loads.

RECOMMENDATIONS FOR FUTURE RESEARCH AND DEVELOPMENT

To allow for the inclusion of alternative FRC based composites for confinement of concrete in the current practice for strengthening of existing infrastructure, or conservation of historic buildings, further research is needed. It is recognized that fiber impregnation needs to be improved to more efficiently use the constituent materials of the developed composite. While, the investigation of alternative reversible systems that minimize tradeoffs in deformability, particularly for seismic retrofit applications, ought to be explored further. The characterization of the proposed FRC composite is essential to develop analytical and design models for its implementation within the current practice. The ICE methodology is a reliable candidate test method to provide initial material properties of FRC composites.

Additionally, due to the cement-matrix's large thickness in comparison to FRP composites (where it is assumed to be negligible), when applied in confinement applications with glass fibers, numerous layers will need to be installed, thus yielding an

overall thick jacket. Therefore, a GFRC confined concrete column under bending needs to be investigated as it would provide longitudinal shear between concrete core and the jacket introducing pre- and post-debonding issues between at the concrete-jacket interface.

The recycling and/or disposal of current polymeric based composite systems needs to be further evaluated quantitatively to determine a full LCA. Additionally, research implementing thermal gas chromatography to identify the components and relative concentrations within the VOC emissions of composites, may potentially provide data to assess the end-point and damage potential indicators to implement them in LCA to determine relative long term environmental and health impacts caused by the use of composite strengthening systems.

The ICE methodology needs to be further validated with different composite material systems and compared to existing standardized test methods. Nonetheless, the ICE methodology can respond numerous fundamental unanswered questions regarding the behavior of FRP composites used in infrastructure rehabilitation such as: behavior multiply composites, non-circular laminates under hydrostatic loading, characterization of hybrid-fiber sheets, and assess the influence of fiber-sheet orientation, or the overlap region.

BIBLIOGRAPHY

- [1] Kaw, A. K. "Mechanics of composite materials (second edition)." *Taylor and Francis* 2005, Boca Raton, FL.
- [2] Bakis, C. E., Bank, L. C., Brown, V. L., Cosenza, E., Davalos, J. F., Lesko, J. J., Machida, A., Rizkalla, S. H., and Triantafillou, T. C. "Fiber reinforced polymer composites for construction – state of the art review." *Journal for Composites for Construction* 2002; 6(2): 73-87.
- [3] Fardis, M. N., and Khalili, H. "FRP-Encased concrete as a structural material." *Magazine of Concrete Research* 1982; 34(121): 191–202.
- [4] Iyer, S. L., and Sen, R. Editors. "Advanced Composite Materials in Civil Engineering Structures." *Proceedings American Society of Civil Engineers* 1991, New York, NY.
- [5] Nanni, A., and Dolan, C.W., Editors. "FRP Reinforcement for Concrete Structures." *Proceedings ACI SP-138, American Concrete Institute* 1993, Detroit, MI.
- [6] American Concrete Institute (ACI) Committee 440. "Report on fiber-reinforced Polymer (FRP) reinforcement for concrete structures." *ACI 440R-07* 2007, Farmington Hills, MI.
- [7] Nanni, A., and Bradford, N. M. "FRP jacketed concrete under uniaxial compression." *Construction Building Materials* 1995; 9(2): 115–124.
- [8] Toutanji, H. "Stress-strain characteristics of concrete columns externally confined with advanced fiber composite sheets." *ACI Materials Journal* 1999; 96(3): 397-404.
- [9] Saadatmanesh, H., Ehsani, M. R., and Jin, L. "Seismic strengthening of circular bridge pier models with fiber composites." *ACI Structural Journal* 1996; 93(6): 639-647.

- [10] Seible, F., Priestley, M. J. N., Hegemier, G. A., and Innamorato, D. "Seismic retrofit of RC columns with continuous carbon fiber jackets." *Journal of Composites for Construction* 1997; 2(1): 52-62.
- [11] American Concrete Institute (ACI) Committee 440. "Guide for the design and construction of externally bonded FRP systems for strengthening concrete structures." *ACI 440.2R-08* 2008. Farmington Hills, MI.
- [12] Canadian Standards Association (CSA). "Canadian highway bridge design code." *CAN/CSA-S6-06* 2006. Mississauga, Ontario, Canada.
- [13] Bisby, L. A., Green, M. F., and Kodur, V. K. R. "Response to fire of concrete structures that incorporate FRP." *Progress in Structural Engineering and Materials* 2005; 7(3): 136-149.
- [14] Van Balen, K. E. P., Ercan, S., Patricio, C. T. "Compatibility and retreatability versus reversibility: a case study at the late hellenistic nymphaeum of Sagalassos (Turkey)." In: Sickels-Taves, L. B., editor. The use of and need for preservation standards in architectural conservation – ASTM STP 1355. West Conshohocken, PA. *American Society for Testing and Materials* 1999; 105-118.
- [15] Civil Engineering Research Foundation (CERF). "Gap analysis for durability of fiber reinforced polymer composites in civil infrastructure." *American Society of Civil Engineers* 2001. New York, NY.
- [16] Bakis, C. "Life cycle analysis issues in the use of FRP composites in civil infrastructure." *Proceedings US-Japan Workshop on Life Cycle Assessment of Sustainable Infrastructure Materials* 2009. Sapporo, Japan.
- [17] Burgoyne, C. "Fibre reinforced polymers – strengths, weaknesses, opportunities and threats." In: Oehlers, D., Griffith, M., and Seracino, R., editors. *Proceedings of the 9th international symposium on fiber reinforced polymer reinforcement for concrete structures (FRPRCS-9)* 2009. Sydney, Australia.
- [18] FMI Corporation. "The U.S. Markets construction overview 2009". *FMI Corporation* 2009. Raleigh, NC.
- [19] National Surface Transportation Policy and Revenue Study Commission. "Transportation for tomorrow." *U.S. Dept. for Transportation* 2007. Volume II, Chapter 4.
- [20] McGraw Hill Construction. "2009 Green outlook: trends driving change." *McGraw Hill Construction* 2009. Washington, DC.
- [21] Bank, L. "Structural materials and mechanics program (SMM)." *National Science Foundation (NSF)* 2010. Arlington, VA.

- [22] United States Green Building Council, (USGBC). "Green building facts." *United States Green Building Council* 2009. Washington, DC.
- [23] De Lorenzis, L., and Tepfers, R. "Comparative study of models on confinement of concrete cylinders with fiber reinforced polymer composites." *Journal of Composites for Construction* 2003; 7(3): 219–237.
- [24] Xiao, Y., and Wu, H. "Compressive behavior of concrete confined by carbon fiber composite jackets." *Journal of Materials in Civil Engineering* 2000; 12(2): 139–146.
- [25] Pessiki, S., Harries K. A., Kestner, J. T., Sause, R., and Ricles, J. M. "Axial behavior of reinforced concrete columns confined with FRP jackets." *Journal of Composites for Construction* 2001; 5(4): 237–245.
- [26] Lam, L., and Teng, J. G. "Ultimate condition of fiber reinforced polymer-confined concrete." *Journal of Composites for Construction* 2004; 8(6): 539-548.
- [27] De Caso y Basalo, F., Matta, F., and Nanni, A. "Fiber reinforced cementitious-matrix composites for infrastructure rehabilitation." *Proceedings Fiber Reinforced Polymer Reinforcement for Concrete Structures (FRPRCS-9)* 2009. Sydney, Australia.
- [28] Foden, A., Lyon, R., Balaguru, P., and Davidovitz, J. "High temperature inorganic resin for use in fiber reinforced composites." In: Saadatmanesh, H., and Ehsani, M. R., editors. *Proceedings of the 1st International Conference on Composites in Infrastructures* 1996; 166-177. Tucson, AZ.
- [29] Papakonstantinou, C., and Balaguru, P. "Bond characteristics and structural behavior of inorganic polymer FRP." In: *Measuring, monitoring and modeling concrete properties*. Dordrecht, Netherlands: Springer Netherlands; 2006. p. 735-741.
- [30] Balaguru, P., and Kurtz, S. "Use of inorganic polymer-fiber composites for repair and rehabilitation of infrastructures." In: Silva-Araya, W. F., deRincón, O. T., and Pumarada O'Neill, L., editors. *Repair and rehabilitation of reinforced concrete structures: the state of the art*. American Society of Civil Engineers; 1998. p.155-168. Reston, VA.
- [31] Kurtz, S., and Balaguru, P. "Comparison of inorganic and organic matrices for strengthening of RC beams with carbon sheets." *Journal of Structural Engineering* 2001; 127(1): 35-42.
- [32] Garon, R., Balaguru, P., and Toutanji, H. "Performance of inorganic polymer-fiber composites for strengthening and rehabilitation of concrete beams." In: Burgoyne, C., editor. *Fibre-reinforced plastics for reinforced concrete structures FRPRCS-5* 2001. Thomas Telford, Vol. 1, p. 53-62. London, UK.

- [33] Triantafillou, T. C., and Papanicolaou, C. G. "Shear strengthening of reinforced concrete members with textile reinforced mortar (TRM) jackets." *Materials and Structures* 2006; 39(1): 93-103.
- [34] Wu, H. C., and Teng, J. "Innovative cement based thin sheet composites for retrofit." In: *Proceedings of the 3rd international conference on composites in infrastructure (ICCI'02)* 2002. San Francisco, CA.
- [35] Wu, H.C., and Sun, P. "Fiber reinforced cement based composite sheets for structural retrofit." In: Chen, J. F., Teng, J. G., editors. *Proceedings of the international symposium on bond behaviour of FRP in structures*. International Institute for FRP in Construction, 2005; 343-348. Hong Kong, China.
- [36] Triantafillou, T. C., Papanicolaou, C. G., Zissimopoulos, P., and Laourdekis, T. "Concrete confinement with textile-reinforced mortar jackets." *ACI Structural Journal* 2006; 103(1): 28-37.
- [37] Bournas, D. A., Lontou, P. V., Papanicolaou, C. G., and Triantafillou, T. C. "Textile-reinforced mortar versus fiber-reinforced polymer confinement in reinforced concrete columns." *ACI Structural Journal* 2007; 104(6): 740-748.
- [38] Di Ludovico, M., Prota, A., and Manfredi, G. "Structural upgrade using basalt fibers for concrete confinement." *Journal of Composites for Construction* 2010; in press, preview available at:
<http://ascelibrary.aip.org/getabs/servlet/GetabsServlet?prog=normal&id=JCCOX X000001000001000067000001&idtype=cvips&gifs=Yes&ref=no>.
- [39] American Society for Testing and Materials (ASTM). "Standard test method for compressive strength of hydraulic cement mortars (using 2-in. or [50-mm] cube specimens) – ASTM C 109". *ASTM International* 2007. West Conshohocken, PA.
- [40] American Society for Testing and Materials (ASTM). "Standard test method for splitting tensile strength of intact rock core specimens – ASTM D 3967". *ASTM International* 2005. West Conshohocken, PA.
- [41] Czigány, T., Vad, J., and Pölöskei, K. "Basalt fiber as a reinforcement of polymer composites." *Periodica Polytechnica – Mechanical Engineering* 2005; 49(1): 3-14.
- [42] Sim, J., Park, C., and Moon, D-Y. "Characteristics of basalt fiber as a strengthening material for concrete structures." *Composites Part B: Engineering* 2005; 36(6-7): 504-512.
- [43] American Society for Testing and Materials (ASTM). "Standard test method for compressive strength of cylindrical concrete specimens – ASTM C 39." *ASTM International* 2005. West Conshohocken, PA.

- [44] American Society for Testing and Materials (ASTM). "Standard test method for tensile properties of polymer matrix composite materials - ASTM D 3039." *ASTM International* 2008. West Conshohocken, PA.
- [45] Haldar, A., and Mahadevan, S. "Probability, reliability and statistical methods in engineering design." *John Wiley & Sons* 2000. New York, NY.
- [46] Pantazopoulou, S. J., and Mills, R. H. "Microstructural aspects of the mechanical response of plain concrete." *ACI Materials Journal* 1995; 92(6): 605-616.
- [47] Mirmiran, A., Shahawy, M., Samaan, M., El Echary, H., Mastrapa, J. C., and Pico, O. "Effect of column parameters on FRP-confined concrete." *Journal of Composites for Construction* 1998; 2(4): 175-185.
- [48] Teng, J. G., Huang, Y.L., Lam, L., and Ye, L. P. "Theoretical model for fiber reinforced polymer-confined concrete." *Journal of Composites for Construction* 2007; 11(2): 201-210.
- [49] United States Environmental Protection Agency, Science Advisory Board. "Toward integrated environmental decision-making." EPA-SAB-EC-00-011, *Environmental Protection Agency (EPA)* 2000. Washington, DC.
- [50] European Commission (CE), "Directives on dangerous substances.", 97/69/CE, European Parliament 1997. Brussels, Belgium
- [51] Hammond, G. P., and Jones, C.I. "Inventory of carbon & energy (ICE), version V1.6a." *Sustainable Energy Research Team, Department of Mechanical Engineering* 2008. University of Bath, UK.
- [52] De Caso y Basalo, F., Nanni, A., and James, J. P. "Qualitative and quantitative environmental impact analysis of BFRC vs GFRP: green building construction rehabilitation systems." *Engineering Sustainability* 2009. Pittsburgh, PA.
- [53] Lieu, T., and Meyer, C. "Recycling concrete and other materials for sustainable development." *American Concrete Institute (ACI), SP-219* 2004. Farmington Hills, MI.
- [54] Fava, J., Dennison, R., Jones, B., Curran, M. A., Vigon, B., Selke, S., and Barnum, J. "A technical framework for life-cycle assessment." *Society of environmental Toxicology and Chemistry* 1991. Washington D.C.
- [55] Environmental Protection Agency (EPA). "Life cycle assessment: inventory guidelines and principles." *EPA/600/R-92/245 Office of Research and Development* 1993. Cincinnati, Ohio.

- [56] American Society for testing and Materials (ASTM). "Standard guide for environmental life cycle assessment of building materials/products - E1991-05." *ASTM International* 2005. West Conshohocken, PA.
- [57] International Organization for Standardization (ISO). "Environmental management - life cycle assessment - principles and framework." *ISO14040* 2005. Geneva, Switzerland.
- [58] Shapira, A., and Bank, L. C. "Constructability and economics of FRP reinforcement cages for concrete beams." *Journal of Composites for Construction* 1997; 1(3): 82-89.
- [59] Ehlen, M. A. "Life-cycle costs of fiber-reinforced-polymer bridge decks." *Journal of Materials in Civil Engineering* 1999; 11(3): 224-230.
- [60] Hastak, M., and Halpi, D. W. "A model for life-cycle cost-benefit assessment of composite materials in construction." *Journal of Composites for Construction* 2000; 4(3): 103-111.
- [61] Kappos, A. J., and Dimitrakopoulos, E. G. "Feasibility of pre-earthquake strengthening of buildings based on cost-benefit and life cycle cost analysis with the aid of fragility curves." *Natural Hazards* 2008; 45(1): 33-54.
- [62] Jayaraman, K., and Xu, X. W. "Life cycle assessment of products made of composite materials." *International Journal Product lifecycle Management* 2009; 4(1): 11-22.
- [63] Tanaka, H., Tazawa, H., Kurita, M., and Shimomura, T. "A case study on life-cycle assessment of environmental aspect of FRP structures." *Conference on FRP Composites in Civil Engineering* 2006, Miami, FL.
- [64] American Chemistry Council (ACC). "The resin reviewed." *American Chemistry Council Inc.* 2010. Silver Spring, MD.
- [65] Kouparttsas, C. E., Kawtalis, C. N., Varelidis, P. C., Tsenoglou, C. J., and Papispyrides, C. D. "Recycling of the fibrous fraction of reinforced thermoset composites." *Polymer Composites* 2002; 23(4): 682-689.
- [66] Ware, J. H., Spengler, J. D., Neas, L., Samet, J., Wagner, G., Coultas, D., Ozkaynak, H., and Schwab, M. "Respiratory and irritant health effects of ambient volatile organic compounds." *American Journal of Epidemiology* 1993; 137(12): 1287-1301.
- [67] Brinke, J.T., Selvin, S., Hodgson, A. T., Fisk, W. J., Mendell, M. J., Koshland, C. P., and Daisey, J. M. "Development of new volatile organic compound (VOC) exposure metrics and their relationship to 'sick building syndrome' symptoms." *International Journal of Indoor Environment and Health* 1998; 8(3): 140-152.

- [68] Bare, J. C., Norris, G. A., Pennington, D. W., and McKone, T. "TRACI, the tool for the reduction and assessment of chemical and other environmental impacts." *Journal of Industrial Ecology* 2003; 6(3):49-78.
- [69] Hofstetter, P. "Perspectives in life cycle impact assessment – a structure approach to combine models of the technosphere, ecosphere, and valuesphere." *Kulwer Academic Press* 1998. 359-366. Boston, MA.
- [70] Bare, J. C., and Gloria, T. P. "Critical analysis of the mathematical relationships and comprehensiveness of life cycle impact assessment approaches." *Environmental Science and Technology* 2006; 40(4): 1104-1113.
- [71] United Nations Environment Program (UNEP). "Evaluation of environmental impacts in life cycle assessment." *UNEP Report, Division of Technology, Industry and Economics, Production and Consumption Branch* 2003. Paris, France.
- [72] Bare, J., Hofstetter, P., Pennington, D., and Udo de Haes, H. "Life cycle impact assessment midpoints vs. endpoints: the sacrifices and the benefits." *International Journal of Life Cycle Assessment* 2000; 5(6): 1104-1113.
- [73] Udo de Haes, H., and Lindeijer, E. "The conceptual structure of life-cycle impact assessment. In life-cycle impact assessment: striving towards best practice." Udo de Haes, Ed; *Society of Environmental Toxicology and Chemistry Press* 2002: 209-225. Pensacola, FL.
- [74] United States Environmental Protection Agency (EPA). "TRACI, the tool for the reduction and assessment of chemical and other environmental impacts." *National Risk Management Research Laboratory, Sustainable Technology Division - Systems Analysis Branch* 2009. Cincinnati, OH.
- [75] American Society for testing and Materials (ASTM). "Standard guide for small-scale environmental chamber determinations of organic emissions from indoor materials/products - D5116." *ASTM International* 2006. West Conshohocken, PA.
- [76] Commission of European Communities (CEC). "Guideline for the characterization of volatile organic compounds emitted from indoor materials and projects using small test chambers." *Commission of European Communities* 1991; Project 613, Report No. 8. Brussels, Belgium.
- [77] United States Environmental Protection Agency (EPA). "Title 40 of the Code of Federal Regulations Part 50." *National Ambient Air Quality Standards (NAAQS)*, 1999. Washington D.C.
- [78] Shannon, J. D. "Atmospheric pathways module. In tracking and analysis framework (TAF) model documentation and user's guide: An interactive model for integrated assessment of Title IV of the clean air act amendments." ANL/DIS/TM-36. *Argonne National Laboratory* 1996. Argonne, IL.

- [79] Carter, W. "Development of ozone reactivity scales for volatile organic compounds." *Journal of the Air and Waste Management Association* 1999; 44(1): 881-899.
- [80] American Concrete Institute (ACI) Committee 440. "Guide test methods for fiber-reinforced polymers (FRPs) for reinforcing or strengthening concrete structures – *ACI 440.3R-04* 2004. Farmington Hills, MI.
- [81] De Caso y Basalo, F., Matta, F., and Nanni, A. "Fiber reinforced cement-based composite system for concrete confinement." *Journal of Construction and Building Materials* 2010; under review.
- [82] American Society for Testing and Materials (ASTM). "Standard test method for apparent hoop tensile strength of plastic or reinforced plastic pipe by split disc method –D 2290." *ASTM International* 2008. West Conshohocken, PA.
- [83] American Society for Testing and Materials (ASTM). "Standard test method for preparation and tension testing of filament-wound pressure vessels – ASTM D 2585." *ASTM International* 1968. West Conshohocken, PA.
- [84] Thompson, R. C., Pak, T. T., and Rech, B. M. "Hydroburst test methodology for evaluation of composite structure." *Composite Materials: Testing and Design* 2003. ASTM STP 1436, West Conshohocken, PA.
- [85] Cain, J., Case, S., and Lesko, J. "Testing of hygrothermally aged e-glass/epoxy cylindrical laminates using a novel fixture for simulating internal pressure." *Journal of Composites for Construction* 2009; 13(4): 325-331.
- [86] Toombes, G. R., Swanson, S. R., and Cairns, D. S. "Biaxial testing of composite tubes." *Journal of Experimental Mechanics* 1985; 25(2): 186-192.
- [87] Johnson, A. K., Cohen, D., Hansen, M. F., and Toombes, Y. T. "Pressurized ring test for composite pressure vessel hoop strength and stiffness evaluation." *Journal of Composites Technology and Research* 1995; 17(4): 331-340.
- [88] Walsh, E. J., and Adams, D. O. "Development and evaluation of the quadrant ring test method." *Journal of Experimental Mechanics* 2008; 48(3); 319-326.
- [89] Fletcher, N. H. "The chemical physics of ice." *Cambridge University Press* 1970. England, UK.
- [90] Chaplin, M. "Hexagonal ice structure." *Water Structure and Science* 2007.
- [91] Petrenko, V. F., and Whitworth, R. W. "Physics of ice." *Oxford University Press* 1999. Oxford, NY.

- [92] Eisenberg, D., and Kauzmann, W. "The structure and properties of water." *Oxford Press*, 2005. Oxford, NY.
- [93] Mason, B. J., Bryant, G. W., and Van den Heuval, A. P. "Growth habits and surface structure of ice crystals." *Philosophical Magazine* 1963; 8: 505–509.
- [94] Shaw, R. A., Durant, A. J., and Mi, Y. "Heterogeneous surface crystallization observed in undercooled water." *Journal of Physical Chemistry B* 2005; 109(20): 9865-9868.
- [95] Lam, L., and Teng, J. G. "Design-oriented stress–strain model for FRP-confined concrete." *Journal of Construction and Building Materials* 2003; 17(6-7): 471-489.
- [96] Jiang, T., and Teng, J. G. "Strengthening of short circular RC columns with FRP jackets: a design proposal." *Proceedings of the 3rd International Conference on FRP Composites in Civil Engineering* 2006, Miami, FL.
- [97] Bisby, L. A., Green, M. F., and Kodur, V. K. R. "Response to fire of concrete structures that incorporate FRP." *Progress in Structural Engineering and Materials* 2005; 7(3): 136-149.
- [98] Luo, S., and Wong, C. P. "Thermo-mechanical properties of epoxy formulations with low glass transition temperatures." *Proceedings of the 8th International Symposium on Advanced Packaging Materials* 2002. Braselton, GA.
- [99] Nardone, F., Di Ludovico, M., De Caso y Basalo, F., Prota, A., and Nanni, A. "Experimental investigation on the tensile behavior of epoxy based composites under extreme service temperatures." *Composites Part B* 2010. Under Review.
- [100] Nielsen, L. E., and Landel, R. F. "Mechanical properties of polymers and composites." *Marcel Dekker* 1994.
- [101] Peters, S. T. "Handbook of composites." *Chapman and Hall* 1998.
- [102] Head, P. R. "Advanced composites in civil engineering – a critical overview at this high interest, low usage stage of development." Badry, E. ed. *Proceeding of Advance Composite Materials in Bridges and Structures* 1996. Montreal, Canada.
- [103] Yang, X., Nanni, A., and Chen, G. "Effect of corner radius on performance of externally bonded FRP reinforcement." *Non-Metallic Reinforcement for Concrete Structures FRPRCS-5* 2001. Cambridge, UK.
- [104] Seely, F. B., and Smith, J. O. "Advance mechanics of materials." *John Wiley* 1978.

- [105] Lignola, G. P., Prota, A., Manfredi, G., and Cosenza, E. “Effective strain in FRP jackets on circular RC columns.” *Fourth International Conference on FRP Composites in Civil Engineering (CICE)* 2008. Zurich, Switzerland.
- [106] American Concrete Institute (ACI) Committee 318. “Building code requirements for structural concrete.” *ACI 318-71* 1971. Farmington Hills, MI.
- [107] European Norm (EN). “Eurocode 8: Design of structures for earthquakes resistance, Part 5.5.1.2.2 Columns.” *European Norm* 1998. Brussels, Belgium.
- [108] Rocca, S., Galati, N., and Nanni, A. “Experimental evaluation of FRP strengthening of large-size reinforced concrete columns.” *Report No. UTC-142* 2006. University of Missouri-Rolla, MO.
- [109] Toutanji, H., Han, M., Gilbert, J., and Matthys, S. “Behavior of large-scale rectangular columns confined with FRP composites.” *Journal of Composites for Construction* 2010; (14)1: 62-71.
- [110] Yang, X., Wei, J., Nanni, A., and Dharani, L. R. “Shape effect on the performance of carbon fiber reinforced polymer wraps.” *Journal of Composites for Construction* 2004; (8) 5: 444-451.

VITA

Francisco J. De Caso y Basalo was born in Madrid, Spain, on October 4, 1984, where he attended King's College. In September, 2002, he entered the University of Bath, England, United Kingdom, where he received the degree of MEng in Civil and Architectural Engineering, with first class honors in July, 2007. He was appointed Graduate Researcher at the Center for Repair of Buildings and Bridges with Composites (RB²C) at the University of Miami, Florida, in August, 2007, where his research focused on the use of sustainable advanced composite material systems for concrete repair and rehabilitation, and developing new test methodologies for composite characterization. He also served as President of the Graduate Student Association (GSA) in 2009. In December, 2010, he received his Ph.D. in Civil Engineering from the University of Miami. He is a member of the American Society of Civil Engineers (ASCE), the American Concrete Institute (ACI), Society of Hispanic Engineers (SHPE), and the Institution of Civil Engineers (ICE) in the UK.

Permanent Address: Pedro Teixeira 10, 28020, Madrid, Spain.